ASSESSMENT OF RARE EARTH ELEMENT POTENTIAL IN DIFFERENT GEOLOGICAL FORMATIONS OF SRI LANKA

Batapola Dewage Nadeera Madhubhashani Batapola

198087R

Degree of Master of Philosophy

Department of Earth Resources Engineering

University of Moratuwa

Sri Lanka

July 2023

ASSESSMENT OF RARE EARTH ELEMENT POTENTIAL IN DIFFERENT GEOLOGICAL FORMATIONS OF SRI LANKA

Batapola Dewage Nadeera Madhubhashani Batapola

198087R

Thesis submitted in fulfillment of the requirements for the degree of Master of Philosophy in Earth Resources Engineering

Department of Earth Resources Engineering

University of Moratuwa

Sri Lanka

July 2023

DECLARATION OF THE CANDIDATE

"I declare that this is my own work, and this thesis does not incorporate without acknowledgment of any material previously submitted for a Degree or Diploma in any other University or institute of higher learning and to the best of my knowledge and belief it does not contain any material previously published or written by another person except where the acknowledgment is made in the text.

Also, I hereby grant to the University of Moratuwa the non-exclusive right to reproduce and distribute my thesis, in whole or in part in print, electronic, or other mediums. I retain the right to use this content in whole or part in future works (such as articles or books)."

Signature: Date: 31/07/2023

DECLARATION OF THE SUPERVISORS

The above candidate has carried out research for the MPhil thesis under my supervision.

Name of the supervisor: Pof. A.M.K.B. Abeysinghe

03.08.2023

Signature of the supervisor: Date:

Name of the supervisor: Prof. H.M.R. Premasiri

UOM Verified Signature

03.08.2023

Signature of the supervisor: Date:

Name of the supervisor: Dr. L.P.S. Rohitha

UOM Verified Signature

03.08.2023

Signature of the supervisor: Date:

ACKNOWLEDGEMENTS

First of all, I wish to express my sincere gratitude to my M. Phil supervisors, Pof. A.M.K.B. Abeysinghe, Prof. H.M.R. Premasiri, and Dr. L.P.S. Rohitha of the Department of Earth Resources Engineering, the University of Moratuwa for their proper guidance, supervision, and support to complete my research. I would also like to acknowledge the financial support provided by the research project "Potential of Rare Earth Elements (REE) in Sri Lankan Onshore and Offshore Terrains and Development of Extraction Techniques" under the Accelerating Higher Education and Development (AHEAD) Operation of the Ministry of Higher Education of Sri Lanka funded by the World Bank (AHEAD/DOR/6026-LK/8743-LK). Furthermore, my heartfelt gratitude goes to the rest members of the afore-mentioned project – Prof. N.P. Ratnayake (Principal Investigator), Dr. I.M.S.K. Ilankoon, Prof. D.M.D.O.K. Dissanayake, Prof. P.G.R. Dharmaratne, and Eng. N.P. Dushyantha for their immense guidance and support.

Moreover, I sincerely thank Dr. S.P. Chaminda, Head and the Research Coordinator of the Department of Earth Resources Engineering, University of Moratuwa, and all the academic staff members. I also wish to admire the continuous assistance provided by the non-academic staff of the Department of Earth Resources Engineering, the University of Moratuwa, in field visits and laboratory tests, especially to Mrs. A.R. Amarasinghe, Mr. S.S.U. Silva, Mrs. W.A.S.M. Wickramarachchi, Mr. W.R.M.D.M.B. Wickramasinghe, Mr. W.W.S. Perera, and Mr. S.D. Sumith. Furthermore, I would like to express my sincere thanks to Mrs. R.M.P. Dilshara for her assistance during the field visits, sample preparation, and laboratory testing.

Finally, I wish to dedicate my sincere gratitude to my family, friends, and all the individuals for their guidance, support, and encouragement to complete my M.Phil research.

ASSESSMENT OF RARE EARTH ELEMENT POTENTIAL IN DIFFERENT GEOLOGICAL FORMATIONS OF SRI LANKA

Abstract

In recent years, the global demand for rare earth elements (REEs) has been burgeoning due to the wide range of applications in numerous modern and green energy technologies. Although China was dominating the REE market, now the reliance on Chinese REE production has begun to ease with the global attempts to explore new REE resources outside China. This growing global competition coupled with demand escalations provides an opportunity for developing countries like Sri Lanka to start explorations for new viable REE sources to become a potential REE supplier to the global REE market. Therefore, the present study focuses on assessing the REE potential in different geological formations in Sri Lanka based on their origins and occurrences. Accordingly, representative samples from the Eppawala phosphate deposit (EPD) (n=60), Ginigalpelessa serpentinite deposit (n=32), beach placers on the northeast coast (Verugal: n=18 and Pulmoddai: n=26) and the southwest coast (n=18), alluvial placers in the Walave river basin (n=20), granites at Thonigala (n=17), Massenna (n=10), Arangala (n=6), and Ambagaspitiya (n=6), and Ratthota pegmatite (n=6) were analyzed for their REE contents. Based on the results, the EPD, Massenna and Arangala granites, and Pulmoddai deposit were the most prospective REE sources in Sri Lanka. However, due to technological and environmental challenges associated with granitic occurrences and the Pulmoddai deposit when converting them into exploitable mineral reserves, the EPD was identified as the most prospective source in Sri Lanka in the present study. Despite the relatively low REO grade (~0.48% $\sum REE_2O_3$) in the EPD compared to other similar global occurrences, this deposit is significantly enriched in critical and highly demanded REEs like Nd, Pr, and Tb. Therefore, with upgraded extraction techniques, the EPD could become a potential diverse source of REEs that may contribute to maintaining a sustainable REE supply chain in the future.

Keywords: Critical rare earth elements, Eppawala phosphate deposit, Pulmoddai deposit, Rare earth resources

TABLE OF CONTENT

LIST OF FIGURES

LIST OF TABLES

LIST OF ABBREVIATIONS

Abbreviation	Description
Ce/Ce*	Ce Anomaly
CREE	Critical Rare Earth Element
EPD	Eppawala Phosphate Deposit
Eu/Eu*	Eu Anomaly
HREE	Heavy Rare Earth Element
HREO	Heavy Rare Earth Oxide
ICP-MS	Inductively Coupled Plasma Mass Spectrometer
LREE	Light Rare Earth Element
LREO	Light Rare Earth Oxide
RE	Rare Earth
REE	Rare Earth Element
REO	Rare Earth Oxide
TREE	Total Rare Earth Element
TREO	Total Rare Earth Oxide

CHAPTER 1: INTRODUCTION

1.1. Background

As a raw commodity, rare earth elements (REEs) have attracted increased attention in recent years due to their high usage in numerous applications across industries, such as electrical and electronics, renewable energy, automotive, medical, and defense (Dushyantha et al., 2020). Owing to the expected supply risk and the economic importance, they have continuously been recognized as one of the most critical and strategic elements in the world. Therefore, scientists, geologists, exploration geochemists, technology developers, and even policymakers are intrigued by REEs, especially because of their significant role in green energy technologies that drive toward climate change mitigation with zero emissions (Balaram, 2019).

REEs are a set of 17 elements composed of 15 lanthanides, Sc, and Y. All these REEs, except for Sc, are chemically and physically similar but behave differently in natural systems. REEs are primarily grouped into two categories: light REEs (LREEs: La, Ce, Pr, Nd, Sm, and Eu) and heavy REEs (HREEs: Gd, Tb, Dy, Ho, Er, Tm, Yb, Lu, and Y) (McLemore, 2015). Typically, LREEs are more abundant in the earth's crust than higher-priced HREEs (Van Gosen et al., 2014). Despite the term 'rare', most REEs, particularly LREEs have an upper crustal abundance comparable to those of base metals like Cu, Pb, Ni, and Zn. Even the least abundant REE, Lu has an upper crustal abundance 200 times higher than gold (Haxel et al., 2002). However, they are less enriched in major rock-forming minerals and only accessory minerals or RE minerals that are difficult and problematic to process contain high concentrations. Thus, REEs are rarely found as concentrated ore deposits, and even from such deposits, the extraction of REE metal from the ore could be economically unfeasible (Hampel and Kolodney, 1961; Simandl, 2014).

The unique chemical and physical characteristics of REEs offer numerous technological advantages, including low energy consumption, high efficiency, miniaturization, speed, durability, high luster, and thermal stability (Balaram, 2019). Therefore, different chemical forms of REEs, such as metals, alloys, oxides, and chlorides have become crucial in various industrial, medical, and defense sectors and

the advancement of high technologies and green energy applications. Among them, the application of Pr, Nd, Gd, Dy, and Tb for the production of permanent magnets, which are especially used in wind turbines and military weapon systems, is considered the prominent application of REEs (Mancheri et al., 2019). In addition, REEs are highly used in catalytic compounds as stabilizers (e.g., La and Ce), high-efficiency lighting phosphors in compact fluorescent bulbs (CFLs) and light-emitting diode bulbs (LEDs) (e.g., Eu), photovoltaic cells in solar panels (e.g., Pr, Gd, Eu, and Er), and also as fertilizers for crops and feeding additives for farm animals in low concentrations (Dushyantha et al., 2020).

Over the last three decades, the global demand for REEs has grown significantly and expects to increase further owing to their immense consumption in the aforementioned applications. Experts in the field predict a surge in this demand over the coming decades (an annual growth rate of 7-8%) (Kingsnorth, 2010), primarily because of the emphasis given at the United Nations Climate Change Conference in Paris in 2015 on the criticality of REEs in the global shift to the carbon-neutral technologies (Dushyantha et al., 2020; Schmid, 2019). The production of REEs, however, is concentrated in only a few countries, particularly in China, where there is a monopoly in REE mining, processing, and purification (Ilankoon et al., 2022).

Until the mid-1990s, the USA was the world's leading producer of REEs and then China superseded their place by exploiting inexpensive and abundant labor, low-energy costs, and lack of environmental regulations (Folger, 2011). Despite the importance of REEs in high-tech applications, there was very little interest in the exploration, mining, and extraction of these metals, before the rare earth crisis that happened during 2010-2012. In 2010, China restricted REE exports to Japan because of a dispute over maritime boundaries, and consequently, REE prices experienced a historical spike (Cox and Kynicky, 2018; Simandl, 2014). Although this supply restriction was removed later, China reduced the export quotas to reduce environmental degradation and to build up a strategic stockpile of REEs. This highlights the vulnerability of the global REE supply chain to disruptions and the

necessity of exploring new REE deposits and opening new and abandoned mines to increase the global production of REEs (Batapola et al., 2020; Dushyantha et al., 2020).

The enrichment and distribution of REEs are controlled by primary geological processes (i.e., magmatic and hydrothermal alteration) and secondary weathering processes. Thus, there are two groups of REE deposits, namely primary deposits formed by igneous and hydrothermal processes and (2) secondary deposits enriched by sedimentary and weathering processes (Jaireth et al., 2014). Key examples of primary deposit types include carbonatites, alkaline igneous rocks, pegmatites, and iron-oxide copper-gold deposits, whereas placers, laterites, bauxites, and ion adsorption clays belong to the secondary deposit type (Goodenough et al., 2018). In addition to this traditional classification scheme of REE deposits, different approaches have been proposed by various researchers, based on the geological associations, evolutionary framework, the relative abundance of REEs in the deposit, and mineral-system associations (Jaireth et al., 2014).

Currently, only a few types of mineral deposits are utilized to produce REEs, such as carbonatites, alkaline igneous rocks, placers, laterites, and ion adsorption clays being carbonatites and ion adsorption clays the major sources of the world's REE supply (Orris and Grauch, 2002). REEs in these natural sources do not exist as individual metals, instead, they occur in different mineral assemblages. Over 250 RE minerals have been identified in these deposits, but only bastnaesite, monazite, xenotime, loparite, and ion-adsorption clay minerals are commercially processable (Dostal, 2017). Four major REE deposits in the world contribute to a large proportion of the global REE production: Bayan Obo in China, Mountain Pass in the USA (after suspending production in 2002, it was started again in 2018), Mount Weld in Australia, and ion adsorption clay deposits in China. Bayan Obo deposit is the world's largest REE deposit, whereas Mount Weld is considered one of the richest REE deposits in the world. While the majority of the world's LREE production comes from the Bayan Obo deposit, the global HREE production largely depends on the ion adsorption clay deposits in China (Balaram, 2019; Dushyantha et al., 2020). This also implies China's

dominancy in the REE industry. In addition, the overconsumption of REEs coupled with the rapid depletion of natural, finite deposits makes us pace towards the recycling of REE-containing waste, such as e-waste, phosphogypsum, and mine-tailings.

However, natural deposits are still considered promising sources of the global REE supply chain as secondary sources possess certain challenges, such as extraction efficiency and selectivity, and process economic considerations (Peelman et al., 2016). Therefore, a global exploration boom for REEs happened after the rare earth crisis in 2011, discovering new REE resources outside China, which accounted for 98 million tonnes of total rare earth oxides (TREO) as of 2015 (Paulick and Machacek, 2017). It highlights the presence of a substantial amount of viable REE resources worldwide and the timely need for delineating such REE resources to stabilize the global REE supply chain.

1.2. Research problem

Currently, the global REE supply chain is highly uncertain due to accelerating REE demand and skewed dominance of REE production by one country. Moreover, the political conflicts between China and other countries like the US, Japan, and the EU also cause occasional supply disruptions. Therefore, the exploration of new and alternative REE deposits worldwide has given increasing interest as a mitigation strategy for the elevated supply risk of REEs. In this global attempt to discover more REE deposits to alleviate the impending supply risk in the REE industry, Sri Lanka also has the potential for REE-enriched geological occurrences, given its favorable geological setting. However, despite a few geochemical research, there have been no significant attempts to either explore these occurrences in detail or develop novel extraction techniques to recover REEs from them. Therefore, a detailed exploration study is needed to determine the potential of REEs in different geological formations of Sri Lanka and to assess their economic significance in terms of becoming viable future sources in Sri Lanka.

1.3. Objectives

Main objective

- To assess the REE potential in different geological formations of Sri Lanka based on their origins and occurrences.

Specific objectives

- To analyze REE concentrations in selected geological formations of Sri Lanka.
- To characterize the enrichment and distribution of REEs in different types of geological formations in Sri Lanka.
- To identify the most prospective REE source/s in Sri Lanka and to assess their economic significance and recovery potential in terms of REEs.

1.4. Scope and significance of the research

In this study, three categories of geological formations in Sri Lanka are explored, namely residual laterites, placers, and magmatic deposits, which in turn consist of six types of resources: residual laterites – carbonatite-associated and serpentinite-associated; placers – beach placers and alluvial placers; and magmatic – granites and pegmatites. Precise geochemical analyses are conducted for the preceding resources to determine their REE concentration levels, followed by the characterization of REE enrichment and distribution in the studied geological resources. Overall, this research provides a detailed exploration of REE potential in different geological environments with an emphasis on the economic significance and recovery potential of REEs in the most prospective source/s in Sri Lanka. Moreover, the present study helps to bring attention to the development of sustainable mining and extraction processes to recover REEs from local resources.

CHAPTER 2: LITERATURE REVIEW

2.1. Rare earth elements

REEs are a group of 17 metallic elements comprising 15 lanthanides, scandium (Sc), and yttrium (Y) (Table 2.1). Due to similar chemical properties of REEs, they tend to occur in the same ore deposits in the form of minerals, except for Sc (Balaram, 2019). Generally, these elements are found as trivalent ions, however, cerium (Ce), terbium (Tb), and praseodymium (Pr) can also occur in tetravalent oxidation states while europium (Eu), samarium (Sm), and ytterbium (Yb) can be found as divalent ions (Wang and Liang, 2016).

Table 2.1: Description of rare earth elements. * Promethium does not occur naturally.

Rare earth element	**Symbol**	**Oxide**		**Conversion factor (% element × conversion factor = % oxide)**	**Atomic number**	**Abundance in the upper crust (ppm)**
Scandium	Sc	Sc_2O_3		1.5338	21	14
Yttrium	Y	Y_2O_3		1.269	39	21
Lanthanum	La	La_2O_3		1.173	57	31
Cerium	Ce	Ce_2O_3		1.171	58	63
Praseodymium	Pr	Pr_2O_3		1.17	59	7.1
Neodymium	Nd	Nd_2O_3		1.166	60	27
Promethium	Pm	*		*	61	*
Samarium	Sm	Sm_2O_3		1.16	62	4.7
Europium	Eu	Eu_2O_3		1.158	63	1.0
Gadolinium	Gd	Gd_2O_3		1.153	64	4.0
Terbium	Tb	Tb_2O_3		1.151	65	0.7
Dysprosium	Dy	Dy_2O_3		1.148	66	3.9
Holmium	Ho	Ho_2O_3		1.146	67	0.83
Erbium	Er	Er_2O_3		1.143	68	2.3
Thulium	Tm	Tm_2O_3		1.142	69	0.30
Ytterbium	Yb	Yb_2O_3		1.139	70	2.2
Lutetium	Lu	Lu_2O_3		1.137	71	0.31

Source: (Dushyantha et al., 2020; McLemore, 2015; Taylor and McLennan, 1985)

REEs are known to have diverse chemical reactivities due to lanthanide contraction: the decreasing of atom radii with the increase of atomic numbers (Aide and Smith-Aide, 2003). REEs are typically categorized into two subgroups, namely LREEs from La to Eu and HREEs from Gd to Lu and Y (McLemore, 2015), where LREEs are often more enriched in deposits than HREEs. However, Sc is not grouped under any of the preceding categories since its occurrence differs from other REEs (Van Gosen et al., 2014). Therefore, here in this study, only 15 lanthanides and Y were considered REEs.

Despite the name 'rare', these elements have a total crustal abundance of 220 ppm (Table 2.1), which is even higher than that of carbon (200 ppm). Moreover, some REEs are more abundantly found in the earth's crust than several frequently used industrial metals like copper (Cu), cobalt (Co), lead (Pb), and tin (Sn) (Gupta and Krishnamurthy, 2005). The term 'rare' is used to imply that REEs hardly occur as concentrated ore deposits, instead, they are evenly distributed in the earth's crust (Haxel et al., 2002). Furthermore, the commercial availability of a metal does not depend only on its crustal abundance, but on factors, such as its degree of enrichment in the deposit, the relative feasibility of separating the ore, and the feasibility of extracting the metal from the ore (Batapola et al., 2020; Hampel and Kolodney, 1961).

2.2. REE applications

The unique physical, chemical, magnetic, and luminescent properties of REEs result in numerous technological advantages, such as low energy consumption, high efficiency, miniaturization, speed, durability, and thermal stability (Zepf, 2013). Therefore, REEs are considered critical and strategic raw materials in a myriad of high-tech applications across various industrial sectors, such as electrical and electronics, automotive, renewable energy, medical, and military (Balaram, 2019; Dushyantha et al., 2020). Table 2.2 illustrates the major applications of REEs in various industrial sectors.

The technological shift towards carbon neutralization has promoted the usage of REEs in renewable energy applications, making permanent magnets the prominent

Table 2.2: Applications of REEs in different industrial sectors.

Area	Applications
Electronics	Television screens, computers, cell phones, silicon chips, monitor displays, long-life rechargeable batteries, camera lenses, light-emitting diodes (LEDs), compact fluorescent lamps (CFLs), baggage scanners, and marine propulsion systems.
Manufacturing	High-strength magnets, metal alloys, stress gauges, ceramic pigments, colorants in glassware, chemical oxidizing agents, polishing powders, plastics creation, additives for strengthening other metals, and automotive catalytic converters.
Medical Science	Portable X-ray machines, X-ray tubes, magnetic resonance imagery (MRI) contrast agents, nuclear medicine imaging, cancer treatment applications, and genetic screening tests, medical and dental lasers.
Technology	Lasers, optical glass, fiber optics, masers, radar detection devices, nuclear fuel rods, mercury-vapor lamps, highly reflective glass, computer memory, nuclear batteries, and high-temperature superconductors.
Renewable Energy	Hybrid automobiles, wind turbines, next-generation rechargeable batteries, and biofuel catalysts.
Others	The europium is being used as a way to identify legitimate bills for the Euro bill supply and to dissuade counterfeiting. An estimated 1 kg of REE can be found inside a typical hybrid automobile. Holmium has the highest magnetic strength of any element and is used to create extremely powerful magnets. This application can reduce the weight of many motors.

Source: (Balaram, 2019; Dushyantha et al., 2020)

application for REEs, especially for Nd, Pr, Dy, and Tb. The second-highest usage of REEs is catalytic compounds, in which high amounts of La and Ce are applied as stabilizers (Mancheri et al., 2019). In addition, Eu is increasingly used in color-producing phosphors of video screens along with Tb and Y, resulting in Eu as one of the highly demanded REEs in the last half of the 20^{th} century (Mertzman, 2019). The uses of REEs in some applications are shown in Table 2.3.

Table 2.3: REE requirements by application (Percentages are from the total REE content required in a given application).

REE application	La%	Ce%	Pr%	Nd%	Sm%	Eu%	Gd%	Tb%	Dy%	Y%	Others%
Magnets	-	-	23.4	69.4	-	-	2.0	0.2	5.0	-	-
Battery alloys	50.0	33.4	3.3	10.0	3.3	-	-	-	-	-	-
Metal alloys	26.0	52.0	5.5	16.5	-	-	-	-	-	-	-
Auto catalysts	5.0	90.0	2.0	3.0	-	-	-	-	-	-	-
Petroleum refining	90.0	10.0	-	-	-	-	-	-	-	-	-
Polishing compounds	31.5	65.0	3.5	-	-	-	-	-	-	-	-
Glass additives	24.0	66.0	1.0	3.0	-	-	-	-	-	2.0	4.0
Phosphors	8.5	11.0	-	-	-	4.9	1.8	4.6	-	69.2	-
Ceramics	17.0	12.0	6.0	12.0	-	-	-	-	-	53.0	-
Other	19.0	39.0	4.0	15.0	2.0	-	1.0	-	-	19.0	-

Source: (Jordens et al., 2013; Long et al., 2012)

2.3. Global REE demand and supply

The extensive REE consumption in the development of modern high technologies has caused a rapid increase in their demand over the past few decades. According to Kingsnorth (2010), it is predicted that the REE demand will increase by 7-8% annually. According to Figure 2.1, the global demand for rare earth oxides (REOs) has increased from about 156,000 to 208,000 metric tonnes throughout 2017–2019. Moreover, it is forecasted that REO demand will increase to about 304,000 metric tonnes by the year 2025. On top of that, the global REE demand is expected to skyrocket due to the immense usage of REEs in renewable energy applications. For example, it is predicted that the demand for Nd and Dy will grow by 700% and 2600%, respectively within the next few decades (Alonso et al., 2012). Consequently, REE prices will also rise dramatically along with the demand. The neodymium oxide price, for example, was U.S. $49,144 per tonne in 2020 and it is forecasted that it will increase up to U.S. $77,500 per tonne by 2025 (Pell et al., 2019).

The global productions of REOs were at 220 and 240 thousand tonnes in 2019 and 2020, respectively, in which China owned about 60% in both years. The United

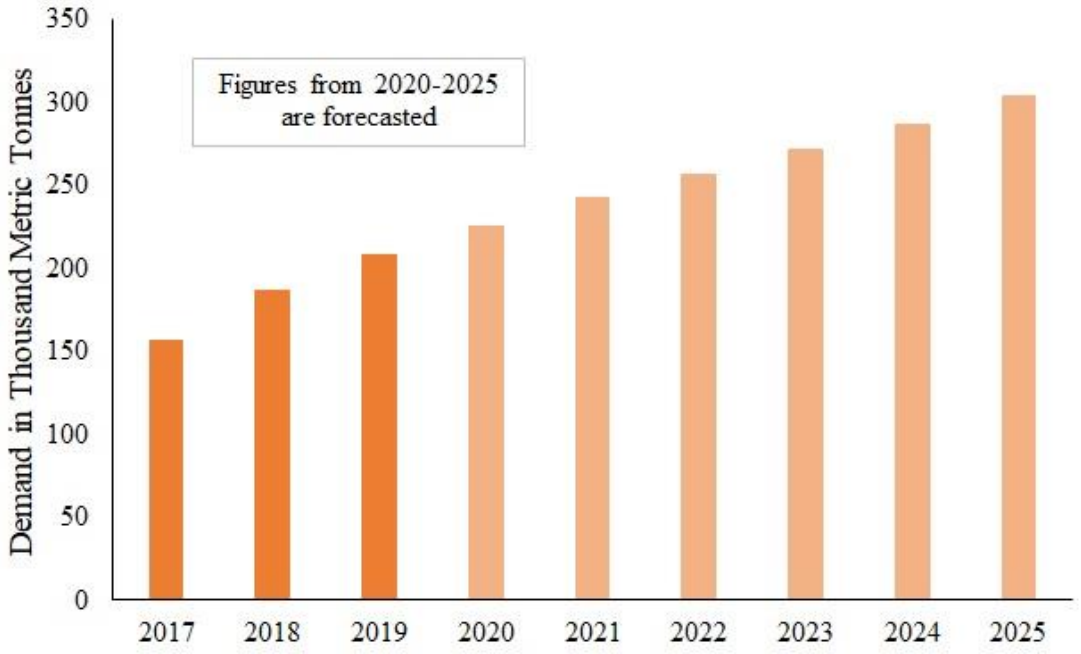

Figure 2.1: The global REO demand estimates (2017–2019) and forecasts (2020–2025).

Source: (Statista, 2020)

States (US) is the second largest supplier of REEs, producing roughly 13% and 16% of the global total in 2019 and 2020, respectively. Other major global suppliers of REEs are Burma (12.5% in 2020), Australia (7% in 2020), and Madagascar (3% in 2020) (Table 2.4). Since the mining and processing of REEs are expensive and environmentally hazardous, China was able to dominate the global REE market by exploiting its low labor cost and lax environmental regulations (Dushyantha et al., 2020). In 2010, China reduced its export quotas by 37%, resulting in a global spike in REE prices (from $9,461 per tonne in 2009 to about $66,957 in 2011) and disruptions to the global REE supply chain. This encouraged key REE stakeholders in the world like the USA, European Union (EU), and Japan to take strategic solutions to prevent such supply chain disruptions, such as re-opening abandoned mines, opening new mines, and exploring new REE resources outside China (Center for Strategic and International Studies, 2020).

Table 2.4: The distribution of global REO production based on countries.

Country	REO production in tonnes		Share (%)	
	2020	2021	2020	2021
United States	39,000	43,000	16.0	15.0
Australia	21,000	22,000	8.0	8.0
Brazil	600	500	0.25	0.2
Burma	31,000	26,000	13.0	9.0
Burundi	300	100	0.12	0.04
China	140,000	168,000	58.0	60.0
India	2,900	2,900	1.2	1.0
Madagascar	2,800	3,200	1.2	1.1
Russia	2,700	2,700	1.1	1.0
Thailand	3,600	8,000	1.5	3.0
Vietnam	700	400	0.3	0.14
Other countries	100	300	0.04	0.11
World total production (rounded)	240,000	280,000	-	-

Source: (USGS, 2023)

As a result, China's share of global REE production has recently decreased from 97.7% in 2010 to 58% in 2020 (USGS, 2021). However, China's dominancy as the global supplier of REOs, RE metals and alloys, and permanent magnets has not similarly reduced. Nevertheless, it is predicted that China's monopoly in the downstream products may also be diluted in the coming years since several REE processing facilities are being constructed outside China (Center for Strategic and International Studies, 2020). Although China's monopoly in the REE market is being reduced as a consequence of growing global competition over REEs, the supply risk for REEs has not yet decreased. The ever-increasing global demand coupled with geopolitical concerns and environmental impacts may pose a significant supply risk for REEs, thus exploring new REE resources, worldwide is important for maintaining a stable and reliable REE supply chain (Dushyantha et al., 2020).

2.4. Rare earth mineralogy

An understanding of deposit types, geology, and mineralogy is important for prospecting new REE deposits as well as determining the feasibility of REE mining,

processing, and refining (Batapola et al., 2020; Weng et al., 2015). Therefore, rare earth (RE) mineralogy plays a crucial role in identifying the REE potential in a particular deposit (Goodenough et al., 2016). Different types of RE minerals, including carbonates, phosphates, silicates, oxides, and halides have been identified to date (over 250 in number) (Gupta and Krishnamurthy, 2005). Table 2.5 illustrates a list of important REE-bearing minerals and their formulae. Generally, carbonate and phosphate RE minerals act as carriers for LREEs, whereas oxide and a part of phosphate minerals are enriched in HREEs (Kanazawa and Kamitani, 2006). However, only bastnaesite, monazite, xenotime, loparite, and ion adsorption clay minerals are processed to produce REEs on a commercial scale (Zhou, 2017).

Table 2.5: Primary REE-bearing minerals and their formula.

REE-bearing minerals	Formula
Allanite	$(Y, La, Ca)_2(Al,Fe^{3+})_3(SiO_4)_3(OH)$
Apatite	$(Ca, La)_5(PO_4)_3(F,Cl,OH)$
Bastnaesite	$(La, Y)(CO_3)F$
Eudialyte	$Na_4(Ca,La)_2(Fe^{2+},Mn^{2+},Y)ZrSi_8O_{22}(OH,Cl)_2$
Fergusonite	$(La, Y)NbO_4$
Gittinsite	$CaZrSi_2O_7$
Limorite	$Y_2(SiO_4)(CO_3)$
Kainosite	$Ca_2(Y,La)_2Si_4O_{12}(CO_3).H_2O$
Loparite	$(La, Na, Ca)(Ti, Nb)O_3$
Monazite	$(La, Th)PO_4$
Mosandrite	$(Na, Ca)_3Ca_3La\ (Ti,Nb,Zr)(Si_2O_7)_2(O,OH,F)_4$
Parisite	$Ca(La)_2(CO_3)_3F_2$
Pyrochlore	$(Ca, Na, La)_2Nb_2O_6(OH,F)$
Rinkite (Rinkolite)	$(Ca, La)_4Na(Na,Ca)_2Ti(Si_2O_7)_2(O,F)_2$
Steenstrupine	$Na_{14}La_6Mn_2Fe_2(Zr,Th)(Si_6O_{18})_2(PO_4)_7 \cdot 3H_2O$
Synchysite	$Ca(La)(CO_3)_2F$
Xenotime	YPO_4
Zircon	$(Zr, La)SiO_4$

Source: (Dostal, 2017)

2.5. REE deposits and their global distribution

2.5.1. Classification of REE deposits

The enrichment and distribution of REEs in mineral deposits are governed by either rock-forming primary processes (magmatic and hydrothermal) or secondary processes (separation into mineral species and precipitation; enrichment through weathering and subsequent transportation) (Jaireth et al., 2014). Although the traditional classification of REE deposits is primarily based on the aforementioned deposit formation processes, the classification of some of the deposits is difficult due to uncertainty in geological associations and/or overlapping of many geological processes (Singh, 2020). Hence, different approaches for the classification of REE deposits have been proposed by various researchers, based on the geological associations, evolutionary framework, the relative abundance of REEs in the deposit, and mineral-system associations (Jaireth et al., 2014).

According to the traditional classification schemes, REE deposits are categorized into (1) primary deposits associated with magmatic and hydrothermal processes, and (2) secondary deposits enriched by weathering and erosion processes (Jaireth et al., 2014; Walters and Lusty, 2010). In contrast, Cassidy et al. (1997) proposed a classification scheme based on the relative abundance of REEs in the deposit, in which REE deposits are categorized into deposits with REEs occur as a (i) primary or co-product and (ii) by-product of the deposit. Moreover, some researchers have suggested a mineral-system classification for the REE deposits that follows a hierarchical structure based on the mineralizing processes of the deposits (Hoatson et al., 2011; Jaireth et al., 2014). This mineral-system approach has been useful for developing process-based conceptual models of ore systems (Skirrow et al., 2009), creating flexible probabilistic structures for conducting risk analysis in mineral exploration (Kreuzer et al., 2010), mapping essential ingredients of fertile mineral systems, and conducting prospective analysis (Barnes et al., 1999; Jaques et al., 2002). Hence, the mineral-system classification scheme (Table 2.6) is used in the present study to discuss the prospective REE resources in the Sri Lankan context.

Table 2.6: Mineral-system classification of REE deposits and its key examples. Deposit types used for the present study are underlined.

Mineral-system association	**Deposit group and type**				**Key examples**
Regolith	Residual lateritic	• <u>Carbonatite-associated</u>			Tantalus, Madagascar; Mount Weld, Australia; Ngulla, Tanzania; Araxa, Brazil; Mabounie, Gabon
		• <u>Ultramafic/mafic rock-associated</u>			Lucknow, Australia
	Residual clay				Ion adsorption clay deposits in Jiangxi, Hunan, Fujian, Guangdong, and Guangxi provinces in China; Dong Pao, Vietnam
	Bauxite				karst-type bauxite deposits from Greece, Bosnia, Montenegro, Hungary, Bulgaria, Croatia, Romania, Italy, Turkey, Iran, and China
Basinal	Sedimentary	• Placer	▪ Quartz-pebble conglomerate		Elliot Lake, Canada
			▪ <u>Alluvial</u>		Charley Creek, Australia; India; Sri Lanka; Florida, USA
			▪ <u>Heavy-mineral sands</u>	✓ Beach	WIM150, Australia; monazite stockpile in India (IREL); Eneabba, Australia; North
				✓ High dune	

				✓ Offshore-shallow-marine tidal	Stradbroke Island, Australia; Calypso, Australia
				✓ Channel	
		• Phosphorite			Korella, Australia; Idaho, USA
		• Sea-floor manganese nodule			
		• Lignite			Mulga Rock, Australia
	Diagenetic-hydrothermal	• Unconformity-related			Killi Killi Hills, Australia; Palaeozoic nodular monazites in UK, Belgium, France, Portugal
Metamorphic	Migmatised gneiss				Mary Kathleen, Australia [a]
	Calc-silicate				
Magmatic	Orthomagmatic	• Alkaline igneous rocks			Khibina and Lovozero, Russia; Norra Kärr, Sweden; Bokan, USA; Thor Lake, Canada; Kipawa Lake, Canada; Kola Peninsula, Russia; Round Top, USA; Foxtrot, Canada; Brockman, Australia
		• Carbonatite			Bayan Obo, China; Karonge, Burundi; Mountain Pass, USA; Nolans Bore, Australia; Steenkampskraal, South Africa; Yangibana, Australia

		• Granites and granitic pegmatite	Khibina Massif, Russia; Motzfeldt, Greenland; Ytterby, Sweden; Cooglegong-Pinga Creek, Australia
	Magmatic-hydrothermal	• Albitite	
		• Porphyry	
		• Skarn	Mary Kathleen, Australia[a]; John Galt, Australia; Saima, China; Mount Gee, Australia
		• Apatite and /or fluorite vein	Nolans Bore, Australia
		• Iron-oxide breccia complex	Olympic Dam, Australia; Milo, Australia

[a] The Mary Kathleen deposit in Australia was originally a skarn deposit that was later modified into a calc-silicate type deposit during the regional metamorphism.

Source: (Cocker, 2014; Goodenough et al., 2016; Jaireth et al., 2014; Sinclair et al., 1992; Weng et al., 2015)

The top level of the mineral-system classification of REE deposits is divided into four major mineral-system associations, namely Regolith, Basinal, Metamorphic, and Magmatic. These major categories are further divided into deposit groups or types based on their REE enrichment and distribution processes. Regolith deposit types are formed either by the enrichment of REEs in the residual material and/or by local remobilization of REEs. Various basinal deposit types can occur from mechanical (e.g., placers) and chemical (e.g., phosphorites) processes and from diagenetic fluids generated in sedimentary basins. Metamorphic deposits are mainly associated with regional and/or contact metamorphism, where metamorphic-derived fluids can also influence the enrichment of REEs. Magmatic deposits are based on the emplacement of REE-enriched melt that can be derived either directly from the crystallization of the melt and/or fluids predominantly derived from the melt (Jaireth et al., 2014).

Since these natural REE resources are finite and will be depleted in the future with the extensive consumption of REEs, substantial research and developments are being carried out on recovering REEs from wastes, such as electrical and electronic waste (or e-waste), mine tailings, red mud, and phosphogypsum (Binnemans et al., 2013). This could also help to overcome the challenges of REE mining and processing, such as handling and storage of radioactive materials, energy requirements, and resource accessibility (Schüler et al., 2011).

2.5.2. Primary REE deposits

2.5.2.1. Carbonatites

Carbonatites are carbonate-rich (carbonate minerals > 50% and SiO_2 < 20%) igneous rocks derived from the mantle. They are found as flows, plugs, dykes, cone sheets, and sills, usually with associations of concurrent ultramafic and alkaline silicate rocks (Chakhmouradian and Zaitsev, 2012). According to the International Union of Geological Sciences (IUGS), carbonatites are subdivided into three major types; magnesiocarbonatites, ferrocarbonatites, and calciocarbonatites, based on their compositions of the major oxides (MgO, CaO, FeO, MnO, Fe_2O_3, etc.) (Simandl and Paradis, 2018). Carbonatite-related REE deposits are currently the predominant source of REEs, which account for over 60% of the global REE resources (Zhou, 2017).

Amongst more than 500 known occurrences of carbonatites disseminated worldwide, only a part (about 58 occurrences) has been identified as REE-bearing carbonatites, which are currently in production, partially mined, well-explored, or under-explored stages (Woolley and Kjarsgaard, 2004). The best-known examples are Bayan Obo and Maoniuping in China, Mountain Pass in the USA, Manavalakurichi in India, Araxá in Brazil, Kangankunde Hill in Malawi, Gallinas Mountains in New Mexico, and Steenkampskraal in South Africa. Out of them, Bayan Obo in China is presently the largest REE deposit in the world (Dushyantha et al., 2020; Long et al., 2012).

Although almost all the carbonatites show higher REE concentrations compared to the crustal abundances, mostly the latest and most highly evolved parts of a carbonatite intrusion contain economic enrichments of REEs (Wall and Mariano, 1995). Generally, in carbonatites, REE enrichments are in the range between 250–8000 ppm, which is comparatively higher than that of other igneous rocks. Even though REE-bearing carbonatites are typically high-grade and large occurrences, they are highly enriched in LREEs compared to HREEs (Smith et al., 2016). While carbonatites mostly contain carbonate RE minerals, such as bastnaesite, parisite, and synchysite, they also consist of phosphate RE minerals like apatite and monazite. However, only bastnaesite is considered the primary ore mineral in many carbonatite-related REE deposits, particularly in Bayan Obo, China, and REEs are produced from this mineral commercially (Goodenough et al., 2018; Gupta and Krishnamurthy, 2005; Smith et al., 2016).

2.5.2.2. Alkaline igneous rocks

Alkaline igneous rocks are the second major group of REE deposits accounting for about 16% of the global REE resources. Even if they are considered as one group, the origin of their RE mineralization varies largely from magmatic to hydrothermal alteration. REEs are highly enriched in alkaline to peralkaline intrusions (Dostal, 2016). These REE-enriched peralkaline intrusions are again classified based on their silica saturation as nepheline syenites (undersaturated) and peralkaline granites (oversaturated) (Marks et al., 2011).

The only active REE mine associated with peralkaline igneous rocks is Lovozero agpaitic nepheline syenite complex in Russia, where the major RE mineral is loparite. In addition, several other agpaitic nepheline syenite complexes are in either development or exploration stages (e.g., Ilı´maussaq and Motzfeldt in Greenland, Norra Ka¨rr in Sweden, and Red Wine and Kipawa in Canada). Eudialyte is the main ore mineral in most of these complexes (Dostal, 2016; Goodenough et al., 2018, 2016). Despite the large occurrences of agpaitic nepheline syenite complexes, their TREO grades are low (generally ≤1 wt%). However, since they have a flatter REE distribution pattern with a negative Eu anomaly, unlike in the carbonatites, they can produce a considerable amount of the most critical HREEs (Dy and Tb) with lesser amounts of La and Ce. Moreover, agpaitic nepheline syenite deposits contain lesser concentrations of U and Th making them more suitable for sustainable mine development (Goodenough et al., 2018).

The peralkaline granites are also another type of REE-enriched peralkaline intrusions, which have been altered by late-stage magmatic fluid and hydrothermal activities (e.g., Strange Lake in Canada, Khaldzan-Buregtey in Mongolia, and Bokan Mountain) (Dostal, 2016; Goodenough et al., 2016). Moreover, similar REE deposits can occur in alkaline syenitic complexes (e.g., Thor Lake in Canada and Ditra˜u in Romania) (Goodenough et al., 2016; Timofeev and Williams-Jones, 2015) and felsic volcanic suites (e.g., Brockman and Dubbo Zirconia deposits in Australia and Round Top deposit in Texas) (Dostal, 2016; Spandler and Morris, 2016), which have been formed by late-stage hydrothermal alteration. Generally, the peralkaline granite deposits show a relatively flatter chondrite normalized REE distribution pattern with a strong negative Eu anomaly, which is similar to agpaitic nepheline syenite deposits (Goodenough et al., 2018).

The interplay of alkaline igneous rocks between magmatic and hydrothermal results in a large variation of the RE mineralogy from silicate and phosphate RE minerals, such as allanite, zircon, monazite, and xenotime to RE carbonates and oxides (Goodenough et al., 2018). Due to this complex RE mineralogy, the grade and tonnage of REOs of these deposits could greatly vary resulting in significant challenges in the separation of ore minerals. However, the recovery of REEs could be feasible, if they

are concentrated in easily-leachable minerals that are either late-stage or secondary (Jowitt et al., 2017).

2.5.2.3. Granites and granitic pegmatites

Another type of igneous-related REE resource is granites and granitic pegmatites, although only a few mined or well-explored deposits have been reported, worldwide (Weng et al., 2015). Granites are large intrusive rocks that occur in the magmatic arcs along the subduction zones. Granitic magma derived from the melting of the lower crustal materials forms these granitic occurrences. The chemical compositions of these rocks, especially trace element concentrations, are dependent upon the compositions of the source materials (Hoshino et al., 2016; Winter, 2013). In the granites, REEs are mostly concentrated in the accessory minerals, such as allanite, monazite, and xenotime while Ca-bearing minerals like garnet, epidote, apatite, titanite, and fluorite also contain REEs as isomorphous admixture (Hoshino et al., 2016).

On the other hand, granitic pegmatites are an extreme version of granites containing exceptionally large crystals and several minerals that are hardly found in other types of rocks. The composition of these pegmatites, however, is similar to granites with high contents of quartz, feldspars, and mica (King, 2015). They are mostly found in cratons and metamorphic belts, surrounding areas of large granitic bodies, contact zones of granite, and skarns associated with granite as dykes, lenses, or veins (Jackson and Christiansen, 1984). Based on the metamorphic environment of the host rocks, mineralogy, elemental composition, and texture, granitic pegmatites are divided into four classes, namely abyssal, muscovite, rare-element, and miarolitic. However, the rare-element class is the most REE-enriched class out of these pegmatite classes (Černý et al., 2012). Depending upon the bulk composition, typical assemblages of trace elements, and types of associated granites, rare-element pegmatites are again classified into three families, namely, LCT (LCT is for Lithium, Cesium, and Tantalum enrichment), NYF (NYF is Niobium, Yttrium, and Fluorine enrichment), and mixed (with both LCT and NYF characteristics). Generally, NYF pegmatites have higher contents of REEs than LCT pegmatites (Černý and Ercit, 2005). In the NYF pegmatites, high amounts of RE minerals, such as zircon,

fergusonite-(Y), columbite-(Fe), allanite-(Ce), xenotime-(Y), monazite-(Ce, Nd), thorite, and gummite are present while other families contain mostly silicate phases (Mahmoud, 2019; Novák et al., 2012).

To date, only the Platt mine pegmatite deposit in Wyoming, USA had been industrially mined for REEs and there was a small pegmatite REE deposit in Western Australia (Cooglegong Pinga Creek) (Jaireth et al., 2014). In addition, high REE enrichments are evident in the Strange Lake Complex in Quebec-Labrador, Canada, a peralkaline A-type granitic pluton hosted by hydrothermally altered pegmatites and adjacent granites (Siegel et al., 2018). Other granites- or granitic pegmatite-related REE resources are Khibina Massif in Russia, Motzfeldt in Greenland, and Ytterby in Sweden (Weng et al., 2015).

2.5.2.4. Iron oxide copper-gold deposits (IOCG)

Iron oxide copper–gold deposits (IOCG) are an important source of U, Cu, and Au, but also contain economic contents of REEs. REE enrichment and mobilization of these deposits have been highly debated over the years due to the lack of research and studies on them. While Groves et al. (2010) has suggested that RE mineralization in IOCG deposits is derived from a metal-rich, metasomatized subcontinental lithospheric mantle, several other studies have argued that REEs are originated from either crustal source, such as felsic magmas, felsic intrusions/volcanic rocks, and sedimentary rocks or from magmatic/non-magmatic REE-carrying fields (e.g., Chen and Zhou, 2015; Skirrow et al., 2007). Generally, REE mobilization in the IOCG deposits occurs in the later Cu-mineralizing stage. Over many years, it was assumed that REE-fluoride complexes facilitate the hydrothermal REE transport in IOCG deposits, due to abundant fluorite and REE-bearing fluor-carbonate occurrences (Oreskes and Einaudi, 1990). The recent modeling of experimental data, however, suggests that fluoride ions promote depositions of RE minerals, such as monazite, apatite, and allanite by acting as binding ligands, rather than being carriers in REE mobilization (Li and Zhou, 2018; Migdisov and Williams-Jones, 2014; Williams-Jones et al., 2012).

RE mineralization of the IOCG deposits is associated with various mineral phases, such as iron oxide, sulfide, silicate, carbonate, and phosphate. Generally, major ore minerals in these deposits are iron oxide minerals, whereas other minor or accessory minerals are found in concentrations between 1–5% (Williams et al., 2005). RE mineralogy in IOCG complexes differs based on the host rock. For example, in the magnetite-dominated ores, REEs are mostly enriched in rock-forming minerals, such as apatite, titanite, and epidote-allanite, whereas in the hematite-rich assemblages, they are concentrated in apatite. Generally, the total REE (TREE) content of IOCG deposits is between 0.2–3%, however, it could also get 10% on some rare occasions (Mazdab et al., 2008). The most known occurrences of REE-enriched IOCG deposits are the Olympic Dam and Milo in Australia (Weng et al., 2015).

2.5.3. Secondary REE deposits

2.5.3.1. Placers

For a long time, placers have been one of the most valuable REE resources, which accounts for about 5% of the total global REE resources (Sengupta and Van Gosen, 2016). Mainly, there are five types of placer deposits: alluvial, colluvial, eluvial, beach placers, and paleo placers, which occur in streams and rivers, beaches, and shallow marine environments. Generally, REE-enriched placers are derived from primary sources associated with granitic or high-grade metamorphic rocks and the degree of RE mineral enrichment in these placers depends on the source of eroded sediments (Garnett and Bassett, 2005).

The most common economic minerals found in placer deposits are ilmenite, rutile, magnetite, zircon, monazite, and xenotime and they are usually processed to produce titanium (Ti) or tin (Sn). However, REEs can also be produced as a by-product (Goodenough et al., 2018). The major REE-bearing mineral found in these deposits is monazite and it contains higher concentrations of LREEs than HREEs (Balaram, 2019). Although REEs can be extracted from the placer deposits, the process involved is difficult and problematic due to high concentrations of radioactive elements, such as Th and U (Zhou, 2017). Based on Orris and Grauch (2002), there are over 360 REE-enriched placers in the world, such as tin-rich river placers in Malaysia, paleo-

placers in South Africa, Elliot Lake in Ontario, and beach sand deposits in Kerala, Andhra Pradesh, Tamil Nadu, and Odisha in India.

2.5.3.2. Laterites

Laterites are residual soils enriched in hydrated iron and aluminum oxides and are formed by deep weathering of rocks under tropical and subtropical climatic conditions (Ugbe, 2011). If the laterites are derived from REE-bearing rocks like carbonatites, pegmatites, and granites, then they could be enriched in REEs. During the formation of laterites, REEs are remobilized into secondary minerals that are concentrated in particular layers within the profile (Berger et al., 2014).

For example, at the Mount Weld mine in Australia, a REE-enriched laterite layer (about 70 m thick), formed by the weathering of a carbonatite was observed (Jaireth et al., 2014). It has a diversified RE mineralogy, containing minerals, such as monazite, churchite, and plumbogummite-group minerals (Lottermoser, 1990). The Tantalus laterite deposit in Madagascar is also another great example of the REE-enriched laterite formations. Other than that, there are many REE-enriched laterite deposits found in countries like Brazil, South Africa, and Western Australia (Long et al., 2012; Weng et al., 2015).

2.5.3.3. Ion adsorption clays

Although ion adsorption clays account for only about 1% of the total global REE resources, they are considered an economic source for REEs, especially for HREEs (Ilankoon et al., 2018; Sanematsu and Watanabe, 2016). This is mainly due to the feasibility of REE separation, which can be achieved via leaching at ambient temperature using ammonium sulfates (Bao and Zhao, 2008; Li et al., 2017; Moldoveanu and Papangelakis, 2016). The genesis of ion adsorption clay deposits is poorly understood, but the most established theory is the adsorption of REEs from lateritic sections into clay minerals (e.g., kaolinite and halloysite), instead of being remobilized into secondary minerals. However, a clear understanding of this could be very important to identify similar occurrences in other parts of the world (Li and Zhou, 2020). Ion adsorption clay deposits are mainly divided into LREE- and HREE-dominated types and HREE-enriched deposits are only hosted by granites, most

probably of A-type affinity. Generally, REE contents up to 4000 ppm are observed in ion adsorption clay deposits along with a significant variation within the weathering profile (Bao and Zhao, 2008).

Ion adsorption clays are mostly concentrated in the southern part of China with a few other occurrences in the continents of Southeast Asia, Africa, Serra Verde in Brazil, and Tantalus in Madagascar (Moldoveanu and Papangelakis, 2016). However, the current status of most of these identified deposits, including commercial extraction of REEs, is not explicitly reported. Currently, only South China and a few other localities in northeastern Myanmar are engaged in the mining of ion adsorption clays, mostly for HREEs. However, ion adsorption clays in South China are considered the main source of HREEs in the world (Ilankoon et al., 2018; Wang et al., 2017).

In China, the ion adsorption clay deposits are mostly distributed in southern Jiangxi and Hunan, northern Guangdong, eastern Guangxi, and western Fujian and Yunnan Provinces. They consist of weathered soils of alkaline granites with grades ranging from 0.05 to 0.2 wt% REOs (Sanematsu and Watanabe, 2016; Wang et al., 2017). The primary HREE-bearing accessory minerals in the parent rocks of these deposits (e.g., xenotime and zircon) are converted lately into weathering-susceptible HREE minerals, such as synchysite-(Y) and gadolinite-(Y) (Li et al., 2019). However, most of these deposits are now closed due to environmental issues (e.g. surface vegetation clearing, soil excavation, and subsequent soil erosion, and disposal of wastewater and tailings) caused by commonly used tank/heap leaching techniques and informal mining activities (Ilankoon et al., 2018).

2.5.3.4. Offshore sources

Marine sediments and phosphorites are considered potential marine sources for REEs (Altschuler et al., 1967). Marine phosphorites are mainly found in very shallow, near-shore marine, or low-energy environments, such as estuarine, supratidal zones, and littoral, or intertidal zones. They occur as nodules (spherical concentrations of phosphates that are randomly dispersed), bone beds (concentrations of phosphates as beds, which contain small skeletal particles and coprolites), and rarely as phosphatizations (phosphate enriched-fluids, that are leached from guano) (Filippelli,

2011, 2008). These phosphorites are enriched in marine apatite, where REEs occur in trace quantities between 0.01-0.1 wt%. However, they contain higher HREE concentrations compared to LREEs. Extensive quantities of REEs and other strategic metals, such as U and Th are found in large marine phosphorites (e.g., Florida and Idaho). Other major occurrences of marine phosphorites are found in Bone Valley in central Florida, Phosphoria in Idaho and Montana, northern Florida, and North Carolina (Altschuler et al., 1967).

In addition to marine phosphorites, iron-manganese nodules in the Pacific Ocean also have higher concentrations of HREEs, even more than that of the carbonatite deposits. Furthermore, deep-sea mud in the Pacific Ocean is also considered a low-grade REE resource. Although REEs are not currently being extracted from offshore sources, they have the potential to become a future REE source since terrestrial REE sources alone would not be adequate to cater to the escalating REE demand (Hein et al., 2011; Kato et al., 2011). However, offshore mining is not encouraged due to environmentally challenging issues, such as biodiversity loss and various other ecological impacts on the marine ecosystem. Therefore, leading REE mining companies are reluctant to initiate marine exploration and mining projects (Sakellariadou et al., 2022).

2.5.4. Global distribution of REE deposits

According to Zhou (2017), the total estimated REE resources in the world are 478.14 million tonnes, which are distributed in China (164 million tonnes), Brazil (55 million tonnes), Australia (49 million tonnes), Russia (48 million tonnes), and Greenland (43 million tonnes), whereas the remaining 119 million tonnes belongs to Canada, Sweden, USA, and Vietnam. However, only a handful of these resources are utilized to produce REEs, and the others are either in the economic feasibility stage or the exploration stage. The main global occurrences of REE deposits are illustrated in Figure 2.2, of which some are in the production stage while others are still in the preliminary stages. The resources at the production stage are considered REE reserves, and the estimated world's REE reserves account for about 120 million tonnes (USGS, 2023) (Table 2.7). The global REE resources (i.e., 478.14 million tonnes) are dominated by carbonatite deposits containing 297.6 million tonnes within 66 deposits,

and the rest is alkaline igneous rocks, iron oxide copper–gold (IOCG) deposits, placers, and ion adsorption clays (Zhou, 2017) (Figure 2.3).

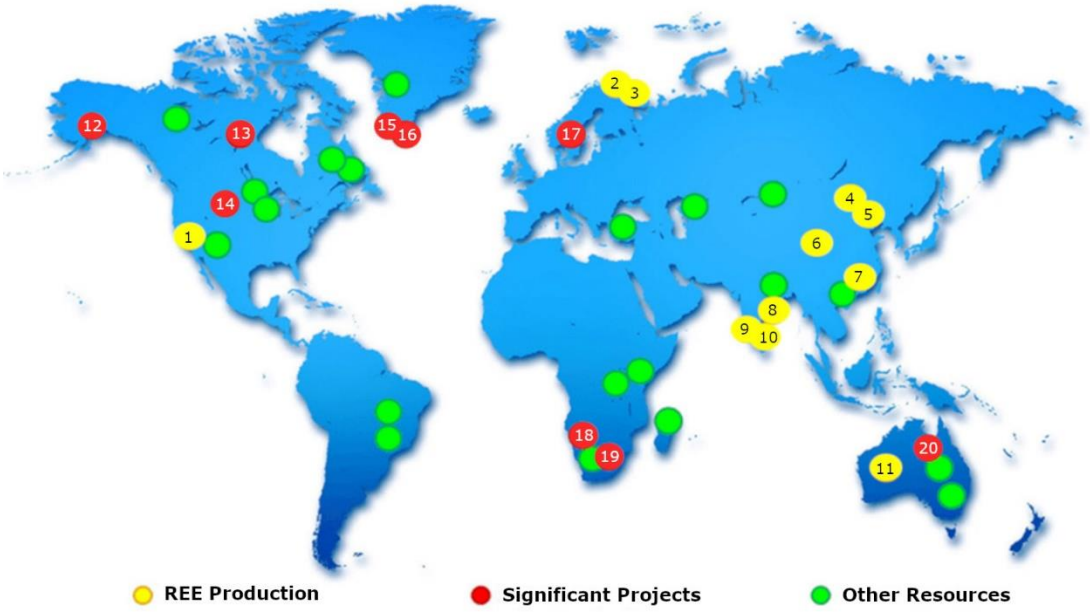

Figure 2.2: The main global occurrences of REE deposits. 1) Mountain Pass, USA; 2) Lovozero, Russia; 3) Khibiny, Russia; 4) Bayan Obo, China; 5) Weisan Lake, China; 6) Maoniuping, China; 7) Longnan, China; 8) Odisha, India; 9) Chavara, India; 10) Manavalakurichi, India; 11) Mount Weld, Australia; 12) Bokan-Dotson, USA; 13) Hoidas Lake, Canada; 14) Bear Lodge, USA; 15) Motzfeldt, Greenland; 16) Kvanefjeld, Greenland; 17) Norra Karr, Sweden; 18) Lofdal, Namibia; 19) Zandkopsdrift, South Africa; 20) Nolans Bore, Australia.
Source: (Barakos et al., 2016)

Table 2.7: The distribution of global REE reserves.

Country	Reserves in tonnes (in terms of REO)	Share (%)
United States	1,800,000	1.5
Australia	4,000,000	3.0
Brazil	21,000,000	17.5
Burma	NA	NA
Burundi	NA	NA
Canada	830,000	0.7
China	44,000,000	37.0

Greenland	1,500,000	1.2
India	6,900,000	5.8
Madagascar	NA	NA
Russia	21,000,000	17.5
South Africa	790,000	0.6
Tanzania	890,000	0.7
Thailand	NA	NA
Vietnam	22,000,000	18.0
Other countries	280,000	0.2
World total reserves (rounded)	120,000,000	-

NA – Not applicable

Source: (USGS, 2023)

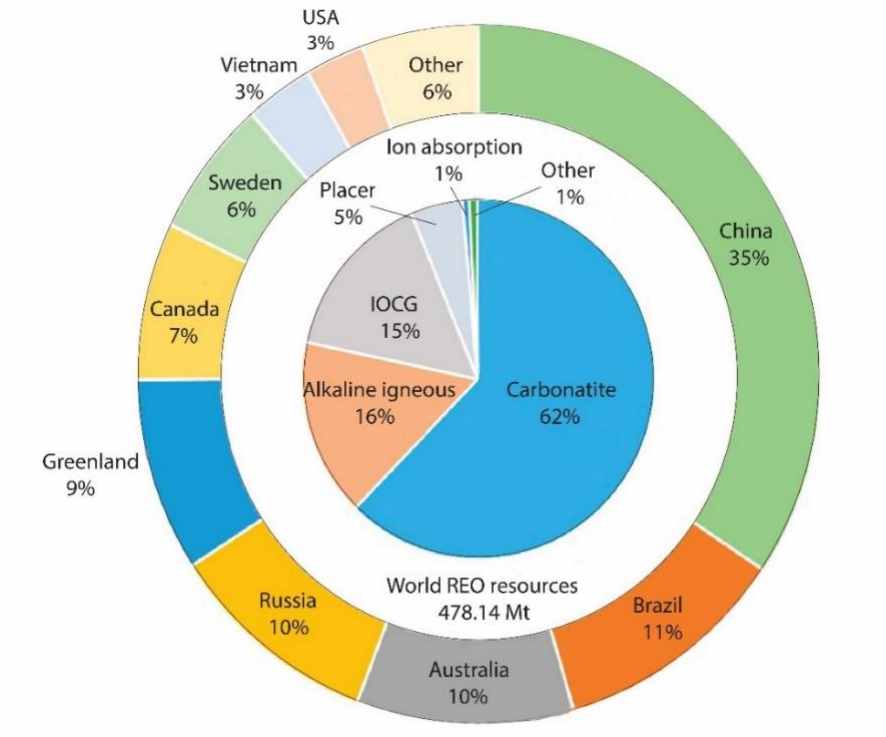

Figure 2.3: The global distribution of REE resources based on deposit type and countries.

Source: (Zhou, 2017)

2.6. Exploration for REEs in Sri Lanka

The first RE mineral detection in Sri Lanka was when monazite enriched with Ce was found in gem gravels during a mineral survey in 1914 (Jayawardena, 2011). Later, Pohl and Emmermann (1991) discovered that there are relatively high

concentrations of REEs (particularly LREEs) in the Precambrian rocks of Sri Lanka (Table 2.8). According to Table 2.8, the chemical compositions of different geological formations and mineral resources have revealed a potential for REEs in Sri Lanka, particularly in the Precambrian terrain.

Table 2.8: REE distribution (ppm) in different geological formations of Sri Lanka.

REE	Metamorphic rocks	Charnockitic gneiss	Granitic gneiss	Granitoid intrusion	Carbonatite	Residual	Blackish Brown Stream Bed Sediments	Buried alluvial deposits
Y	37	39	43	67	57	-	-	-
La	44	44	47	165	151	55.1	79.2	53
Ce	105	98	123	317	354	127	158	252
Pr	10	10	14	33	48.9	14	-	14.3
Nd	36	36	48	102	192	48.4	66.5	32.9
Sm	8.5	6.9	10.9	15.9	31.5	9	11.8	7.8
Eu	1.52	1.38	2.95	2.04	7	1.7	2.3	1.3
Gd	7	5.8	12.3	14.6	20.1	-	-	-
Dy	6.9	5.2	13.2	11.7	1.8	7.5	7.9	-
Ho	1.54	1.06	3.35	2.23	10.2	1.5	-	1
Er	4.3	3.1	9.5	6.4	1.8	-	-	-
Yb	4.3	2.58	9.63	5.3	0.6	4.4	4.3	2.3
Lu	0.67	0.45	1.56	0.8	3.5	0.6	0.7	0.4
TREE	279.73	258.47	352.39	787.97	885.3	270.5	332	366

Source: (Athurupane, 2014; Batapola et al., 2020; Pitawala et al., 2003; Pohl and Emmermann, 1991; Senaratne et al., 1987)

Sri Lanka has been long renowned for its rich monazite deposits in the onshore areas of Beruwala, Induwara, and Pulmoddai, thus beach sand may have a potential for REEs (Jayawardena, 2011). Moreover, gem-bearing gravels have been gaining the attention of geologists, scientists, and researchers as a promising source of REEs (Wadia and Fernando, 1945). Bastnaesite, the most abundant and one of the major REE minerals used for commercial extraction of REEs, has not yet been discovered in Sri Lanka (Batapola et al., 2020). However, the presence of geological formations, such as carbonatites, pegmatites, granites, and contact metamorphic deposits, where bastnaesite commonly occurs implies that potential bastnaesite sources can be found in Sri Lanka. Despite the evidence of REE-bearing minerals and high concentrations of REEs in different geological formations, no detailed studies have been carried out

to explore or quantify the potential of these sources, including economic feasibility. Therefore, detailed explorations are recommended in Sri Lanka, covering all the potential REE sources.

2.7. Geological setting of Sri Lanka

Over 90% of the geological terrain of Sri Lanka is composed of Precambrian high-grade metamorphic rocks while the rest contains Quaternary sediments (Cooray, 1984). In the Precambrian high-grade metamorphic rock terrain, quartzites, high-grade gneisses and granulites, calc gneisses and granulites, crystalline limestones (marbles), dolomites, charnockites, and pelitic gneisses are the major rock types found. They contain numerous economic minerals, such as ilmenite, zircon, sillimanite, REE-bearing minerals, thorium minerals, and precious and semi-precious gemstones (Fernando, 1986).

Based on the geochronology and metamorphic grade, the Precambrian rock terrain is divided into three major lithotectonic complexes: Highland Complex, Vijayan Complex, and Wanni Complex (Cooray, 1994; Kroner, 1991). The Highland Complex, including the Kataragama, Kudu Oya, and Buttala granulite inliers, is the largest unit and consists of supracrustal rocks and miscellaneous igneous intrusions of mostly granitoid composition. Major rock types in the Vijayan Complex are biotite-hornblende gneisses, scattered bands of meta-sediments, and granitic gneisses, whereas small plutons of granite and acid charnockites and NW-trending suite of dolerite dikes are also found (Jayawardena and Carswell, 1976). The Wanni Complex consists of granitoid gneisses, charnockitic gneisses, and granites with rare intercalations of metasediments, mainly calc-silicate rocks and quartzites (Pohl and Emmermann, 1991). In addition to these major complexes, there is a minor lithotectonic terrain called the Kadugannawa Complex, which is located around Kandy in the Central Highlands of Sri Lanka. It mainly comprises hornblende and biotite-gneisses with minor supracrustal rocks (Kröner et al., 1991; Pohl and Emmermann, 1991).

Quaternary sediments are only exposed along the northern and north-western coasts, which belong to the Pleistocene and Recent periods. They are consolidated and

unconsolidated materials formed on the surface, such as laterites, gravels, sands, and clays (Fernando, 1986). Red earth and laterites are Pleistocene sediments occurring along the northwest coast aligning in the north-south direction and the southwest coast from Matara to Tangalle, respectively (Cooray, 1984). The Recent sediments consist of residual laterites, alluvial placers, coral and shell formations, lagoons, estuaries, peat, gem-bearing gravels, and beach mineral sands (Fernando, 1986).

CHAPTER 3: METHODOLOGY

3.1. Study area

Three different types of geological formations, namely residual lateritic regolith, placers, and magmatic were selected to explore the potential resources of REEs in Sri Lanka. Figure 3.1 shows the major lithotectonic complexes of Sri Lanka with the distribution of selected geological formations in the present study.

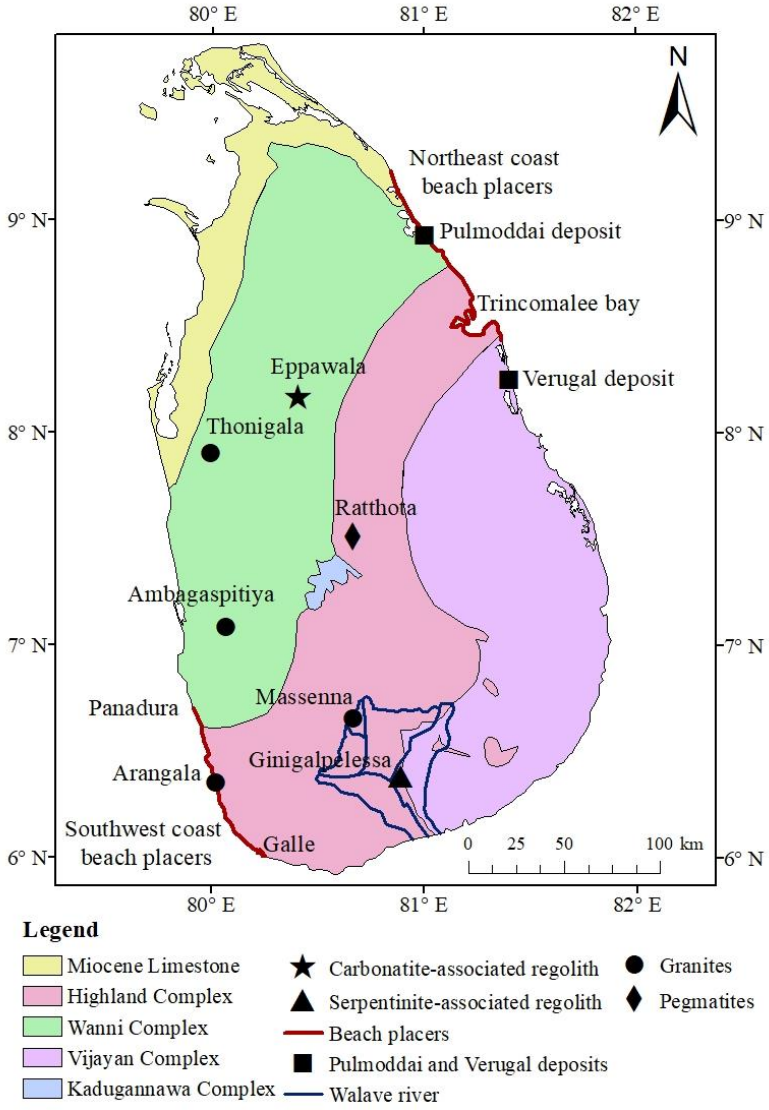

Figure 3.1: The simplified geological map of Sri Lanka showing the distribution of the major lithotectonic complexes of the Precambrian basement and the explored geological formations for REEs.

Source: (Cooray, 1994)

3.1.1. Residual lateritic regolith

3.1.1.1. Carbonatite-associated regolith

The only known occurrence of carbonatite in Sri Lanka is the Eppawala carbonatite, which was discovered by the Geological Survey Department of Sri Lanka in 1971. It is located in Eppawala of the north-central province and extends over 20 km^2. Eppawala carbonatite belongs to the Wanni Complex of the Precambrian basement of Sri Lanka (Figure 3.1). The country rocks of the area consist of biotite-hornblende gneisses, granites and granitic gneisses, charnockitic gneisses, minor quartzites, and marbles (Pitawala and Lottermoser, 2012). The Eppawala carbonatite is exposed as circular or oval outcrops with conspicuous N-S orientation. Most of the outcrops are found along or near the axis of a synform, whereas others are in the core of an antiform in the east of Eppawala (Dahanayake and Subasinghe, 1991; Jayawardena, 1978; Pitawala et al., 2003). Mainly, there are two carbonatite outcrops found at Eppawala, namely northern and southern outcrops (Figure 3.2). The genesis of the Eppawala carbonatite is still a matter of debate, however, the most popular theories are igneous and sedimentary (metamorphosed limestone) (Pitawala et al., 2003).

Due to intense tropical weathering conditions, a secondary phosphate-rich regolith has been developed on the Eppawala carbonatite. It is known as the Eppawala Phosphate Deposit (EPD) and is currently being mined for phosphates (Hewawasam, 2013). The parent carbonatite rock is mainly composed of carbonate minerals, such as calcite (70%) and dolomite (10-20%). In addition, it contains apatite (5-10%) as individual yellowish-green crystals (a few mm to 50-60 cm in size) with minor minerals like ilmenite, magnetite, forsterite, phlogopite, magnesite, enstatite, and tremolite and accessory minerals, such as spinel, pyrite, monazite, and rutile (Manthilake et al., 2008; Pitawala et al., 2003). During weathering, residual minerals, such as apatite, iron-oxide, and silicate minerals are concentrated in the regolith due to their weathering resistance while the carbonate minerals are partially or completely dissolved (Chandrakumara et al., 2021). However, under intense weathering

conditions, secondary supergene phosphates are formed by the dissolution recrystallization of weathering-resistant primary minerals (Dinalankara, 1995).

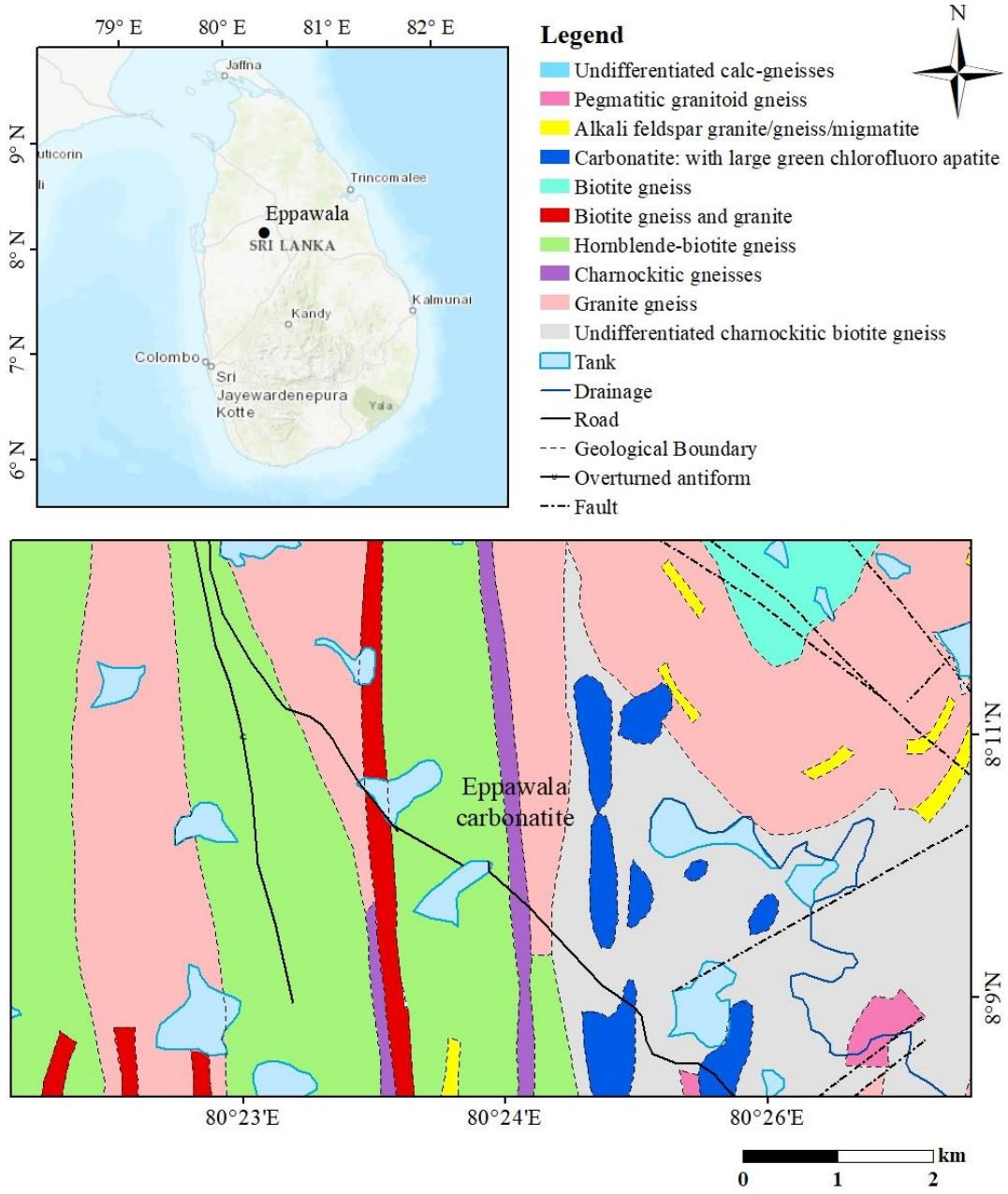

Figure 3.2: The simplified geological map of the Eppawala area.
Source: (GSMB, 2001a)

The northern phosphate-rich regolith, which is currently being mined, consists of thick weathered profiles developed under karstic conditions (Chandrakumara et al., 2021). The two major weathering zones here are leached zone containing primary

apatite crystals that are embedded in a hard, consolidated secondary matrix and the top weathered zone comprising loosely bound primary apatite crystals in a soft, brownish soil-like matrix (Figure 3.3a) (Hewawasam, 2013). In contrast, the southern phosphate-rich regolith is subjected to minimal karstic conditions so that it consists of several distinctive weathering zones, which are fresh to partially weathered carbonatite zone, alloteritic-saprolite zone, intensively leached zone, and lateritic zone (Figure 3.3b) (Chandrakumara et al., 2021).

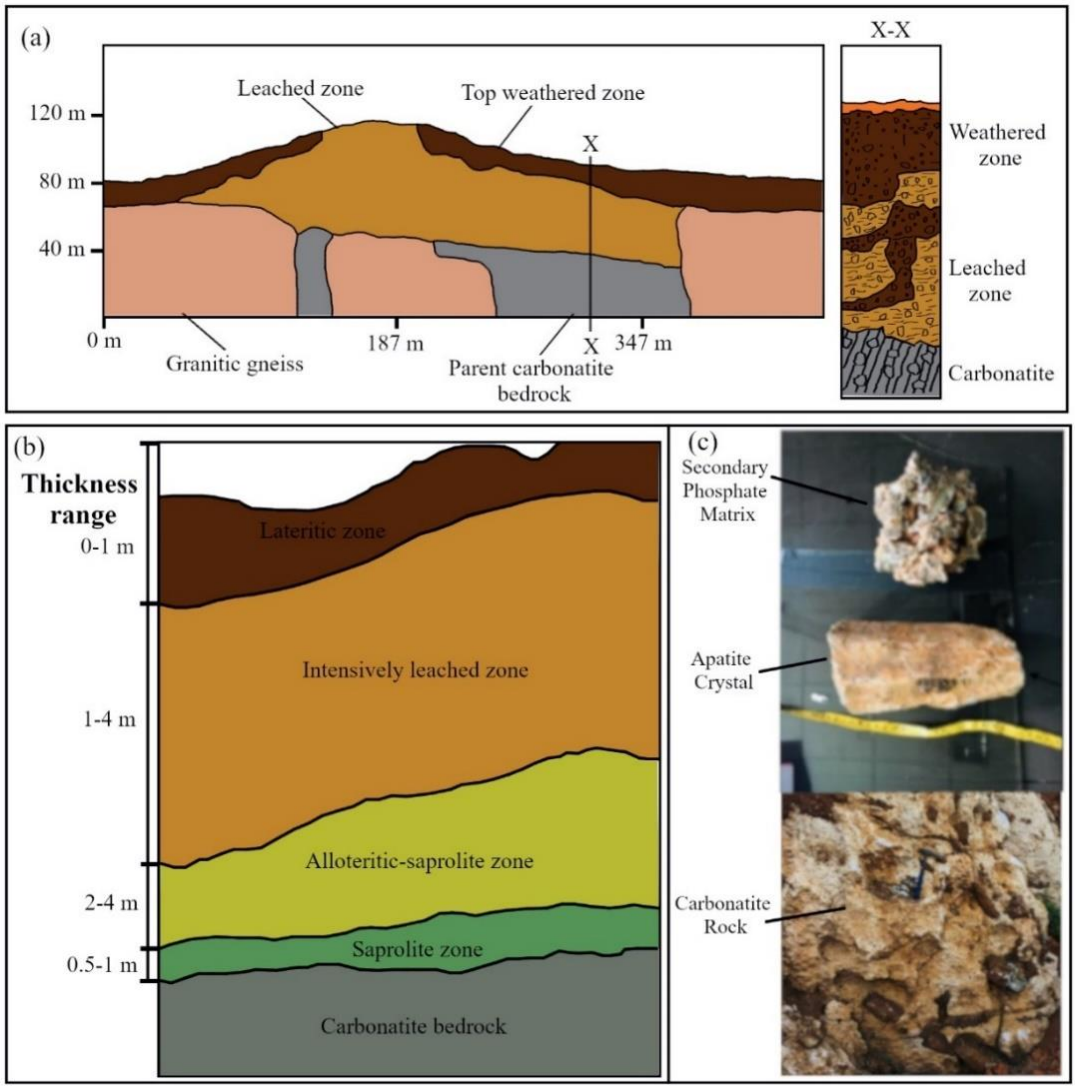

Figure 3.3: The weathering profiles at (a) the northern phosphate-rich regolith; (b) the southern phosphate-rich regolith; and (c) the primary apatite crystal and the secondary phosphate matrix.

Source: (Chandrakumara et al., 2021; Hewawasam, 2013)

This secondary phosphate-rich regolith contains two types of components, namely primary apatite crystals (30-40% P_2O_5) and secondary phosphate matrix (10-30% P_2O_5) (Figure 3.3c). These phosphate components are currently being mined to produce High-Grade Eppawala Rock Phosphate (HERP) and Eppawala Rock Phosphate (ERP), respectively (Dahanayake and Subasinghe, 1991; Dushyantha et al., 2019). In the primary apatite crystals, chloro-fluor-hydroxylapatite is the major mineral while fluorapatite is present as the minor component. However, in the secondary phosphate matrix, these two minerals are only found in the coarser fraction. Secondary minerals, such as crandallite, millisite, wavellite, goethite, gibbsite, kaolinite, and quartz are only present in the finer fraction of the secondary phosphate matrix (Hewawasam, 2013).

3.1.1.2. Serpentinite-associated regolith

In Sri Lanka, six serpentinite bodies have been identified to date, namely Ginigalpelessa, Ussangoda, Indikolapelessa, Yodaganawa, Rupaha, and Katupotha, and all of which lie along the boundary of Highland Complex and Vijayan Complex. It is speculated that these serpentinite outcrops have a deep-seated origin due to their northward orientation close to the litho-tectonic boundary (Hewawasam et al., 2014). Out of them, Ginigalpelessa is the largest serpentinite outcrop covering an area of ~1 $km^{2,}$ and is located near the Embilipitiya town in the Uva province (Figure 3.1). The Ginigalplelessa area consists of crystalline rocks of migmatitic hornblende biotite gneisses and biotitic gneisses metamorphosed under upper amphibolite/granulite facies conditions. In addition, many quartz and feldspar veins along with late pegmatitic intrusions are evident, which have been formed from a residual melt of the ultramafic magma (Dushyantha et al., 2021; Hewawasam et al., 2014) (Figure 3.4). It is reported that these rocks contain more than 90% of ultramafic minerals, such as pyroxene and olivine, whereas the rest is composed of orthoclase, plagioclase, diopside, and magnetite.

A weathered regolith (thickness = ~36 m) (Dissanayaka, 1982) of dark brown color overlies the serpentinite outcrop at Ginigalpelessa with significant metal enrichment, particularly Cr, Ni, and Co (Dushyantha et al., 2021). This lateritic profile

developed on the serpentinite parent rock mainly consists of three zones: soil zone, pisolitic laterite, and limonitic laterite (Dissanayaka, 1982). Over the years, the Ginigalpelessa serpentinite outcrop has been the subject of numerous geochemical, petrological, and ecological research (e.g., Dushyantha et al., 2021; Hewawasam et al., 2014; Rajakaruna and Bohm, 2002; Vithanage et al., 2014). However, this outcrop or

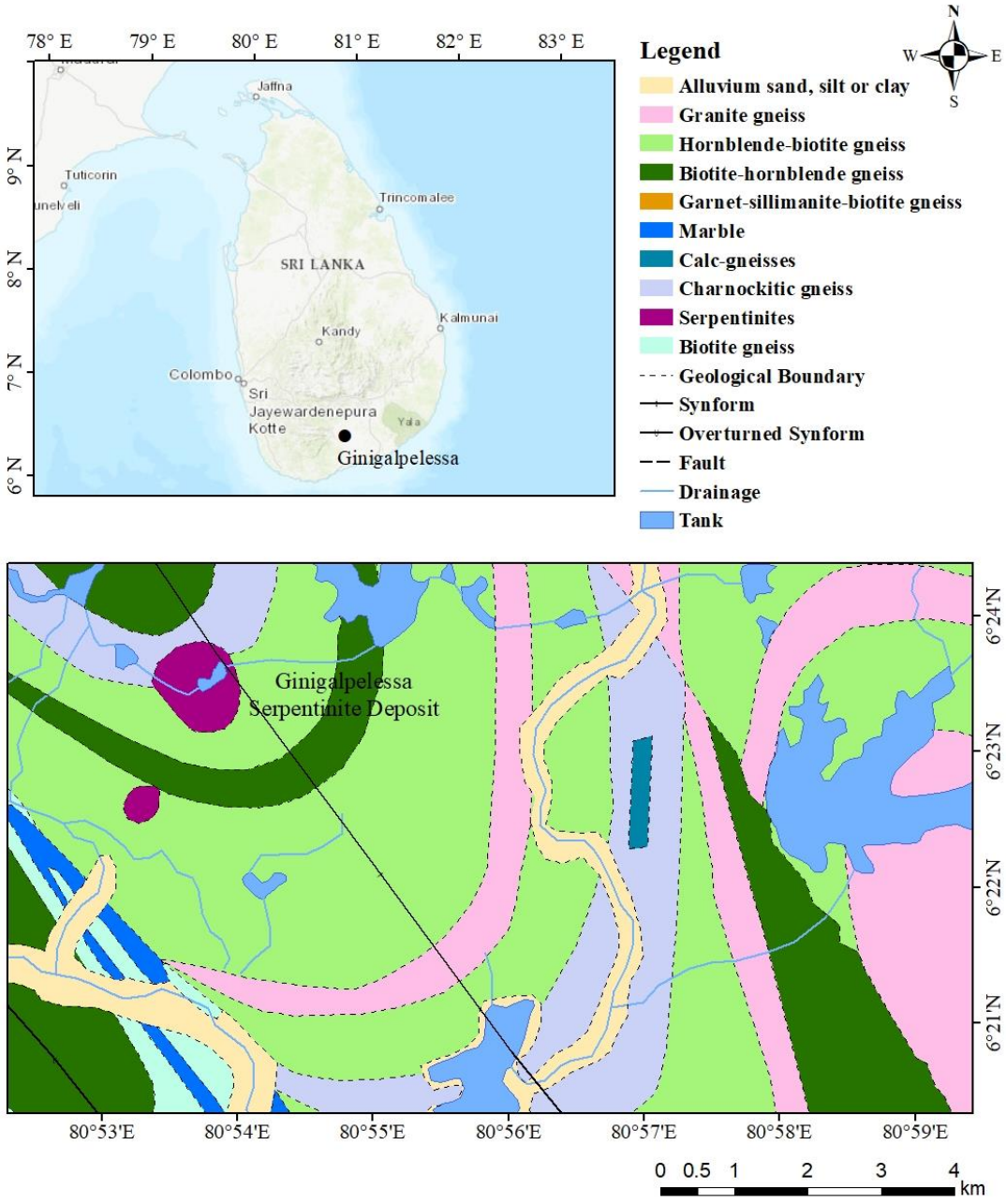

Figure 3.4: The simplified geological map of the Ginigalpelessa area.

Source: (GSMB, 2001b)

any other serpentinite outcrops in Sri Lanka have never been explored for REEs, although laterites derived from serpentinite bodies across the world have been known for their REE potential and thus have been explored widely.

3.1.2. Placers

3.1.2.1. Beach placers

Beach placers of different scales occur around the island with economical concentrations of heavy minerals, such as ilmenite, rutile, monazite, garnet, and zircon (Amalan et al., 2018). For example, Lanka Mineral Sands Ltd of Sri Lanka currently produces 90,000 tonnes of ilmenite, 9,000 tonnes of rutile, 5,500 tonnes of zircon, 100 tonnes of monazite, and 4,000 tonnes of Hi titanium ilmenite annually. However, these mineral sands are exported in raw form without any value addition (Lanka Mineral Sands Ltd, 2022). In the present study, beach placers were divided into two units: (1) beach placers on the northeast coast (Pulmoddai and Verugal deposits) and (2) beach placers along the southwest coast (from Pandura to Galle coasts) (Figure 3.1).

3.1.2.1.1. Beach placers on the northeast coast

The Pulmoddai deposit is the largest heavy mineral beach placer deposit in Sri Lanka, located on the northeast coast, 54 km north of Trincomalee bay (Figure 3.1, Figure 3.5a). It extends over a length of about 7.4 km with an average width of 150 m. The Pulmoddai deposit is considered one of the richest mineral sand deposits in the world as it contains more than 80% of usable heavy mineral sand (Amalan et al., 2018). It is continuously replenished and washed off into the sea during the monsoons, if not mined. The Pulmoddai deposit has been exploited for heavy minerals since 1957 and has a reserve capacity of 6 million tonnes of heavy minerals with 70–72% ilmenite, 8–10% zircon, 8% rutile, 0.3% monazite, and 1% sillimanite (Herath, 1980; Lanka Mineral Sands Ltd, 2022; Thilakanayaka, 2015). Though economic concentrations of monazite are found in the Pulmoddai deposit, to date no value addition or extraction processes are carried out for them (Batapola et al., 2020).

The Verugal deposit is located on the northeast coast, 50 km south of Trincomalee bay extending over a length of more than 3 km (Figure 3.1, Figure 3.5b).

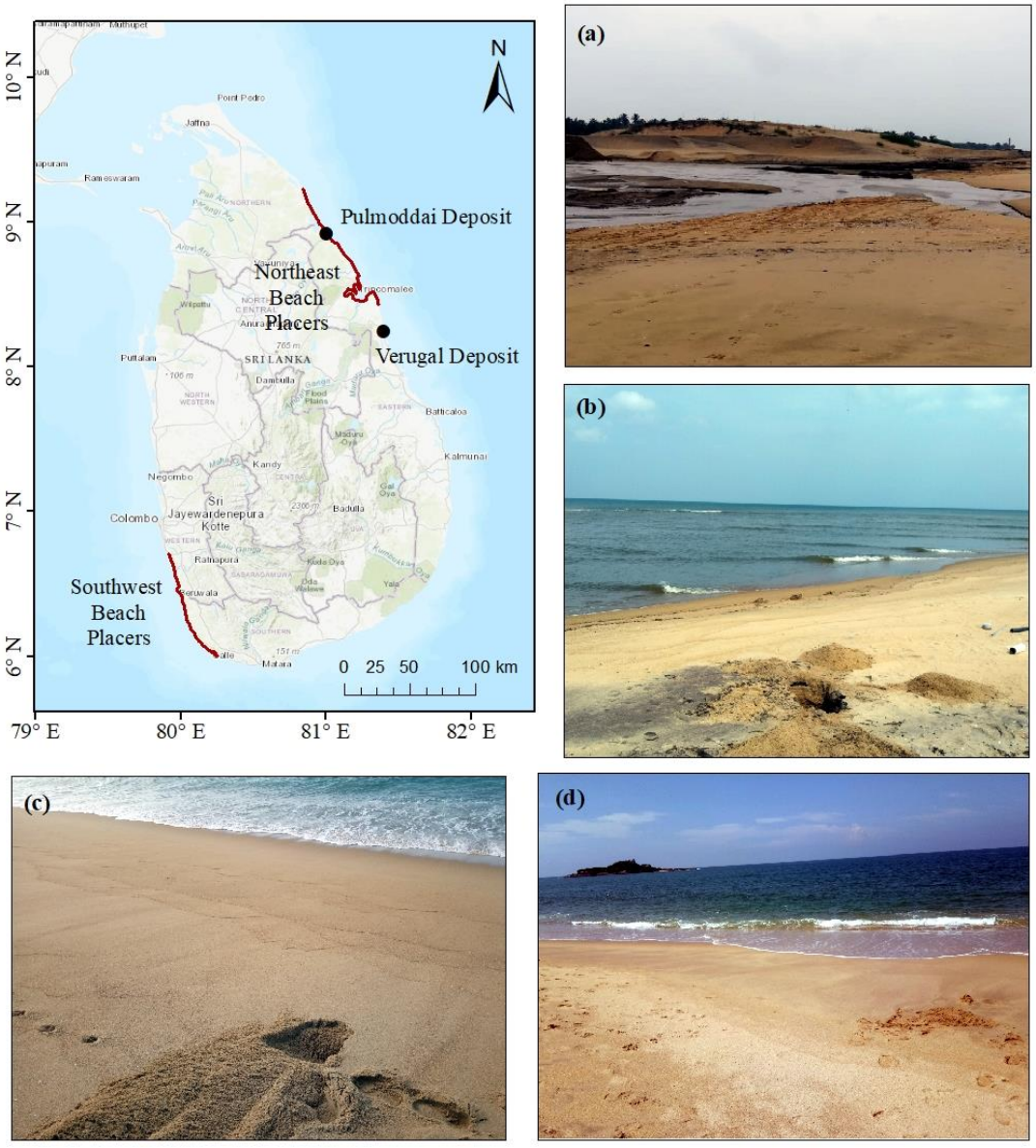

Figure 3.5: Field photographs showing the (a) Pulmoddai deposit; (b) Verugal deposit in the northeast coast; (c) Induwara beach; (d) Beruwala beach in the southwest coast.

ilmenite (average 48.0% in the bottom sediments and average 38.7% in the surface sediments), whereas zircon and garnet are found in fewer concentrations (zircon: 17.4-22.0%, garnet: 11.9-22.5%) (Amalan et al., 2018). However, it has been reported that monazite and rutile occur in low concentrations in the Verugal deposit, compared to the Pulmoddai deposit (Udarika et al., 2016).

3.1.2.1.2. Beach placers along the southwest coast

The southwest coast of Sri Lanka has been long known for its occurrence of monazite-rich heavy mineral placer deposits and had been exploited since 1918. These placer deposits have been studied previously by many researchers (Fernando, 1954; Wadia and Fernando, 1945; Wickremeratne, 1986) and high monazite concentrations (average 4-20%) have been reported at Beruwala, Kaikawala, Polkotuwa, and Induwara coastal areas (Batapola et al., 2020). Until 1971, Beruwala and Kaikawala deposits were commercially exploited, however, their replenishment reduced over time, and currently, no economic exploitations are carried out in these beach placers (Wickremeratne, 1986).

In this study, beach placers along the southwest coast from Panadura to Galle were selected extending over a distance of about 100 km and an average width of 10-40 m, where in some locations the width exceeds 100 m (Figure 3.1, Figure 3.5). The studied southwest beach placers lie in the southwestern part of the Highland Complex and charnockites, charnockitic gneisses, and garnetiferous quartzo-feldspathic rocks are mainly found in the inland terrain near this area along with wollastonite and scapolite-bearing calcgneisses and mappable bands or lenses of cordierite-bearing pelitic gneisses (Kröner et al., 1991; Sameera et al., 2020). Since Sri Lanka is a tropical country, the weathering rates of the rocks are high, which results in a high yield of sediments (Dushyantha et al., 2019). Therefore, the secondary geological processes possess the potential to accumulate valuable minerals in the placers. Ilmenite, rutile, monazite, zircon, and garnet are the major heavy minerals abundantly found in these placer deposits, whereas spinel and sillimanite occur in minor quantities (Batapola et al., 2021).

3.1.2.2. Alluvial placers

Alluvial placers in Sri Lanka are well-known for their high potential of heavy minerals (zircon, garnet, monazite, ilmenite, allanite, and rutile) and particularly sedimentary gem deposits (Batapola et al., 2020). There are four major river basins on the island; Mahaweli, Kalu, Walave, and Kelani, out of which Walave river basin is considered the most geologically and economically important one with significant

potential for alluvial placer deposits of heavy minerals and gem-bearing minerals. Therefore, the Walave river basin was selected to explore the potential of REEs in the present study.

3.1.2.2.1. Walave river basin

The Walave river basin lies within the boundary between the Highland Complex and Vijayan Complex (Figure 3.1, Figure 3.6), which is considered to be a mineralized belt. This area is characterized by a ridge and valley topography with plunging synclinal and anticlinal structures (Chandrajith et al., 2000). In this study, the upper part of the Walave basin was investigated, which is located in the Highland Complex. It is mainly underlain by charnockites with occasional garnetiferous varieties. In addition, major rock types, such as biotite garnet gneiss, quartzite, crystalline limestone, and undifferentiated metasediments occur in the Walave basin. Furthermore, pegmatitic intrusions are evident in the Walave river basin, particularly large syenitic intrusions with zircon crystals in the Balangoda area (Nawaratne and Wijeratne, 1995). Since pegmatite is known as a potential primary source of REEs, a part of the Walave river basin located in the Balangoda area was selected, including two other tributaries connected to the basin, namely Belihul Oya and Kiriketi Oya.

It is reported that about 50% of stream sediments of the Walave river consist of heavy minerals, including zircon, garnet, monazite, ilmenite, sphene, allanite, magnetite, rutile, and ferromagnesian minerals. Moreover, the upper tributaries of the Walave river basin contain a wide variety of gem minerals, even some rare gem minerals like ekanite, alexandrite cat's eye, and aquamarine have been reported in the upper part of the Rakwana Ganga tributary (Chandrajith et al., 2000; Ratnayake et al., 2017). In addition, it has been reported that gold nuggets and flakes are also found in several areas of the Walave river basin (Nawaratne and Wijeratne, 1995).

3.1.3. Magmatic

3.1.3.1. Granites

Granite is the most common intrusive rock type in Sri Lanka, which occurs as small plutons, sheets parallel to the foliation of the surrounding gneisses, cross-cutting

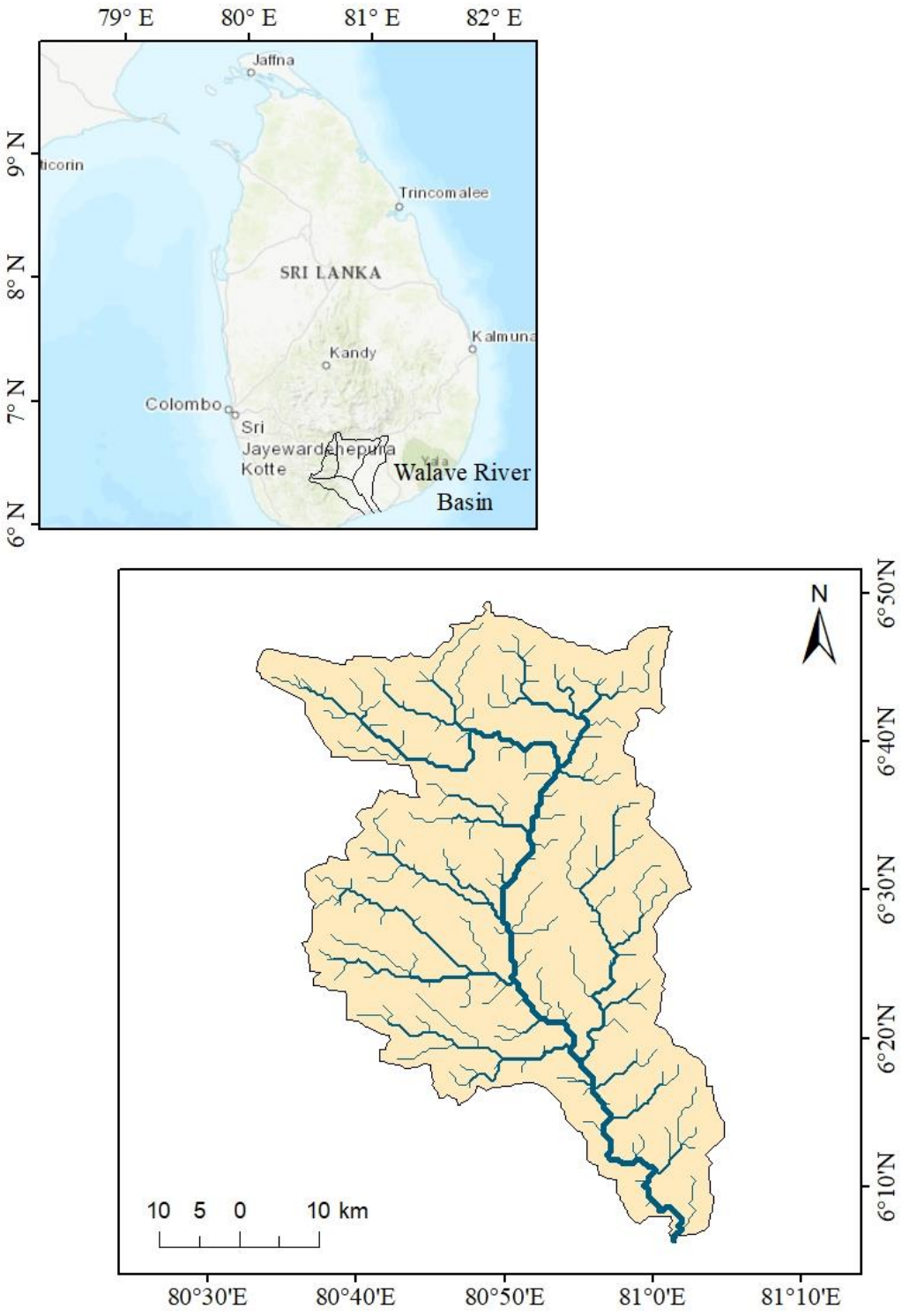

Figure 3.6: The Walave river basin.

Source: (HydroSHEDS, 2023)

dykes and veins, and large irregular bodies associated with the gneisses (Cooray, 1984). Out of them, Thonigala, Massenna, Arangala, and Ambagaspitiya are well-known granitic bodies in Sri Lanka.

3.1.3.1.1. Thonigala granite

Thonigala granite is the largest and the best-known of the granites, located in the northwest part of the country, and belongs to the Wanni Complex (Figure 3.1). Although it is a pinkish, medium-grained granite with a few dark minerals, certain parts of it are gneissic in texture due to the presence of streaks of biotite and hornblende. Thonigala granite occurs as two sub-parallel sheets of a width of 1 to 3 km, and they are vertical or steeply dipping with boundaries parallel to the foliation of the surrounding rocks. The northerly one runs over 24 km, mostly in the E-W direction, whereas the southerly sheet is about 15 km that runs in a WSW-ENE direction (Figure 3.7) (Nawaratne, 2009). The southerly sheet, which is found as several low, turtle--backed outcrops, crossing the road from Puttalam to Kurunagala at Thonigala, near Anamaduwa is the targeted granitic body in this study. Thonigala granite has quartz and feldspar as major minerals with biotite in minute quantity. In addition, coarse, pegmatitic patches are also observed in the Thonigala granite.

3.1.3.1.2. Massenna granite

Another major occurrence of granite is the Balangoda zircon granite occurs in the Highland Complex, in which honey-brown, well-formed crystals of zircons can be observed with the naked eye (Coomáraswámy, 1904). The Balangoda zircon granite exposes at different locations in the Balangoda area and Massenna granite is the finest and longest exposure located in Massenna 9.6 km away from Balangoda (Figure 3.1). The Massenna granite outcrops as a line of large boulders lying in a paddy field with a length of about 3.2 km and a width of about 90 m. It is parallel to the Charnockite foliation-strike, along the trough-like strike valley of the Massenna Oya (Figure 3.8). The Massenna granite is very coarse-grained and almost pegmatitic in texture and is mainly composed of quartz, feldspar, and biotite. In addition, it also contains zircon and ilmenite as accessory minerals with apatite as a minor constituent (Coomáraswámy, 1904).

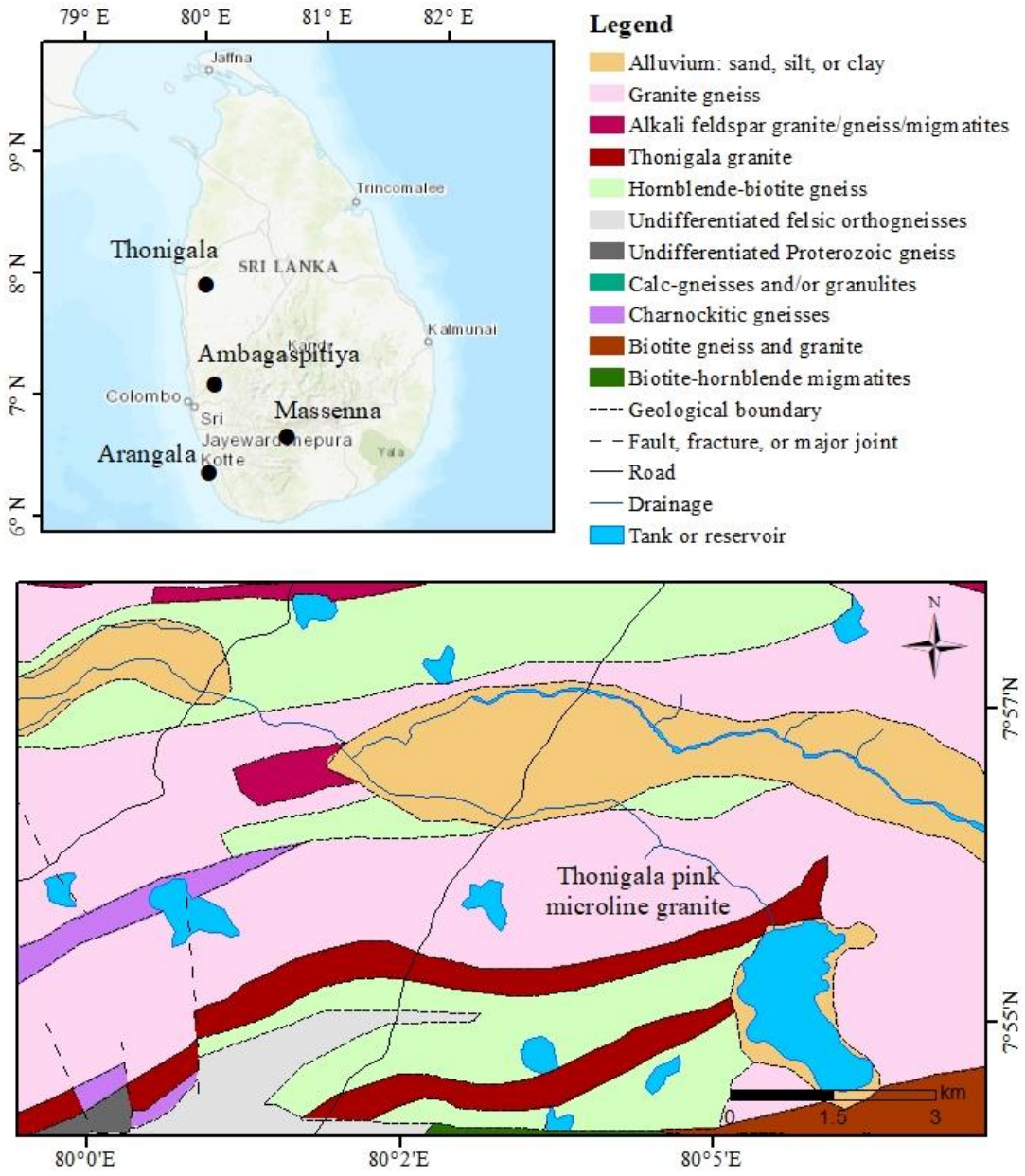

Figure 3.7: The simplified geological map of the Thonigala area.

Source: (GSMB, 2001c)

3.1.3.1.3. Arangala granite

The Arangala granite is a relatively small granitic body in the southwestern part of the island that belongs to the Highland Complex. It is a circular pluton with an average diameter of about 2 km intruding the surrounding rocks and it is located in the

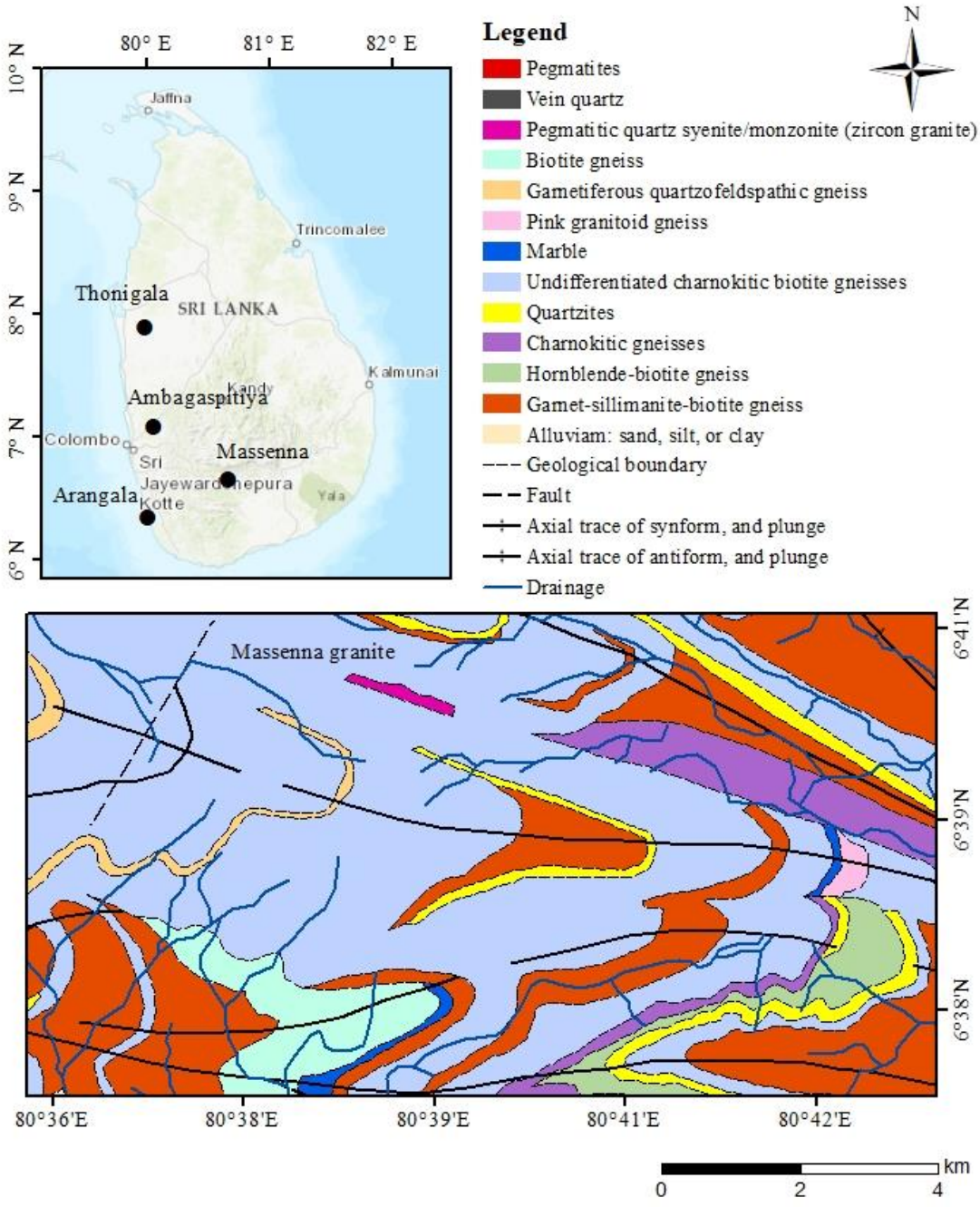

Figure 3.8: The simplified geological map of the Massenna area.
Source: (GSMB, 1997)

Kosgoda area near the beach (Figure 3.1, Figure 3.9). Typically, it has a fluted surface owing to the weathering, which has taken place along parallel lines. The Arangala granite is a coarse-grained, porphyritic rock with hornblende crystals of more than 10 cm in length and purplish brown crystals of zircon. In addition, there are several blocks

of an earlier formed, even-grained variety of the same granite, which were disrupted and moved about by the later coarse-grained variety (Nawaratne, 2009).

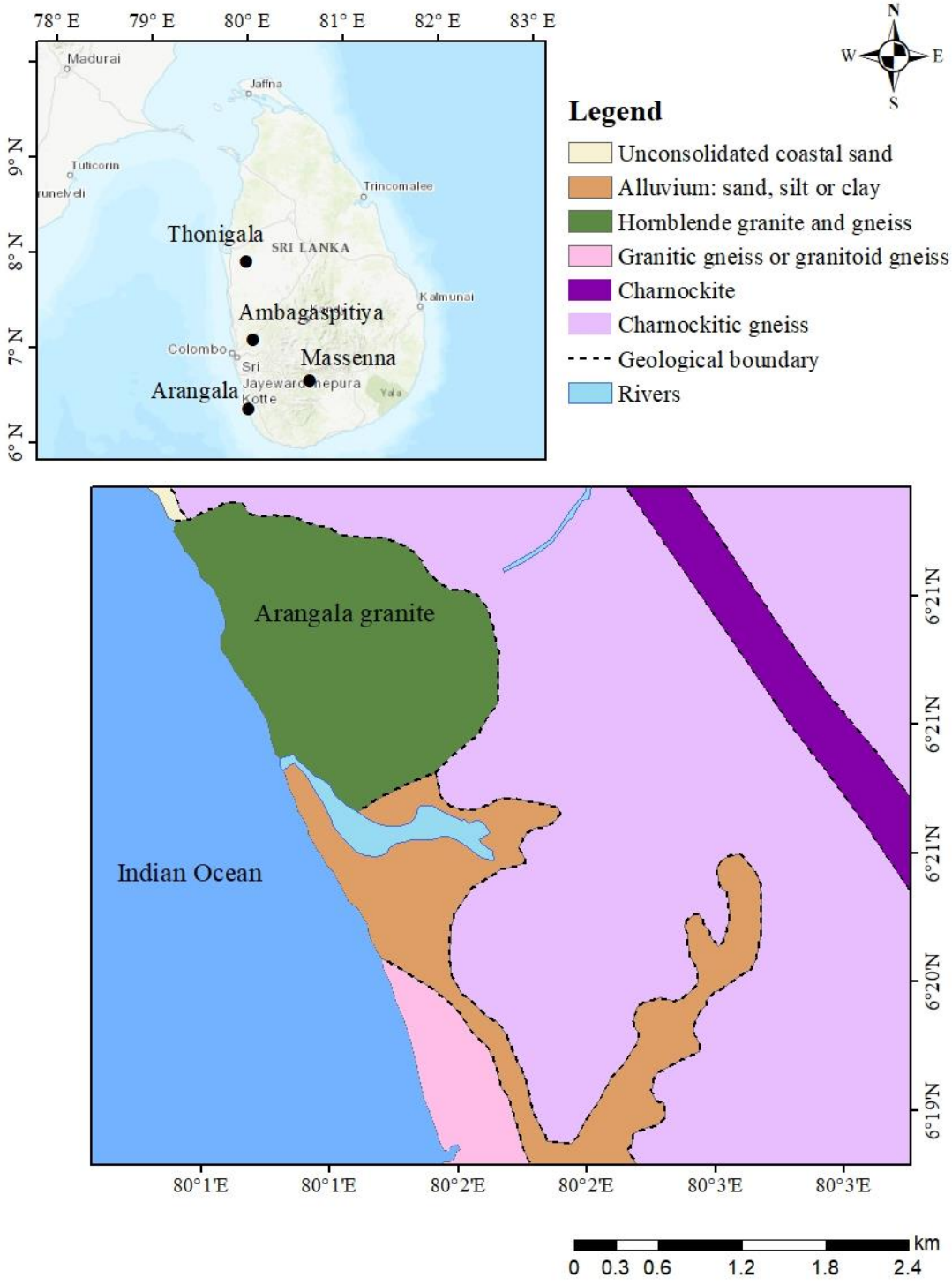

Figure 3.9: The simplified geological map of the Arangala area.

Source: (GSMB, 2001a)

3.1.3.1.4. Ambagaspitiya granite

The Ambagaspitiya granite is also located in the southwestern part of the country but belongs to the Wanni Complex. It is a pink Microline granite, which occurs at Ambagaspitiya, about 6 km south of Veyangoda (Figure 3.1). It is roughly circular with an average diameter of about 7 km, covering an area of about 40 km^2 (Figure 3.10). In comparison to the Thonigala granite, the composition of this granite is less uniform with several gneissic patches on it. There are a few other small granitic outcrops around the main granite body and it suggests that the Ambagaspitiya granite could be larger than the present outcrop, lying at a certain depth from the surface (Nawaratne, 2009).

3.1.3.2. Pegmatites

Numerous pegmatite occurrences in varying sizes are found all over the country, which cut across all the Precambrian rocks. Mainly, two types of pegmatites occur in Sri Lanka, namely (1) narrow (up to 1 m width) concordant or discordant bodies, exposed as dykes, lenses, pods, and veins in the upper-amphibolite- to granulite-facies basement and (2) bodies that may cover several hundreds of square meters to square kilometers. In the present study, Ratthota pegmatite was selected as it is a large occurrence of economic interest that belongs to the above latter group (Dharmapriya et al., 2021; Fernando et al., 2011).

3.1.3.2.1. Pegmatites in Ratthota, Matale

The Ratthota pegmatite is located at the Ratthota-Matale area in the central part of the Highland Complex close to the inferred tectonic boundary between the Highland and Wanni complexes (Figures 3.1 and 3.11). It has been reported that the Ratthota pegmatite shows evidence of hydrothermal activity (Dharmapriya et al., 2021). The host rocks of this pegmatite are mainly composed of marble and biotite–sillimanite gneiss. In addition, several vertical and sub-vertical pipe-like pegmatite bodies with oval to irregular cross-sections are also evident here. Ratthota pegmatite contains large crystals of K-feldspar, quartz, and mica with minor inclusions of fluorite, biotite, and calcic amphibole (Nawaratne, 2009).

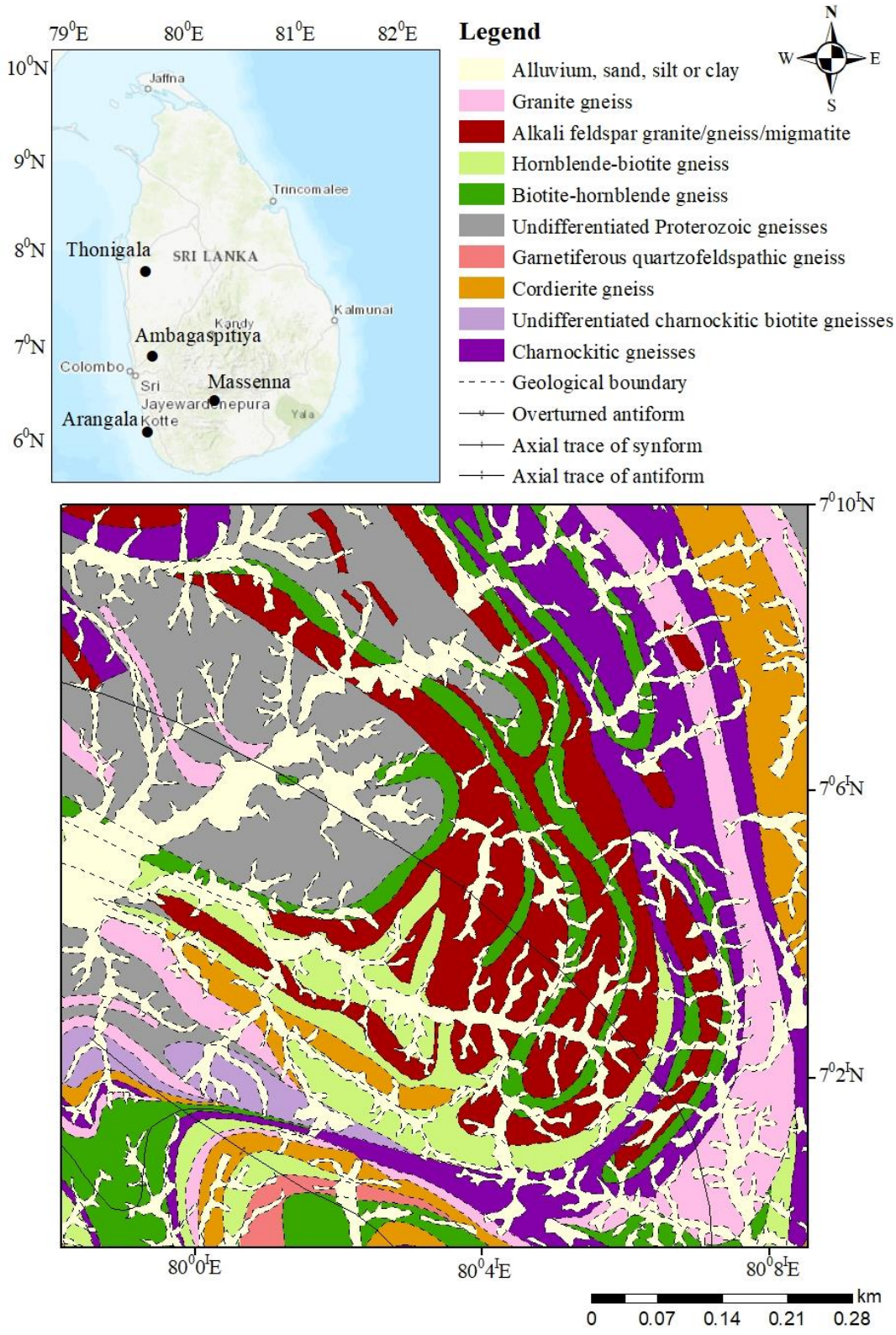

Figure 3.10: The simplified geological map of the Ambagaspitiya area.

Source: (GSMB, 1996a)

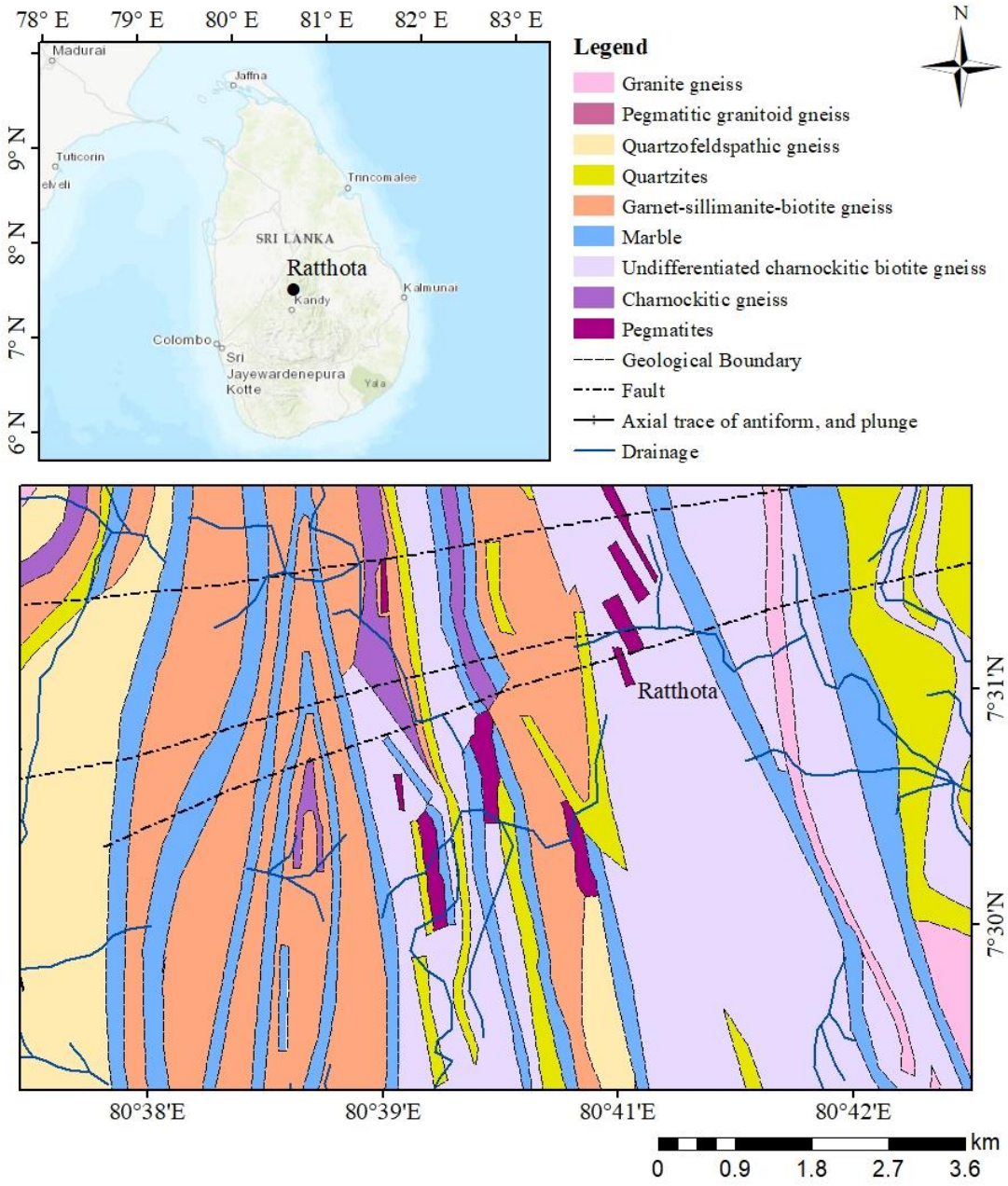

Figure 3.11: The simplified geological map of the Ratthota area in Matale.
Source: (GSMB, 1996b)

3.2. Sample collection

3.2.1. Eppawala phosphate deposit

The sampling locations (EP1-EP18: northern regolith; EP19-EP30: southern regolith) at the EPD are illustrated in Figure 3.12. Sixty samples were obtained from

the EPD: apatite crystals (n=28; apatite crystals were not found in EP12 and EP17 sampling locations), secondary phosphate matrix (n=30), and carbonatite rock (n=2)

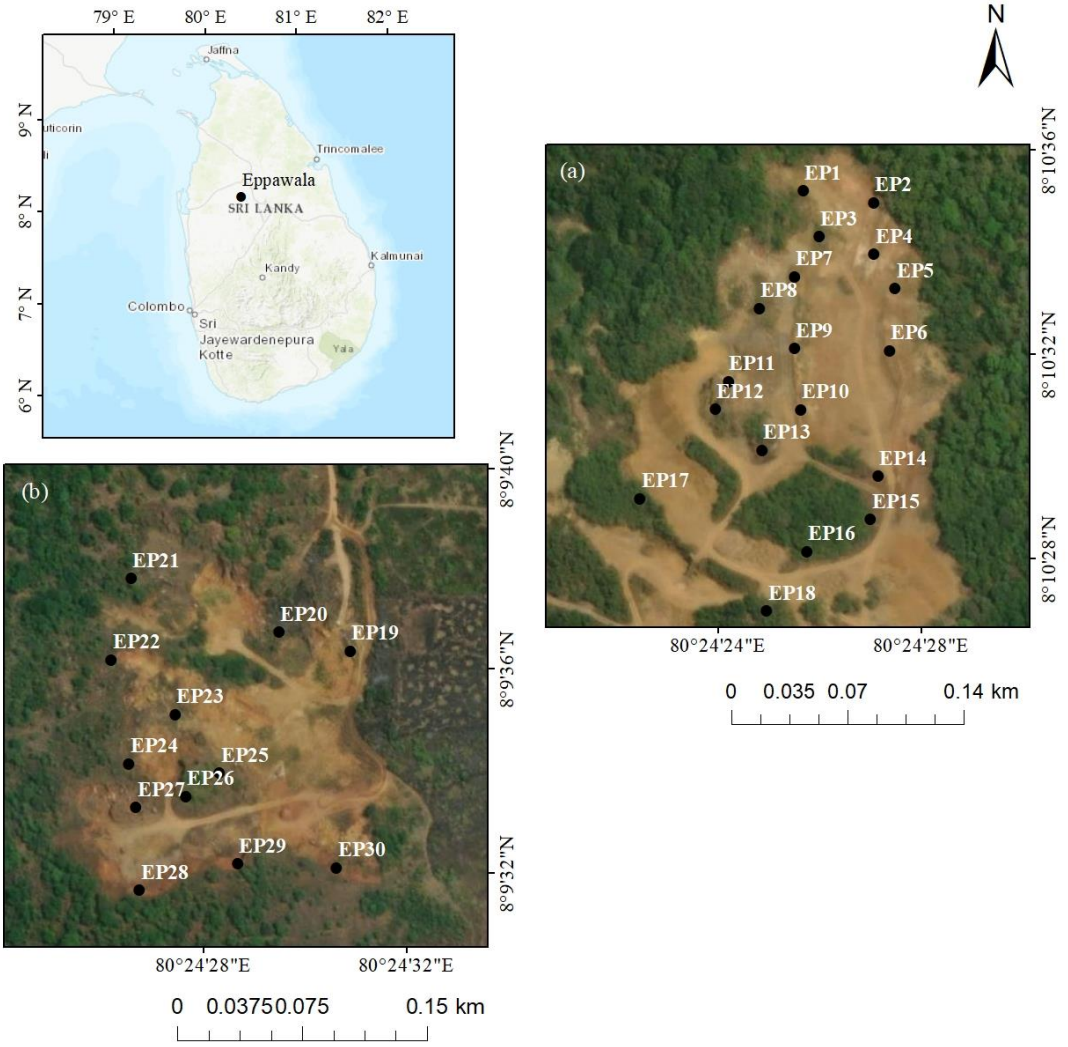

Figure 3.12: Sampling location map of the Eppawala phosphate deposit. (a) northern regolith; (b) southern regolith.

Source: (Google Earth, 2021)

covering 30 sampling locations. Apatite crystals and secondary phosphate matrix samples were collected from the leached zone of both the northern and southern regolith at the EPD. Carbonatite samples were obtained from outcrops exposed at EP11 and EP19 locations in the respective northern and southern areas.

3.2.2. Ginigalpelessa serpentinite regolith

Thirty-two rock (n=13) and soil (n=19) samples were collected from the Ginigalpelessa serpentinite outcrop covering 19 sampling locations (Figure 3.13). Soil samples were obtained from the subsurface layer (about 10-15 cm below the surface) after removing the topsoil layer. Rock samples were collected from serpentinite outcrops evident near some sampling locations.

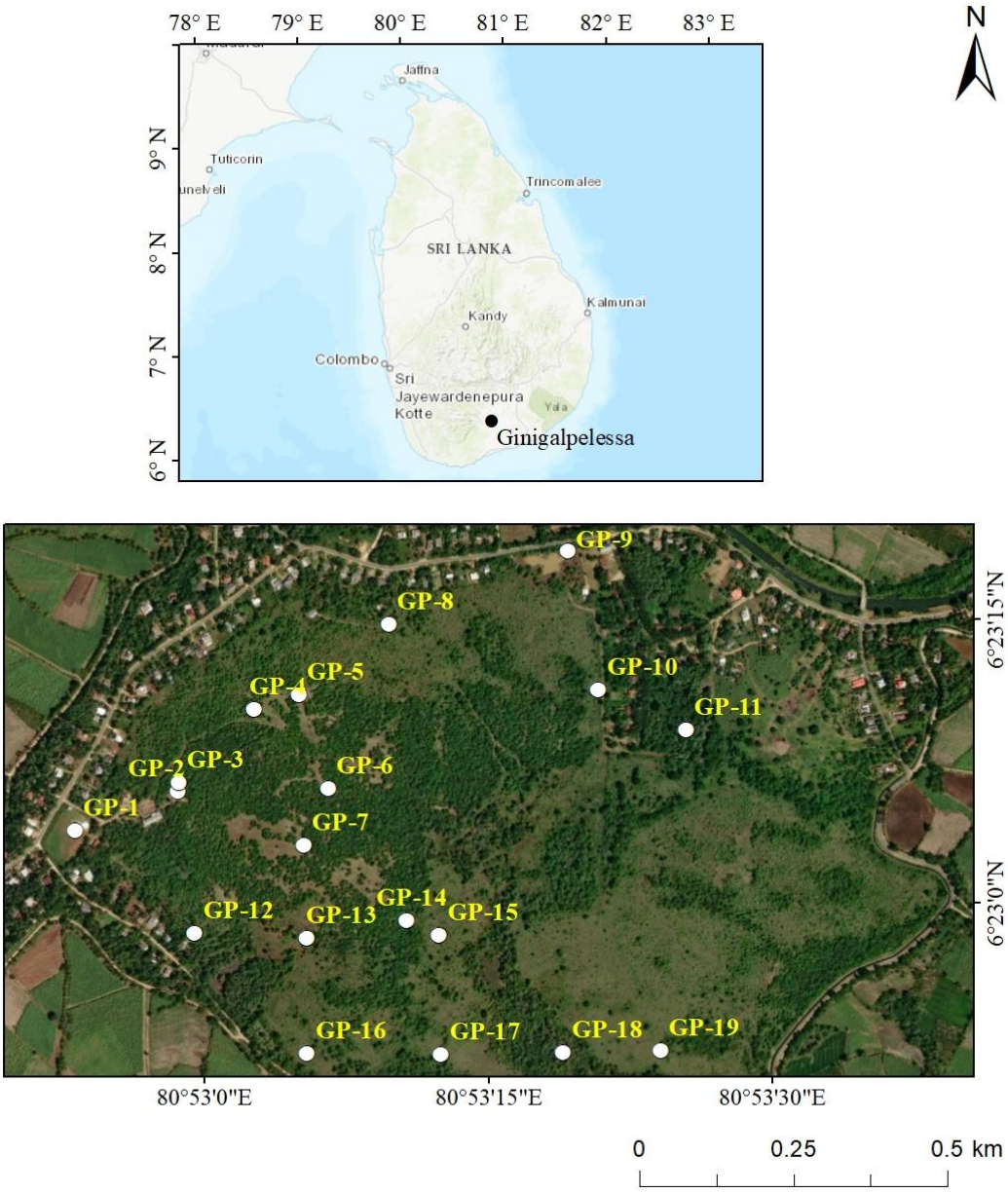

Figure 3.13: Sampling location map of the Ginigalpelessa serpentinite regolith. Source: (Google Earth, 2021)

3.2.3. Beach placers on the northeast coast

Figure 3.14 shows the sampling locations at the Pulmoddai (Figures 3.14a and 3.14b) and Verugal (Figure 3.14c) deposits. A total of 44 beach sand samples were collected systematically from the mean sea level along the coasts of Pulmoddai (n=26) and Verugal (n=18). About 500 g of undisturbed beach sand was collected from each sampling location below the 20 cm surface level.

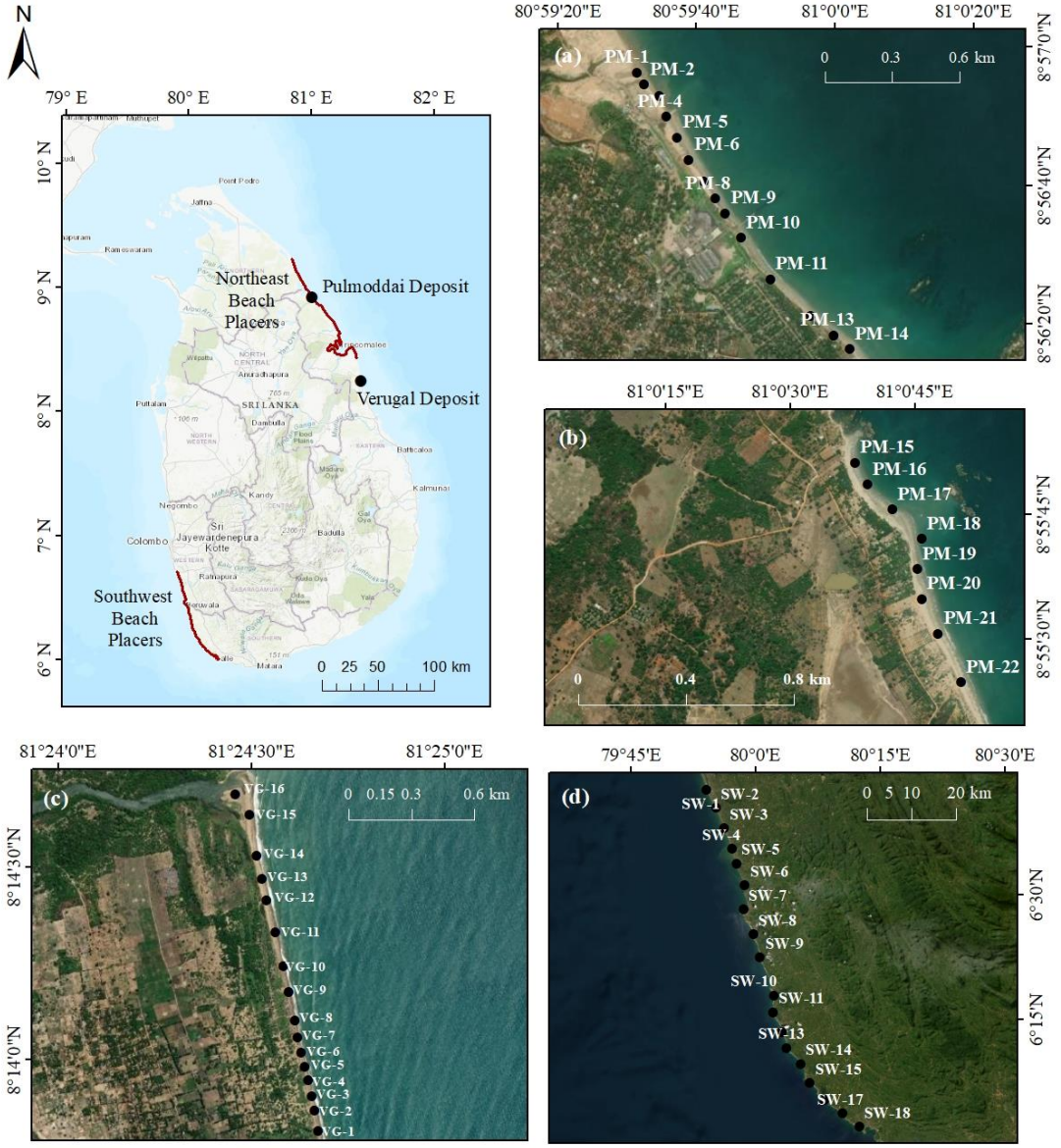

Figure 3.14: Sampling location map of the northeast coast (a), (b) Pulmoddai deposit; (c) Verugal deposit and (d) the southwest coast.

Source: (Google Earth, 2021)

3.2.4. Beach placers along the southwest coast

A total of 18 beach sand samples were collected systematically from the mean sea level along the southwest coast from Panadura to Galle (Figure 3.14d). About 500 g of undisturbed beach sand was collected from each sampling location below the 20 cm surface level.

3.2.5. Alluvial placers in the Walave river basin

In the Walave river basin, 20 sampling locations were selected to collect the stream sediment samples and the sampling locations are illustrated in Figure 3.15. Stream sediment samples were obtained from Walave river (n=7, from WB-WR-1 to WB-WR-7), Belihul Oya (n=9, from WB-BO-1 to WB- BO-9), and Kiriketi Oya (n=4, from WB-KO-1 to WB-KO-4).

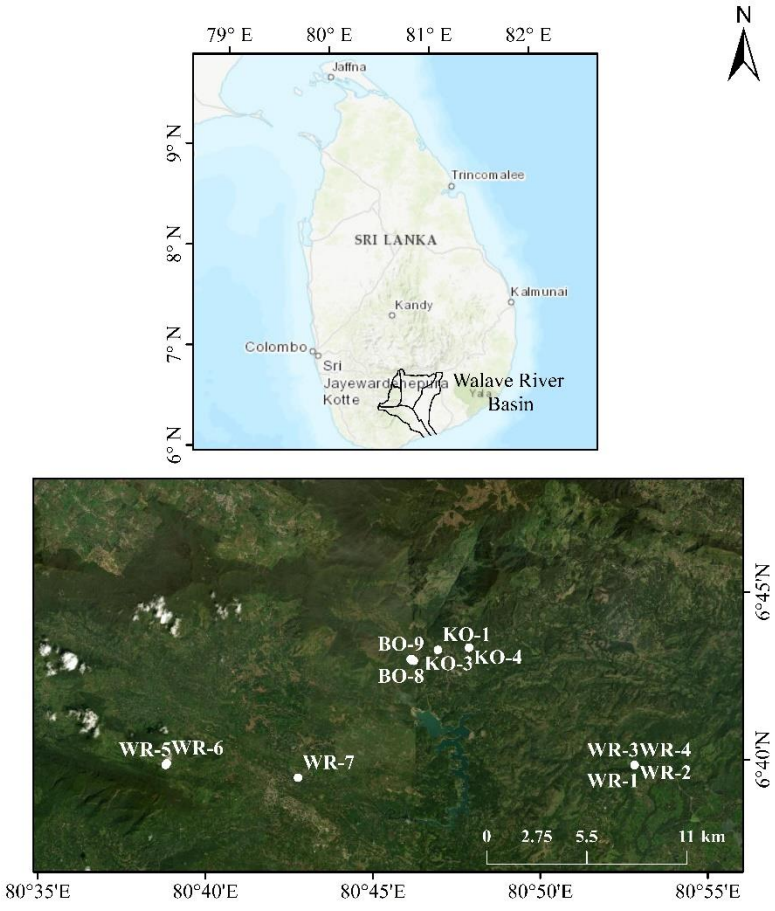

Figure 3.15: Sampling location map of the Walave river basin.
Source: (Google Earth, 2021)

3.2.6. Magmatic deposits

The granitic rocks used for this study were collected from the aforementioned granite bodies in Sri Lanka: Thonigala, Arangala, Massenna, and Ambagaspitiya. From the Thonigala granite, a total of 17 rock samples were collected representing both sub-parallel outcrops (Figure 3.16a). Six rock samples were obtained from the Arangala granite (Figure 3.16b), whereas ten rock samples were collected from two

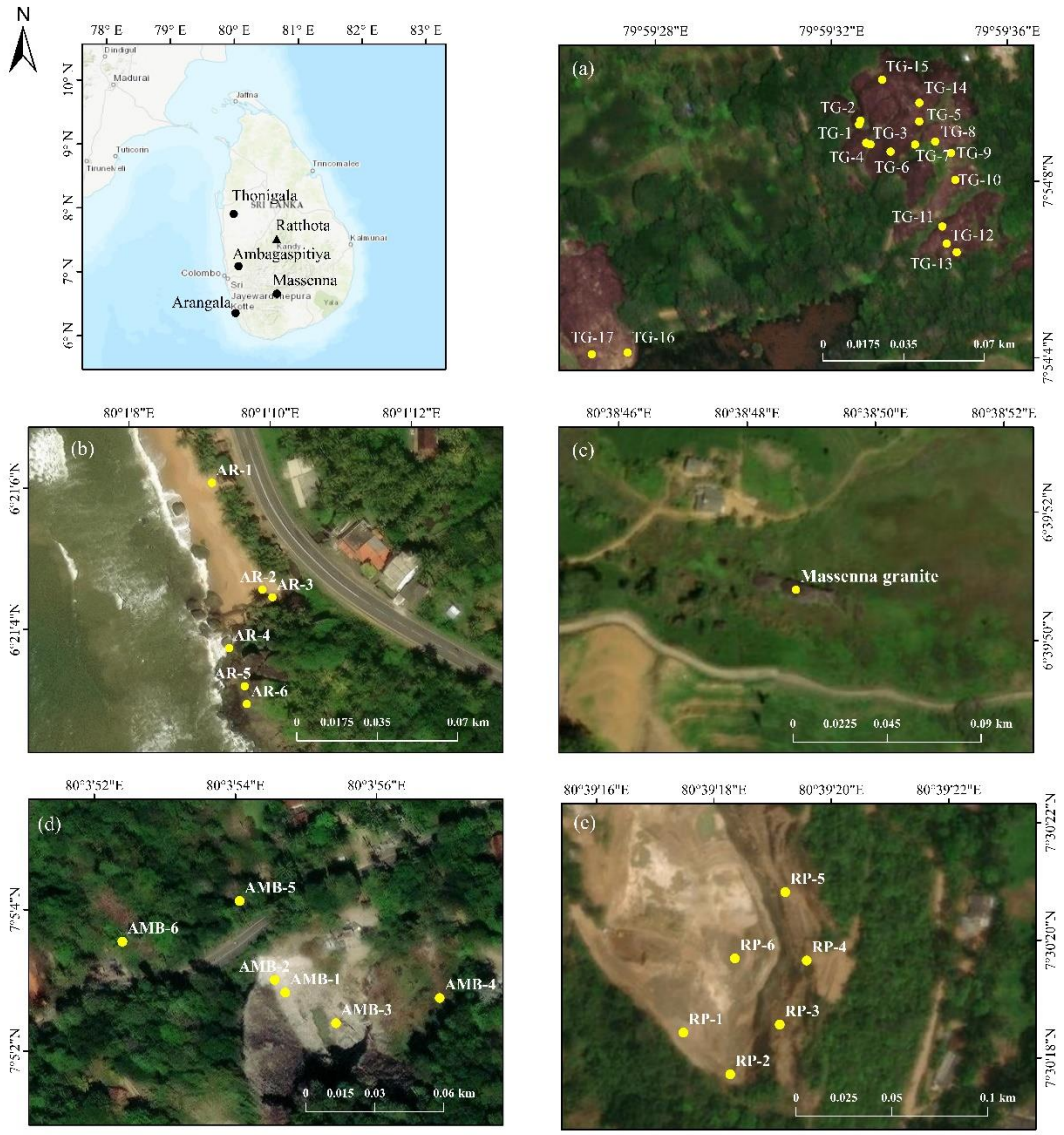

Figure 3.16: Sampling location map of the (a) Thonigala granite; (b) Arangala granite; (c) Massenna granite; (d) Ambagaspitiya granite; (e) Ratthota pegmatite.
Source: (Google Earth, 2021)

exposed outcrops of the Massenna granite across three vertically parallel lines (Figure 3.16c). From the Ambagaspitiya granite, six rock samples were collected (Figure 3.16d), and six rock samples were collected from the Ratthota pegmatite (Figure 3.16e). Figure 3.17 shows field photographs of sample collection in several different geological formations in Sri Lanka.

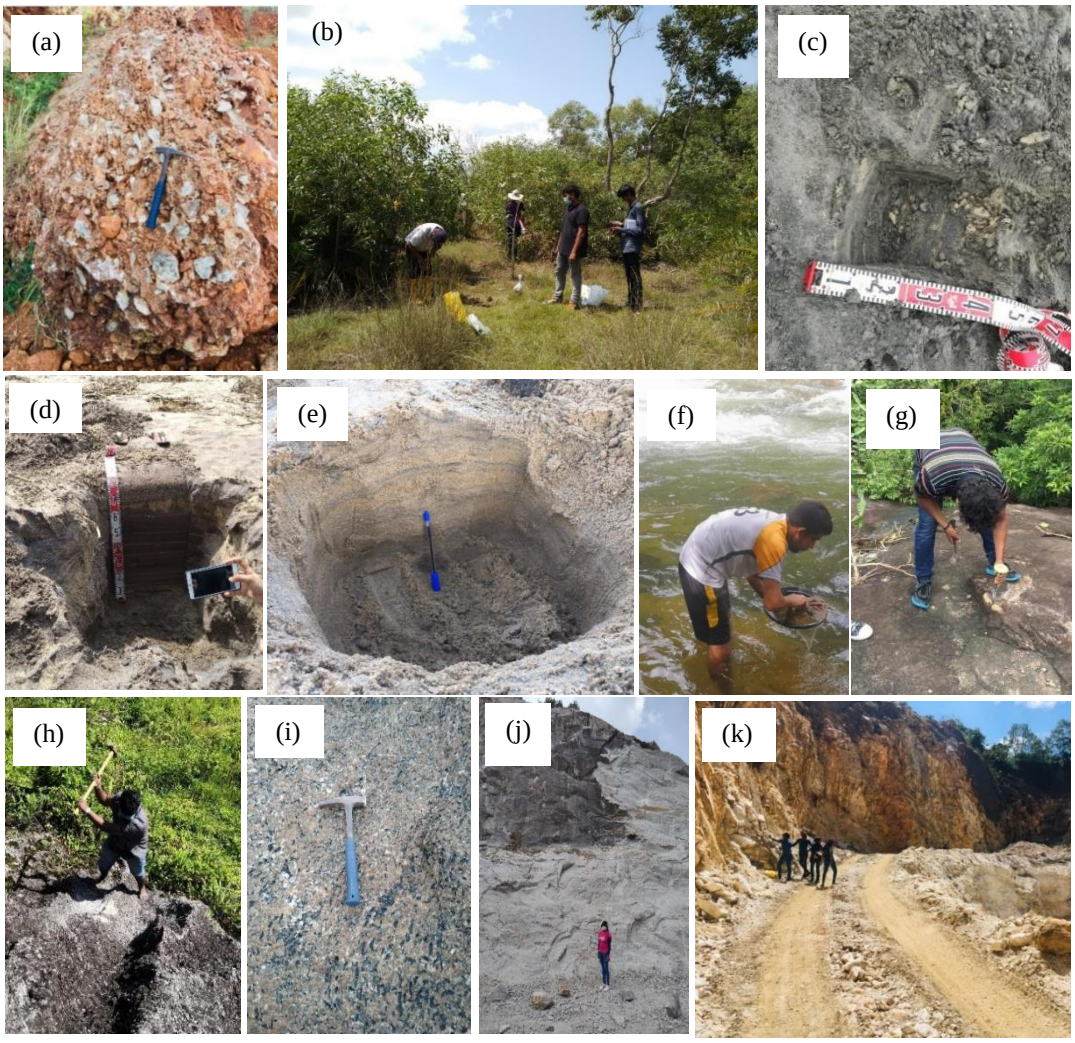

Figure 3.17: Field photographs showing the sample collection in the studied geological formations in Sri Lanka. (a) Weathered regolith at the EPD with embedded large apatite crystals; (b) Soil and rock sample collection from the Ginigalpelessa serpentinite body; Beach sand sampling pits at the (c) Pulmoddai deposit; (d) Verugal deposit; and (e) southwest coast; (f) Stream sediment sampling via panning; (g) Rock sampling at the Thonigala granite; (h) Rock sampling at the Massenna granite; (i) Arangala granitic sample containing biotite; (j) A rock quarry associated with the Ambagaspitiya granite; (k) Rock sampling at the Ratthota pegmatite.

3.3. Sample preparation

All the collected rock samples were air-dried at room temperature while soil and sediment samples were oven dried at 105°C for 24 h. Rock samples were crushed into small pieces by the laboratory Jaw crusher. All the samples were then powdered by the laboratory Tema mill and sieved through a 63 µm sieve to reduce the particle size. Then after, representative samples were obtained using the cone and quartering method. Figure 3.18 presents the sample preparation process carried out for the collected rock, soil, and sediment samples.

Figure 3.18: (a) Powdering rock/soil/sediment samples using the laboratory Tema mill; (b) Sieving through 63 µm sieve to reduce the particles size in samples

3.4. REE analysis using the Inductively Coupled Plasma Mass Spectrometer (ICP-MS)

3.4.1. Sample digestion and dilution

A 0.5 g of each prepared representative sample was measured into a Teflon crucible and treated with HNO_3, HCl, and H_2O_2 in the ratio of 1:3:1 (aqua-regia). The mixture was then heated at 120-130°C for 3 hours. The first dilution was carried out by taking 1 ml of the digested sample (filtered through 0.45 µm syringe filters) and

diluting it to 10 ml with ultrapure water. After that, the diluted sample was again 1:1 diluted with ultrapure water (dilution factor = 1000) (Krzeszowska et al., 2019; Soil & Plant Analysis Laboratory University of Wisconsin, 2005). The diluted samples were then stored in the refrigerator.

3.4.2. Blank sample preparation

A blank sample was prepared to maintain the quality control of sample analysis. Firstly, 1 ml of HNO_3, 3 ml of HCl, and 1 ml of H_2O_2 were measured into a Teflon crucible and heated at 120-130°C for 3 hours. It was then diluted 1000 times with ultrapure water and stored in the refrigerator (Krzeszowska et al., 2019).

3.4.3. Preparation of multi-elemental standard solutions

A multi-elemental standard solution (stock solution) with a concentration of 10 ppm (Sigma-Aldrich, Germany) was used for the preparation of standard solutions. Firstly, an intermediate solution of 500 ppb concentration was prepared from the stock solution. The concentrations of prepared standard solutions were in the range of 1 – 50 ppb (Std A – 1 ppb, Std B – 5 ppb, Std C – 10 ppb, Std D – 25 ppb, and Std E – 50 ppb).

3.4.4. REE analysis by ICP-MS

REE analysis of the prepared samples was carried out by Thermo ICapQ Inductively Coupled Plasma Mass Spectrometer (ICP-MS) (ICapQ-Thermo Fisher, Bremen, Germany) at the analytical laboratory of the Department of Earth Resources Engineering, University of Moratuwa. After checking the operating conditions of the ICP-MS instrument, a standard curve for each element was obtained by feeding the prepared standard solutions to the ICP-MS. If standard curves are correct, prepared blank and samples were fed to ICP-MS, and REE concentrations of the sample solutions were obtained. Figure 3.19 shows the experimental procedure for REE analysis using ICP-MS.

3.4.5. Quality control of the analysis

Certified international reference samples (San Joaquin NIST SRM 2709a from Sigma-Aldrich, Germany) were used to cross-validate the obtained results.

Furthermore, replicate analysis and blanks at every tenth sample were used to maintain the quality control of the analysis. The analytical uncertainty of measurements was ±0.2% (standard deviation).

3.4.6. Back-calculation of actual REE concentrations in the samples

Actual concentrations of REEs in the samples were calculated through the multiplication of REE concentrations in the diluted samples by the dilution factor (1000). REE concentrations of all the analyzed samples were recorded in ppm level.

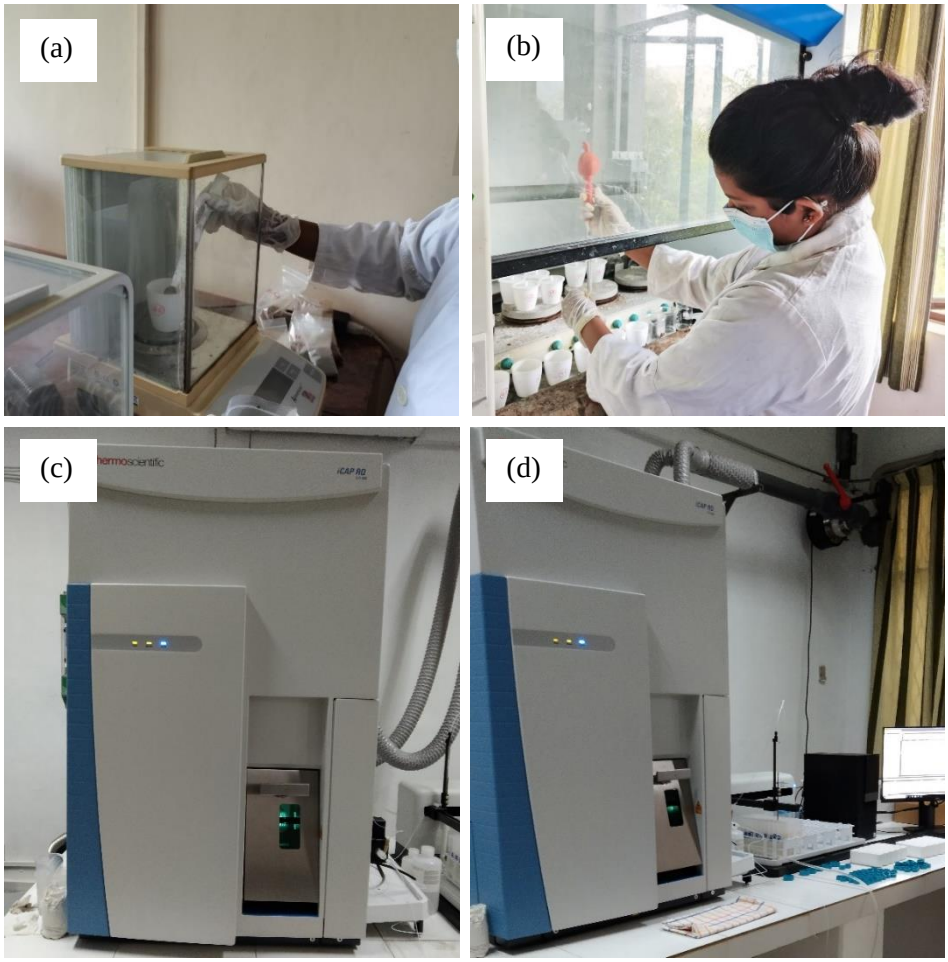

Figure 3.19: (a) Weighing of 0.5 g of each prepared sample; (b) Aqua-regia digestion with adding nitric, hydrochloric, and hydrogen peroxide; (c) ICP-MS instrument; (d) Sample analysis for REE concentrations using the ICP-MS.

3.5. Calculation of chondrite normalized REE concentrations

Chondrite normalized concentrations of individual REEs in each sample of the studied prospects were calculated as follows.

$$\text{Chondrite normalized concentration of X} = \frac{\text{Concentration}_X}{\text{Chondrite value}_X} \quad \text{Eq. (1)}$$

X represents each REE and chondrite values of each element were obtained from McDonough and Sun (1995).

3.6. Calculation of Eu and Ce anomalies

Eu and Ce anomalies of each studied sample were calculated as shown in Eq. (2) and (3).

$$\text{Eu/Eu*} = \frac{Eu_N}{\sqrt{(Sm_N \times Gd_N)}} \quad \text{Eq. (2)}$$

$$\text{Ce/Ce*} = \frac{Ce_N}{\sqrt{(La_N \times Pr_N)}} \quad \text{Eq. (3)}$$

While Eu/Eu* and Ce/Ce* represent the Eu and Ce anomalies, the subscript N denotes the normalization by chondrite values from McDonough and Sun (1995).

CHAPTER 4: RESULTS AND DISCUSSION

In this chapter, REE potential in three major types of geological formations in Sri Lanka, namely residual laterites (carbonatite-associated and serpentinite-associated laterites), placers (beach and alluvial placers), and magmatic deposits (granites and pegmatites) is assessed. Accordingly, REE concentrations and distribution in the Eppawala phosphate deposit, Ginigalpelessa serpentinite deposit, Pulmoddai and Verugal beach placer deposits, beach placers along the southwest coast, alluvial placers in the Walave river basin, granitic intrusions at Thonigala, Massenna, Arangala, and Ambagaspitiya, and pegmatite occurrences at Ratthota, Matale are studied and characterizations of their REE enrichments are discussed in this chapter. Furthermore, a comparative analysis of TREE content, TREO grade, LREE/HREE ratios, and significant individual REE enrichments in these prospects is carried out to identify the most prospective source/s in Sri Lanka, while assessing their position in the global context against similar global occurrences. In addition, the economic potential of the most prospective source is discussed to delineate its possibility to contribute to the local and global supply chains.

4.1. REE content in the studied geological formations

4.1.1. REE content in the Eppawala phosphate deposit

REE content in the EPD can vary depending on the two phosphate components present in the weathering profile (i.e., primary apatite crystals and secondary phosphate matrix). However, the results of this study only reveal minor differences in total REE (TREE) content between primary apatite crystals and secondary phosphate matrix in the EPD. Primary apatite crystals showed TREE contents ranging from 2676 to 6486 mg/kg (avg. = 4072 mg/kg), whereas they were in the range of 3253 to 5120 mg/kg (avg. = 4063 mg/kg) in the secondary phosphate matrix. Similarly, different LREE and HREE contents were observed for the primary apatite crystals and the secondary phosphate matrix in the EPD (primary apatite crystals: LREE = 2325–5698 mg/kg (avg. = 3612 mg/kg), HREE = 313–788 mg/kg (avg. =460 mg/kg); secondary phosphate matrix: LREE = 2768–4509mg/kg (avg. = 3566 mg/kg), HREE = 356–610 mg/kg (avg. = 497 mg/kg)) (Table 4.1). In comparison to REE contents in the

phosphates, carbonatite source rock at the EPD showed rather low contents of TREEs, LREEs, and HREEs. The northern carbonatite at the EP-11 sample location contained TREE, LREE, and HREE contents of 959 mg/kg, 837 mg/kg, and 122 mg/kg, respectively. Relatively low TREE (742 mg/kg) and LREE (614 mg/kg) contents were evident in the southern carbonatite at the EP-19 sample location while HREE content (129 mg/kg) was a little higher than in northern carbonatite.

The individual REE content trends in both primary apatite crystals and secondary phosphate matrix followed a decreasing order of Ce > La > Nd > Pr > Gd > Sm > Y > Er > Dy > Tb > Eu > Yb > Ho > Tm > Lu with the highest concentrations reported for Ce (1565 mg/kg for apatite crystals, 1507 mg/kg for secondary phosphate matrix) and Lu has the lowest concentrations of 2.2 mg/kg (apatite crystals) and 3.1 mg/kg (secondary phosphate matrix). The average ratio of LREE/HREE in apatite crystals was approximately 7.9, whereas the secondary phosphate matrix had a ratio of 7.2 (Table 4.1).

Figure 4.1 illustrates the chondrite normalized REE distribution plots of apatite crystals, secondary phosphate matrix, and carbonatite rock in the EPD. It is observed that apatite crystals, secondary phosphate matrix, and carbonatite rock followed similar REE distribution patterns. However, REE contents of the Eppawala carbonatites were ten times lower than that of apatite crystals and secondary phosphate matrix. Furthermore, the LREE distribution of the present study almost followed the same pattern as from Pitawala et al. (2003) and Manthilake et al. (2008), while the HREE contents were higher in the current study.

Eu anomalies (Eu/Eu*) of apatite crystals and secondary phosphate matrix ranged between 0.30–0.47 and 0.29–0.65, respectively, whereas Ce anomalies (Ce/Ce*) of apatite crystals and secondary phosphate matrix were in the range of 0.37–0.63 and 0.40–0.62 (Table 4.1). Since all the samples of both apatite crystals and secondary phosphate matrix components displayed Eu/Eu* and Ce/Ce* values less than unity, we can generally characterize the leached zone of the EPD by negative Eu and Ce anomalies.

Table 4.1: REE concentrations (mg/kg) of apatite crystals, secondary phosphate matrix, and carbonatite rock samples in the Eppawala phosphate deposit (*Apatite Crystals were not found in the sampling locations EP12 and EP17)

Element	Apatite Crystals*														
	EP-1	**EP-2**	**EP-3**	**EP-4**	**EP-5**	**EP-6**	**EP-7**	**EP-8**	**EP-9**	**EP-10**	**EP-11**	**EP-13**	**EP-14**	**EP-15**	**EP-16**
La	729.1	719.1	1055.6	675.0	596.9	851.7	1070.3	896.3	1071.5	974.4	724.1	865.3	636.0	724.3	961.0
Ce	1901.5	1759.0	2732.8	989.9	952.0	1414.2	1736.8	1487.0	1695.6	1560.8	1830.3	1861.4	971.0	1183.1	1575.5
Pr	236.6	225.6	335.3	193.0	176.9	252.8	310.0	257.1	285.8	289.3	231.1	264.2	185.0	214.9	281.4
Nd	922.7	866.1	1333.1	489.9	464.7	654.9	810.7	717.8	746.6	776.8	894.4	911.5	477.3	559.8	732.8
Sm	126.1	114.0	196.1	127.0	109.8	161.1	204.1	168.4	178.0	184.4	120.1	161.6	118.4	135.5	182.6
Eu	29.4	26.4	45.2	26.8	24.4	36.5	47.8	38.6	42.2	43.6	27.9	36.0	25.6	30.5	42.2
Gd	202.7	195.0	285.3	108.4	153.1	140.8	170.5	140.6	150.0	140.8	198.9	196.9	130.8	147.0	155.7
Tb	39.0	36.3	57.6	31.8	29.0	42.8	50.8	41.3	46.2	44.9	37.7	44.7	30.4	35.9	46.8
Dy	41.8	36.3	66.1	40.1	37.5	53.1	64.3	53.3	57.6	58.4	39.1	53.1	38.8	45.3	58.7
Ho	7.2	6.3	11.8	6.9	6.0	9.2	10.8	8.9	10.3	10.8	6.8	9.4	6.5	7.6	10.0
Er	57.5	49.0	84.5	42.4	38.3	54.0	69.5	56.3	60.4	58.9	53.3	63.5	40.4	46.2	61.8
Tm	2.5	2.1	4.0	2.0	2.0	2.8	3.3	2.9	3.3	3.3	2.3	3.0	2.0	2.4	3.1
Yb	22.2	17.6	32.9	15.7	14.7	20.7	24.8	21.5	23.8	23.1	19.9	24.3	15.2	17.7	22.8
Lu	2.2	1.7	3.4	1.7	1.5	2.3	2.6	2.4	2.5	2.5	2.0	2.6	1.6	1.9	2.5
Y	143.8	117.4	242.7	64.0	69.2	92.3	112.1	97.4	114.3	107.7	130.6	153.4	66.6	80.8	102.2
LREE	3945.3	3710.2	5698.1	2501.6	2324.7	3371.3	4179.6	3565.2	4019.8	3829.2	3827.8	4099.9	2413.2	2848.0	3775.5
HREE	518.9	461.7	788.2	313.0	351.3	417.9	508.7	424.5	468.5	450.4	490.3	550.6	332.2	384.6	463.3
TREE	4464.3	4171.9	6486.3	2814.7	2676.0	3789.2	4688.3	3989.7	4488.2	4279.6	4318.1	4650.5	2745.4	3232.6	4238.8
LREE/HREE	7.6	8.0	7.2	8.0	6.6	8.1	8.2	8.4	8.6	8.5	7.8	7.6	7.3	7.4	8.2
Eu/Eu*	0.32	0.30	0.33	0.39	0.32	0.42	0.44	0.43	0.44	0.47	0.31	0.36	0.36	0.37	0.43
Ce/Ce*	0.62	0.60	0.63	0.37	0.40	0.42	0.41	0.42	0.42	0.40	0.61	0.50	0.39	0.41	0.42

Element	Apatite Crystals*														
	EP-18	EP-19	EP-20	EP-21	EP-22	EP-23	EP-24	EP-25	EP-26	EP-27	EP-28	EP-29	EP-30	EP-1	EP-2
La	983.9	1023.0	805.7	876.3	750.6	680.1	842.7	972.2	794.8	798.5	853.8	972.5	1003.1	744.4	755.5
Ce	1591.3	1628.2	2038.1	2053.6	1416.2	1077.0	1379.3	1593.7	1522.2	1273.2	1397.5	1583.4	1620.1	1843.8	1945.3
Pr	271.5	287.6	255.8	272.3	224.6	199.9	248.1	282.5	239.5	233.2	249.2	276.4	285.6	239.1	244.4
Nd	732.2	761.7	997.0	1005.6	694.4	518.6	646.3	748.5	735.7	605.1	662.0	732.5	763.0	899.2	970.4
Sm	173.2	181.2	137.6	158.3	140.0	126.9	159.0	184.4	148.5	150.5	160.9	177.9	183.7	127.4	133.4
Eu	40.4	42.9	31.9	35.9	30.8	28.0	36.3	42.7	33.2	33.9	36.8	41.3	43.1	29.0	29.2
Gd	145.3	145.4	219.5	218.5	163.8	138.9	151.3	155.6	171.9	143.2	151.3	150.5	150.5	205.1	218.4
Tb	43.8	45.6	42.3	45.8	37.6	33.2	41.4	46.4	40.3	38.6	41.0	45.3	45.8	37.7	38.6
Dy	55.5	58.0	45.1	52.2	46.0	42.1	52.0	58.8	49.2	48.8	52.1	57.1	58.4	41.2	43.1
Ho	9.6	10.6	7.9	9.2	7.9	7.0	8.8	9.9	8.5	8.2	8.7	9.8	10.2	6.8	7.3
Er	58.4	59.7	60.0	65.1	51.9	43.3	54.0	62.3	54.8	51.1	54.5	60.1	61.3	58.2	59.6
Tm	3.1	3.3	2.7	3.0	2.5	2.2	2.7	3.1	2.7	2.5	2.8	3.1	3.2	2.2	2.3
Yb	22.7	23.5	22.6	24.8	19.8	16.5	20.2	23.0	21.0	19.0	20.4	22.7	23.3	21.0	21.6
Lu	2.5	2.5	2.3	2.6	2.1	1.8	2.2	2.5	2.2	2.0	2.2	2.5	2.5	2.0	2.0
Y	105.9	111.0	155.3	166.7	110.0	73.7	91.5	103.5	117.1	84.4	92.8	104.0	107.9	136.9	141.7
LREE	3792.5	3924.5	4266.0	4402.0	3256.5	2630.6	3311.7	3823.9	3473.9	3094.3	3360.2	3784.0	3898.5	3882.9	4078.2
HREE	446.5	459.5	557.6	587.8	441.4	358.4	424.0	465.0	467.6	397.7	425.6	454.9	463.0	511.2	534.7
TREE	4239.0	4383.9	4823.6	4989.8	3697.9	2989.0	3735.7	4288.9	3941.6	3492.1	3785.8	4238.9	4361.5	4394.1	4612.9
LREE/HREE	8.5	8.6	7.7	7.6	7.5	7.3	7.8	8.2	7.5	7.7	7.8	8.3	8.4	7.6	7.6
Eu/Eu*	0.44	0.46	0.31	0.34	0.36	0.36	0.40	0.43	0.37	0.39	0.40	0.43	0.45	0.31	0.29
Ce/Ce*	0.42	0.41	0.61	0.56	0.44	0.40	0.41	0.42	0.46	0.40	0.41	0.42	0.41	0.60	0.62

Element	Secondary Phosphate Matrix														
	EP-3	EP-4	EP-5	EP-6	EP-7	EP-8	EP-9	EP-10	EP-11	EP-12	EP-13	EP-14	EP-15	EP-16	EP-17
La	1099.6	755.2	710.4	1090.5	793.7	774.2	974.9	664.4	750.0	927.6	927.4	732.8	900.5	942.1	784.0

Ce	1869.9	1249.0	1158.1	1787.6	1269.8	1269.5	1650.6	1133.4	1894.6	1907.6	1559.5	1203.6	1472.9	1528.7	1269.7
Pr	325.7	230.5	208.7	316.8	234.1	229.9	319.0	200.9	241.8	285.1	278.1	219.6	262.8	275.5	232.0
Nd	922.7	626.4	554.3	835.9	602.3	612.4	804.7	565.0	934.8	946.6	774.6	590.4	695.1	719.1	607.4
Sm	233.3	182.6	143.1	213.9	150.4	157.2	223.9	159.1	130.4	183.4	208.0	162.9	178.5	182.2	153.8
Eu	58.1	57.9	37.9	52.2	34.8	36.0	52.8	44.8	29.1	43.7	58.0	47.9	45.1	43.5	35.4
Gd	167.9	127.6	163.4	155.5	175.6	104.3	142.3	168.7	211.8	193.2	147.8	145.5	159.5	165.6	140.0
Tb	53.6	41.6	33.8	50.2	34.7	37.3	48.4	34.6	38.2	46.1	47.6	37.7	42.0	42.5	36.0
Dy	78.5	74.3	52.1	68.7	46.0	46.4	74.7	64.4	42.2	60.8	76.4	63.2	60.4	57.4	46.2
Ho	14.6	14.2	9.6	12.6	8.1	8.5	13.9	11.9	7.1	11.0	14.4	11.9	11.1	10.4	8.3
Er	75.4	65.6	49.5	67.6	49.7	51.2	74.2	58.0	58.9	67.5	70.5	57.6	58.6	58.7	50.5
Tm	5.2	5.2	3.1	4.2	2.6	2.5	4.9	4.6	2.3	3.8	5.2	4.2	3.7	3.4	2.6
Yb	33.3	34.5	21.5	29.0	19.2	19.2	33.6	30.2	21.3	27.5	33.9	28.0	25.3	24.1	19.2
Lu	4.2	4.8	2.6	3.2	2.0	2.1	4.3	4.0	2.0	3.1	4.5	3.7	2.9	2.6	2.1
Y	177.5	194.4	105.0	127.6	77.3	84.4	142.0	143.3	139.3	159.6	186.0	149.7	116.3	102.5	80.9
LREE	4509.3	3101.6	2812.5	4297.1	3085.0	3079.1	4025.9	2767.6	3980.6	4293.8	3805.5	2957.1	3554.8	3691.1	3082.1
HREE	610.2	562.2	440.7	518.6	415.1	355.8	538.2	519.9	523.0	572.5	586.2	501.5	479.7	466.9	385.5
TREE	5119.5	3663.8	3253.3	4815.7	3500.1	3434.9	4564.1	3287.5	4503.5	4866.2	4391.7	3458.6	4034.5	4157.9	3467.5
LREE/HREE	7.4	5.5	6.4	8.3	7.4	8.7	7.5	5.3	7.6	7.5	6.5	6.0	7.4	7.9	8.1
Eu/Eu*	0.51	0.65	0.43	0.49	0.37	0.48	0.51	0.47	0.30	0.40	0.58	0.54	0.46	0.43	0.43
Ce/Ce*	0.43	0.41	0.41	0.42	0.40	0.41	0.40	0.42	0.61	0.53	0.42	0.41	0.42	0.41	0.41
Element	**Secondary Phosphate Matrix**													**Carbonatite**	
	EP-18	**EP-19**	**EP-20**	**EP-21**	**EP-22**	**EP-23**	**EP-24**	**EP-25**	**EP-26**	**EP-27**	**EP-28**	**EP-29**	**EP-30**	**EP-11**	**EP-19**
La	874.6	819.7	838.8	927.5	830.1	816.6	921.3	863.0	913.9	837.5	842.2	908.3	801.8	185.395	134.908
Ce	1460.1	1392.0	1901.1	1733.5	1381.5	1338.2	1500.8	1399.2	1516.2	1366.1	1371.3	1494.4	1330.8	290.378	218.294
Pr	274.5	260.0	263.4	281.6	248.9	241.2	269.1	253.7	270.4	247.5	247.4	275.0	246.0	55.217	36.531
Nd	708.6	684.9	940.7	860.6	682.5	642.7	707.1	663.2	734.8	654.7	651.2	713.8	646.1	256.263	184.236
Sm	190.6	191.5	156.9	195.7	185.4	170.7	180.3	168.0	193.2	172.5	166.2	186.4	172.7	40.73	31.32

Eu	44.4	48.8	36.4	50.8	53.0	46.5	44.3	39.5	51.5	45.7	40.2	44.0	42.1	9.313	8.3
Gd	123.3	155.5	202.5	170.5	146.6	152.5	162.5	152.8	153.6	155.5	149.7	144.4	147.7	48.681	33.881
Tb	42.9	41.5	42.1	46.9	42.7	39.9	42.2	39.2	44.8	40.1	39.0	42.7	38.8	9.349	6.936
Dy	60.6	69.6	51.5	68.6	69.8	61.8	58.9	51.8	68.4	60.3	53.3	59.0	57.9	13.632	12.172
Ho	11.2	12.9	9.0	12.7	13.2	11.5	10.7	9.3	12.8	11.1	9.7	10.8	10.6	2.419	2.388
Er	62.7	66.1	63.2	69.0	64.0	58.1	58.6	54.6	64.5	58.1	54.5	60.7	58.3	13.444	11.005
Tm	3.7	4.8	3.0	4.5	4.7	3.9	3.5	3.0	4.4	3.8	3.1	3.6	3.7	0.893	0.946
Yb	26.4	31.9	24.4	30.7	31.0	26.6	24.7	21.7	29.6	26.1	22.2	25.3	25.6	5.87	5.793
Lu	3.2	4.2	2.6	3.8	4.1	3.3	2.8	2.3	3.7	3.2	2.5	2.9	3.1	0.694	0.794
Y	113.2	142.7	149.5	172.8	167.8	133.0	109.4	91.7	151.1	126.1	98.6	107.8	111.8	27.027	54.959
LREE	3552.5	3396.8	4137.2	4049.6	3381.3	3255.9	3622.9	3386.6	3680.1	3324.1	3318.4	3621.8	3239.4	837.3	613.6
HREE	447.0	529.1	547.7	579.3	543.8	490.6	473.3	426.2	532.9	484.2	432.6	456.9	457.3	122.0	128.9
TREE	3999.5	3925.8	4684.9	4628.9	3925.1	3746.5	4096.2	3812.7	4213.1	3808.2	3751.0	4078.7	3696.7	959.3	742.5
LREE/HREE	8.1	6.4	7.6	7.0	6.2	6.7	7.6	8.0	6.9	6.9	7.7	8.0	7.2	6.9	4.8
Eu/Eu*	0.50	0.49	0.35	0.49	0.56	0.50	0.45	0.43	0.52	0.49	0.44	0.46	0.46	0.36	0.42
Ce/Ce*	0.41	0.41	0.57	0.47	0.42	0.41	0.41	0.41	0.42	0.41	0.41	0.41	0.41	0.39	0.14

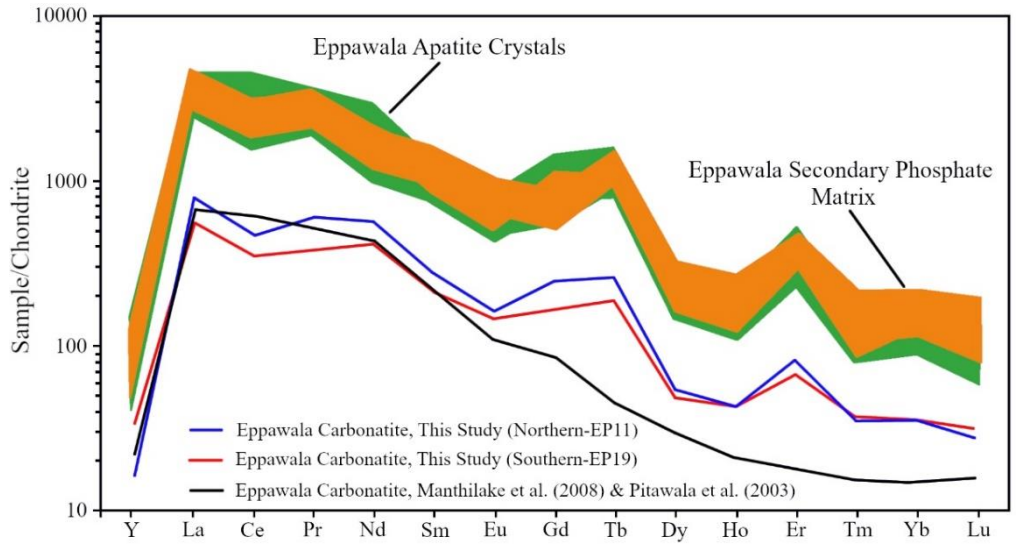

Figure 4.1: Chondrite-normalized REE distribution patterns of apatite crystals (28 samples), secondary phosphate matrix (30 samples), and carbonatite (2 samples) in the Eppawala phosphate deposit. Reference REE contents in the carbonatite are taken from Pitawala et al. (2003) and Manthilake et al. (2008), and Chondrite values are from McDonough and Sun (1995).

4.1.2. REE content in Ginigalpelessa serpentinite regolith

TREE concentrations of soil at the Ginigalpelessa serpentinite deposit ranged from 19.29 to 143 mg/kg, with an average of 90.50 mg/kg (Table 4.2). Moreover, the LREE and HREE contents of serpentine soil were in the ranges of 13.48–95.12 mg/kg (avg. = 51.39 mg/kg) and 5.81–47.55 mg/kg (avg. =25.44 mg/kg), respectively. In contrast, TREE contents of the collected rock samples from the Ginigalpelessa serpentinite regolith were very low ranging from 0.59 to 30.89 mg/kg, with an average of 5.72 mg/kg. Similarly, very low contents of LREEs and HREEs were observed in the serpentinite rocks in the ranges of 0.28-21.41 (avg. = 4.04 mg/kg) and 0.25-9.49 mg/kg (avg. = 1.68 mg/kg). The individual REE content trends in the Ginigalpelessa serpentinite deposit generally followed a decreasing order of Ce > Gd > Nd > La > Y > Sm > Dy > Pr > Eu > Er > Yb > Tb > Ho > Tm > Lu with the highest concentrations reported for Ce (27.63 mg/kg for serpentine soil, 1.41 mg/kg for serpentinite rocks) and Lu has the lowest concentrations of 0.17 mg/kg (serpentine soil) and 0.015 mg/kg (serpentinite rocks). The average ratio of LREE/HREE in serpentine soil was

Table 4.2: REE concentrations (mg/kg) of soil and rock samples in the Ginigalpelessa serpentinite regolith (*Rock samples were not found in the locations GP-11, GP-13, GP-14, GP-16, GP-17, and GP-19)

Element	Serpentine soil																
	GP-1	GP-2	GP-3	GP-4	GP-5	GP-6	GP-7	GP-8	GP-9	GP-10	GP-11	GP-12	GP-13	GP-14	GP-15	GP-16	GP-17
La	9.68	9.93	9.68	7.94	9.77	12.75	5.50	18.95	16.15	10.79	11.74	9.56	3.26	5.38	8.57	3.79	8.02
Ce	27.05	30.91	26.86	31.39	34.75	36.58	21.28	25.16	44.47	24.73	25.78	21.18	7.49	12.38	20.60	12.11	17.35
Pr	2.54	2.37	2.42	2.24	2.42	2.62	2.12	2.46	3.87	2.10	2.55	2.33	0.76	1.18	1.96	0.96	2.28
Nd	14.10	13.76	14.46	13.64	19.96	23.56	10.46	12.36	22.76	11.97	12.90	12.37	4.09	6.47	10.87	5.66	12.01
Sm	3.72	3.14	3.65	5.06	3.95	6.45	2.23	3.63	5.56	3.78	2.54	2.93	1.24	1.68	2.69	2.36	2.76
Eu	1.40	1.34	1.35	1.52	1.48	1.70	1.14	1.31	2.30	1.74	0.88	1.29	0.57	0.74	1.09	1.39	0.84
Gd	13.13	15.78	21.03	21.14	22.43	23.50	10.20	15.80	23.81	12.83	13.70	10.91	4.16	6.78	10.13	6.09	9.64
Tb	0.61	0.45	0.84	0.45	0.85	1.12	0.28	0.62	0.92	0.36	0.44	0.48	0.14	0.21	0.38	0.21	0.59
Dy	3.07	2.29	3.22	3.19	3.36	4.28	1.32	3.26	4.32	1.95	2.32	2.57	0.79	1.03	1.83	1.02	2.97
Ho	0.39	0.29	0.35	0.30	0.46	0.74	0.29	0.24	0.57	0.21	0.29	0.28	0.10	0.09	0.20	0.12	0.46
Er	1.35	1.13	1.19	1.13	1.16	1.22	0.96	1.12	2.29	0.97	1.09	0.97	0.37	0.48	0.85	0.37	1.47
Tm	0.16	0.12	0.24	0.27	0.17	0.59	0.12	0.16	0.27	0.10	0.12	0.12	0.06	0.08	0.10	0.06	0.16
Yb	0.94	0.67	0.92	0.93	0.83	0.98	0.74	0.60	1.56	0.60	0.74	0.81	0.26	0.28	0.51	0.32	1.10
Lu	0.15	0.12	0.26	0.16	0.18	0.32	0.19	0.31	0.25	0.08	0.12	0.14	0.04	0.05	0.09	0.06	0.19
Y	9.27	6.83	9.38	9.57	10.98	11.66	5.34	8.91	13.57	4.76	6.80	6.34	2.10	2.59	4.12	2.73	10.45
LREE	58.49	61.46	58.42	61.80	72.33	83.66	42.72	63.86	95.12	55.11	56.38	49.66	17.40	27.83	45.78	26.26	43.25
HREE	29.08	27.66	37.42	37.13	40.42	44.41	19.44	31.02	47.55	21.86	25.63	22.64	8.00	11.59	18.19	10.99	27.03
TREE	87.56	89.12	95.84	98.93	112.8	128.1	62.16	94.87	142.7	76.97	82.01	72.29	25.40	39.41	63.97	37.25	70.27
LREE/HREE	2.0	2.2	1.6	1.7	1.8	1.9	2.2	2.1	2.0	2.5	2.2	2.2	2.2	2.4	2.5	2.4	1.6
Eu/Eu*	0.34	0.33	0.26	0.25	0.27	0.24	0.41	0.30	0.34	0.43	0.26	0.39	0.43	0.38	0.36	0.63	0.28
Ce/Ce*	0.74	0.87	0.76	1.02	0.98	0.86	0.85	0.50	0.77	0.71	0.64	0.61	0.65	0.67	0.69	0.87	0.55

Element			Serpentinite rocks*												
	GP-18	GP-19	GP-1	GP-2	GP-3	GP-4	GP-5	GP-6	GP-7	GP-8	GP-9	GP-10	GP-12	GP-15	GP-18
La	7.61	2.35	1.86	0.585	1.87	0.67	0.56	0.29	0.37	0.267	0.28	0.043	0.32	4.09	0.26
Ce	18.16	6.11	2.774	0.611	2.41	0.76	0.36	0.51	0.34	0.448	0.34	0.119	0.35	9.20	0.09
Pr	1.70	0.51	0.364	0.095	0.39	0.09	0.15	0.021	0.06	0.022	0.02	Bdl	0.06	0.91	0.04
Nd	9.62	2.92	1.9	0.505	1.75	0.52	0.94	0.226	0.26	0.205	0.17	0.076	0.33	4.88	0.23
Sm	4.17	1.08	0.527	0.527	0.67	0.53	0.17	0.095	0.14	0.583	0.12	0.02	0.16	1.56	0.24
Eu	2.17	0.52	0.165	0.318	0.19	0.35	0.43	0.063	0.15	0.387	0.08	0.017	0.12	0.76	0.19
Gd	9.59	3.35	1.445	0.418	1.42	0.36	0.17	0.304	0.16	0.176	0.18	0.097	0.19	5.04	0.05
Tb	0.36	0.10	0.064	0.032	0.06	0.04	0.02	0.007	0.02	0.008	0.02	0.008	0.01	0.17	0.01
Dy	1.48	0.48	0.439	0.06	0.42	0.05	0.07	Bdl	0.01	0.06	0.04	0.036	0.01	0.86	0.03
Ho	0.19	0.05	0.055	0.014	0.07	0.02	0.09	0.002	0.01	0.003	Bdl	0.009	0.01	0.11	0.01
Er	0.80	0.24	0.137	0.063	0.14	0.08	0.13	Bdl	0.02	0.022	0.01	0.022	0.02	0.43	0.01
Tm	0.12	0.03	0.03	0.011	0.02	0.01	0.10	0.002	Bdl	0.008	Bdl	0.002	Bdl	0.07	0.01
Yb	0.52	0.16	0.116	0.058	0.12	0.07	0.11	0.007	Bdl	0.007	0.01	0.03	Bdl	0.23	0.02
Lu	0.08	0.03	0.02	0.013	0.01	0.01	0.01	Bdl	Bdl	0.007	Bdl	0.008	Bdl	0.05	0.01
Y	4.45	1.37	1.194	0.497	1.19	0.32	0.45	0.086	0.03	0.056	Bdl	0.111	0.04	2.54	0.20
LREE	43.43	13.48	7.59	2.64	7.28	2.92	2.61	1.21	1.31	1.91	1.00	0.28	1.34	21.41	1.05
HREE	17.58	5.81	3.50	1.17	3.43	0.95	1.14	0.41	0.25	0.35	0.26	0.32	0.28	9.49	0.34
TREE	61.02	19.29	11.09	3.81	10.71	3.87	3.75	1.61	1.57	2.26	1.26	0.60	1.62	30.89	1.39
LREE/HREE	2.5	2.3	2.2	2.3	2.1	3.1	2.3	3.0	5.2	5.5	3.9	0.9	4.8	2.3	3.1
Eu/Eu*	0.59	0.47	0.33	1.17	0.34	0.57	4.35	1.80	1.88	1.21	0.96	2.08	1.18	0.47	2.88
Ce/Ce*	0.69	0.77	0.46	0.35	0.27	0.23	0.17	0.22	0.10	0.12	0.60	0.80	0.33	0.65	0.13

Bdl – Below detection limit

approximately 2.1, whereas the serpentinite rocks had a ratio of 3.1 (Table 4.2).

According to Figure 4.2, the chondrite normalized REE distribution patterns of all the serpentine soil samples at the Ginigalpelessa deposit generally followed the same trend, where La and Gd showed distinctive positive anomalies. The average chondrite normalized REE distribution pattern of Ginigalpelessa serpentinite rocks also displayed the same trend as of serpentine soil, however, REEs were about 10 times more enriched in the regolith compared to the serpentinite rocks in the vicinity. Eu/Eu* of soil and rocks in the Ginigalpelessa serpentinite deposit ranged between 0.24–0.63 and 0.33–4.35, respectively, whereas Ce/Ce* were in the range of 0.50–1.02 and 0.10–0.80 (Table 4.2). Therefore, serpentine soils at the Ginigalpelessa can be characterized with negative Eu and Ce anomalies (value<1), while serpentinite rocks may have positive Eu anomalies (value>1) with negative Ce anomalies.

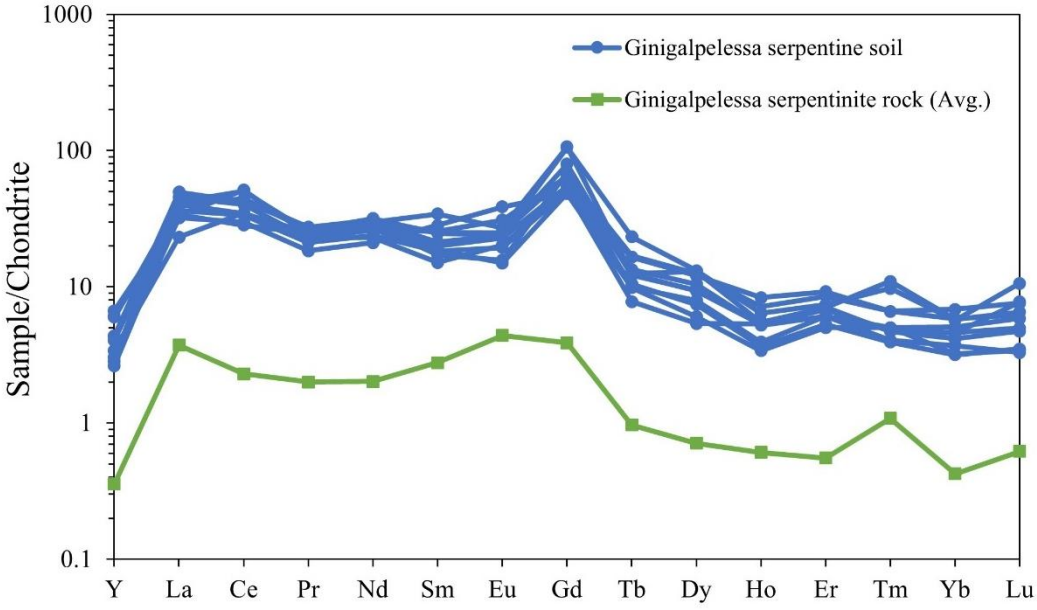

Figure 4.2: Chondrite-normalized REE distribution patterns of soil (19 samples) and rocks (13 samples) in the Ginigalpelessa serpentinite deposit.

4.1.3. REE content in Pulmoddai and Verugal deposits

Table 4.3 shows REE, Th, and U concentrations in the beach placer deposits along the northeast coast (Verugal and Pulmoddai deposits). TREE contents in the Verugal deposit ranged between 144–612 mg/kg (avg. = 274 mg/kg), whereas they were relatively enriched in the Pulmoddai deposit ranging from 137 – 2996 mg/kg

(avg. = 454 mg/kg). In addition, LREE and HREE concentrations in the Verugal deposit were in the range of 106–500 mg/kg (avg. = 215 mg/kg) and 38.98–112 mg/kg (avg. =58.78 mg/kg), respectively. In the Pulmoddai deposit, LREE and HREE concentrations ranged between 93.97–2608 mg/kg (avg. = 359 mg/kg) and 39.95–387 mg/kg (avg. = 94.84 mg/kg), respectively.

Ce was the dominant REE found in both Verugal and Pulmoddai deposits (Verugal deposit: 103 mg/kg, Pulmoddai deposit: 175 mg/kg) while the least abundant REE was Tm (Verugal deposit: 0.35 mg/kg, Pulmoddai deposit: 0.56 mg/kg). According to Table 4.3, beach placers on the northeast coast displayed a general decreasing order of Ce > La > Nd > Gd > Y > Pr > Sm > Dy > Er > Yb > Tb > Eu > Ho > Lu > Tm. The Verugal and Pulmoddai deposits showed average LREE/HREE ratios of 3.4 and 3.1, respectively. Beach placers in the Verugal and Pulmoddai deposits showed high Th and U enrichments. Thorium concentration in the Verugal deposit ranged from 17.61 – 212 mg/kg, whereas it was in the range of 5.48 – 630 mg/kg in the Pulmoddai deposit (Table 4.3). However, U content was significantly lower than Th in both Verugal (1.75 – 9.10 mg/kg) and Pulmoddai (0.63 – 13.73 mg/kg) deposits.

Figure 4.3 shows the chondrite normalized REE distribution patterns of beach placers in Verugal (Figure 4.3a) and Pulmoddai (Figure 4.3b) deposits. The same trend of REE distribution was evident in both Verugal and Pulmoddai deposits, where there is a prominent Eu anomaly. In addition, La and Gd exhibited significant positive anomalies in both deposits. Eu/Eu* of Verugal and Pulmoddai deposits displayed the same range between 0.07–0.29, whereas Ce/Ce* values of Verugal and Pulmoddai deposits were in the ranges of 0.52–0.58 and 0.29–0.34, respectively (Table 4.3). While beach placers on the northeast coast can be characterized by strong negative Eu anomalies, Ce anomalies showed weak positive anomalies.

Table 4.3: REE, Th, and U concentrations (mg/kg) of beach placers in the Verugal and Pulmoddai deposits

Element	Verugal deposit																	
	VG-1	**VG-2**	**VG-3**	**VG-4**	**VG-5**	**VG-5a**	**VG-6**	**VG-7**	**VG-8**	**VG-9**	**VG-10**	**VG-11**	**VG-12**	**VG-13**	**VG-13a**	**VG-14**	**VG-15**	**VG-16**
La	37.62	35.55	36.28	35.07	51.82	45.00	113.8	44.93	44.74	135.4	30.17	29.69	36.40	51.11	116.2	27.26	24.81	41.01
Ce	76.62	72.36	74.17	71.96	103.2	92.70	230.0	90.73	89.66	230.4	59.80	62.23	74.84	100.5	232.0	57.08	50.05	87.29
Pr	8.90	8.36	8.69	8.60	12.48	10.61	26.84	10.56	11.03	26.77	7.35	7.56	8.63	11.97	27.57	6.83	6.08	10.76
Nd	28.79	26.53	27.33	29.02	38.87	34.77	81.93	33.29	34.55	86.83	23.08	24.32	27.67	38.94	80.52	22.16	18.86	34.75
Sm	6.38	6.08	6.57	6.16	7.88	7.43	16.70	6.06	6.27	18.43	5.13	5.44	5.93	8.86	14.12	5.39	4.78	7.84
Eu	0.92	0.86	0.75	1.10	1.02	1.01	1.77	0.70	0.70	1.68	0.79	0.86	0.89	1.27	1.15	1.13	0.93	1.30
Gd	16.44	15.42	15.58	15.67	21.74	19.19	46.48	18.99	18.64	47.22	12.62	14.21	15.89	20.19	43.30	12.53	11.44	18.97
Tb	1.77	1.69	1.80	1.77	2.40	2.08	4.79	1.91	1.80	4.64	1.47	1.47	1.60	2.20	3.91	1.48	1.40	2.08
Dy	5.14	4.80	5.50	5.05	6.99	6.17	12.04	5.04	4.71	12.41	3.92	4.51	4.80	6.22	9.36	4.67	4.20	6.61
Ho	0.79	0.86	0.69	0.91	1.05	1.07	1.82	0.87	0.94	1.89	0.69	0.82	0.94	1.21	1.38	0.85	0.66	1.30
Er	3.02	3.18	3.15	3.62	4.42	4.23	8.00	3.59	3.53	8.29	2.77	3.16	3.23	4.29	6.47	2.96	2.49	4.90
Tm	0.30	0.29	0.25	0.34	0.38	0.32	0.61	0.28	0.28	0.57	0.28	0.30	0.29	0.38	0.39	0.31	0.29	0.49
Yb	1.88	1.96	1.83	2.20	2.64	2.35	4.26	1.81	2.00	4.27	1.75	1.91	1.72	2.48	3.07	1.97	1.62	3.00
Lu	0.33	0.31	0.34	0.34	0.41	0.39	0.68	0.32	0.35	0.70	0.30	0.33	0.29	0.48	0.50	0.33	0.31	0.53
Y	16.81	16.01	16.45	19.38	21.54	20.79	33.61	15.91	16.97	32.01	16.28	17.21	16.99	22.83	23.98	18.64	16.58	28.99
Th	41.86	36.20	37.52	36.24	86.68	47.34	165.1	81.19	71.70	154.7	32.92	35.41	39.56	53.04	212.2	20.42	17.61	64.47
U	2.30	2.44	2.68	3.59	5.95	2.74	7.75	4.18	3.89	7.01	1.95	2.39	2.23	4.13	9.11	1.84	1.75	4.28
LREE	159.2	149.7	153.8	151.9	215.3	191.5	471.1	186.3	186.9	499.6	126.3	130.1	154.4	212.7	471.5	119.8	105.5	183.0
HREE	46.47	44.52	45.59	49.29	61.58	56.58	112.3	48.70	49.21	112.0	40.08	43.91	45.74	60.27	92.35	43.74	38.98	66.86
TREE	205.7	194.2	199.4	201.2	276.9	248.1	583.4	235.0	236.2	611.5	166.4	174.0	200.1	273.0	563.9	163.6	144.5	249.8
LREE/HREE	3.43	3.36	3.37	3.08	3.50	3.38	4.20	3.82	3.80	4.46	3.15	2.96	3.37	3.53	5.11	2.74	2.71	2.74
Eu/Eu*	0.15	0.15	0.13	0.19	0.13	0.15	0.11	0.11	0.11	0.10	0.17	0.17	0.16	0.16	0.08	0.24	0.22	0.18
Ce/Ce*	0.57	0.57	0.57	0.57	0.55	0.58	0.57	0.57	0.55	0.52	0.55	0.57	0.58	0.55	0.56	0.57	0.56	0.57

Element	Pulmoddai deposit												
	PM-1	**PM-2**	**PM-2a**	**PM-3**	**PM-4**	**PM-5**	**PM-6**	**PM-7**	**PM-7a**	**PM-8**	**PM-9**	**PM-9a**	**PM-10**
La	35.19	24.04	110.0	627.8	56.71	41.01	47.12	51.55	120.4	24.88	162.4	93.91	52.64
Ce	67.20	42.15	192.8	1385.2	99.99	81.46	106.2	106.0	199.1	48.70	293.9	186.3	102.8
Pr	8.98	5.81	24.46	134.6	13.07	10.70	12.92	13.38	22.49	6.12	30.41	20.30	12.83
Nd	29.59	19.70	75.95	395.1	41.18	36.24	47.61	46.70	66.39	22.27	97.00	61.41	41.97
Sm	7.02	4.58	15.53	61.25	8.65	8.27	11.42	11.88	12.54	5.28	18.83	11.19	9.30
Eu	1.70	1.03	3.22	4.61	1.66	2.14	2.81	2.54	1.89	1.28	2.76	1.24	2.15
Gd	16.69	10.84	40.29	212.5	22.12	19.40	26.19	25.47	37.77	12.39	52.84	31.10	23.74
Tb	1.99	1.18	3.88	18.33	2.48	2.40	3.32	3.47	3.64	1.40	4.86	3.23	2.59
Dy	6.19	4.52	11.64	38.78	7.13	8.22	12.05	11.49	9.55	4.52	14.06	8.68	9.33
Ho	1.05	0.82	1.89	4.60	1.35	1.57	2.16	2.13	1.69	0.89	1.95	1.34	1.58
Er	3.99	2.68	8.14	28.79	4.87	5.27	7.90	7.04	6.65	3.09	9.24	5.50	5.85
Tm	0.42	0.29	0.64	1.17	0.47	0.56	0.87	0.82	0.49	0.35	0.63	0.39	0.56
Yb	2.67	1.87	4.69	10.07	2.95	3.27	5.05	4.99	3.53	2.18	4.19	3.17	3.65
Lu	0.44	0.32	0.82	1.56	0.49	0.55	0.86	0.78	0.59	0.34	0.72	0.46	0.59
Y	23.17	17.44	30.95	71.59	22.51	35.98	56.27	53.22	29.50	22.03	40.08	25.48	39.53
Th	19.48	11.82	84.98	630.4	40.43	22.68	10.97	18.78	89.05	11.33	148.9	177.0	34.27
U	1.49	1.08	3.12	13.73	1.82	1.56	1.74	1.91	3.02	1.16	4.30	7.84	1.97
LREE	149.7	97.31	422.0	2608.5	221.3	179.8	228.1	232.1	422.8	108.5	605.3	374.4	221.7
HREE	56.60	39.95	102.9	387.4	64.36	77.22	114.6	109.4	93.40	47.19	128.6	79.36	87.41
TREE	206.3	137.2	525.0	2995.9	285.6	257.0	342.7	341.5	516.2	155.7	733.8	453.8	309.1
LREE/HREE	2.64	2.44	4.10	6.73	3.44	2.33	1.99	2.12	4.53	2.30	4.71	4.72	2.54
Eu/Eu*	0.27	0.25	0.22	0.07	0.21	0.29	0.28	0.25	0.15	0.27	0.15	0.11	0.25
Ce/Ce*	0.29	0.29	0.30	0.34	0.30	0.29	0.31	0.30	0.32	0.30	0.33	0.32	0.30
Element	**Pulmoddai deposit**												

	PM-10a	PM-11	PM-12	PM-13	PM-14	PM-15	PM-16	PM-17	PM-18	PM-19	PM-20	PM-21	PM-22
La	85.32	237.8	45.81	43.57	184.6	21.77	35.30	48.36	32.58	41.39	31.34	28.06	25.49
Ce	152.2	449.3	95.34	90.18	337.3	41.95	66.28	92.31	63.77	79.37	60.33	51.06	47.72
Pr	18.82	49.20	11.36	11.32	39.05	5.44	9.00	11.80	8.31	10.49	8.03	6.53	6.42
Nd	59.48	141.4	39.41	39.79	113.7	18.87	30.75	40.14	29.44	36.60	29.19	22.16	21.43
Sm	12.42	26.08	9.97	10.22	21.74	4.78	7.52	9.27	6.35	8.57	7.02	5.26	4.85
Eu	2.08	2.74	2.59	2.38	3.03	1.16	1.75	2.40	1.68	2.16	1.61	1.19	1.13
Gd	32.00	78.15	24.10	22.44	62.45	10.61	17.07	22.21	15.31	20.25	14.48	12.19	11.42
Tb	2.99	6.96	2.80	2.66	5.84	1.31	1.98	2.70	1.84	2.54	1.91	1.33	1.49
Dy	9.56	16.93	9.89	9.54	14.17	4.28	7.77	8.95	6.21	8.26	6.25	4.70	4.87
Ho	1.57	2.25	1.86	1.83	1.98	0.76	1.40	1.66	1.21	1.78	1.20	0.91	0.88
Er	6.70	11.09	6.11	6.40	9.59	2.65	4.76	5.60	3.91	5.50	4.14	3.11	2.98
Tm	0.51	0.65	0.70	0.72	0.62	0.31	0.54	0.62	0.46	0.64	0.41	0.32	0.30
Yb	3.55	5.42	4.09	4.26	4.41	1.80	2.86	3.83	2.84	3.51	2.41	1.88	1.98
Lu	0.61	0.77	0.65	0.66	0.70	0.26	0.47	0.58	0.48	0.58	0.45	0.31	0.31
Y	29.11	39.52	51.03	45.71	34.05	21.27	33.72	43.41	28.96	41.02	28.11	21.02	21.88
Th	74.60	231.0	58.91	18.31	159.8	5.48	6.64	20.60	8.24	6.79	7.15	8.71	7.26
U	2.69	5.49	2.13	1.69	4.27	0.63	1.19	1.78	1.10	1.25	1.05	0.95	1.04
LREE	330.3	906.5	204.5	197.5	699.3	93.97	150.6	204.3	142.1	178.6	137.5	114.2	107.0
HREE	86.61	161.8	101.2	94.20	133.8	43.25	70.57	89.55	61.21	84.08	59.35	45.77	46.10
TREE	416.9	1068.2	305.7	291.7	833.1	137.2	221.2	293.8	203.3	262.6	196.9	160.0	153.1
LREE/HREE	3.81	5.60	2.02	2.10	5.23	2.17	2.13	2.28	2.32	2.12	2.32	2.50	2.32
Eu/Eu*	0.18	0.10	0.29	0.27	0.14	0.28	0.26	0.29	0.29	0.28	0.27	0.26	0.26
Ce/Ce*	0.30	0.32	0.31	0.30	0.31	0.30	0.29	0.30	0.30	0.29	0.29	0.30	0.29

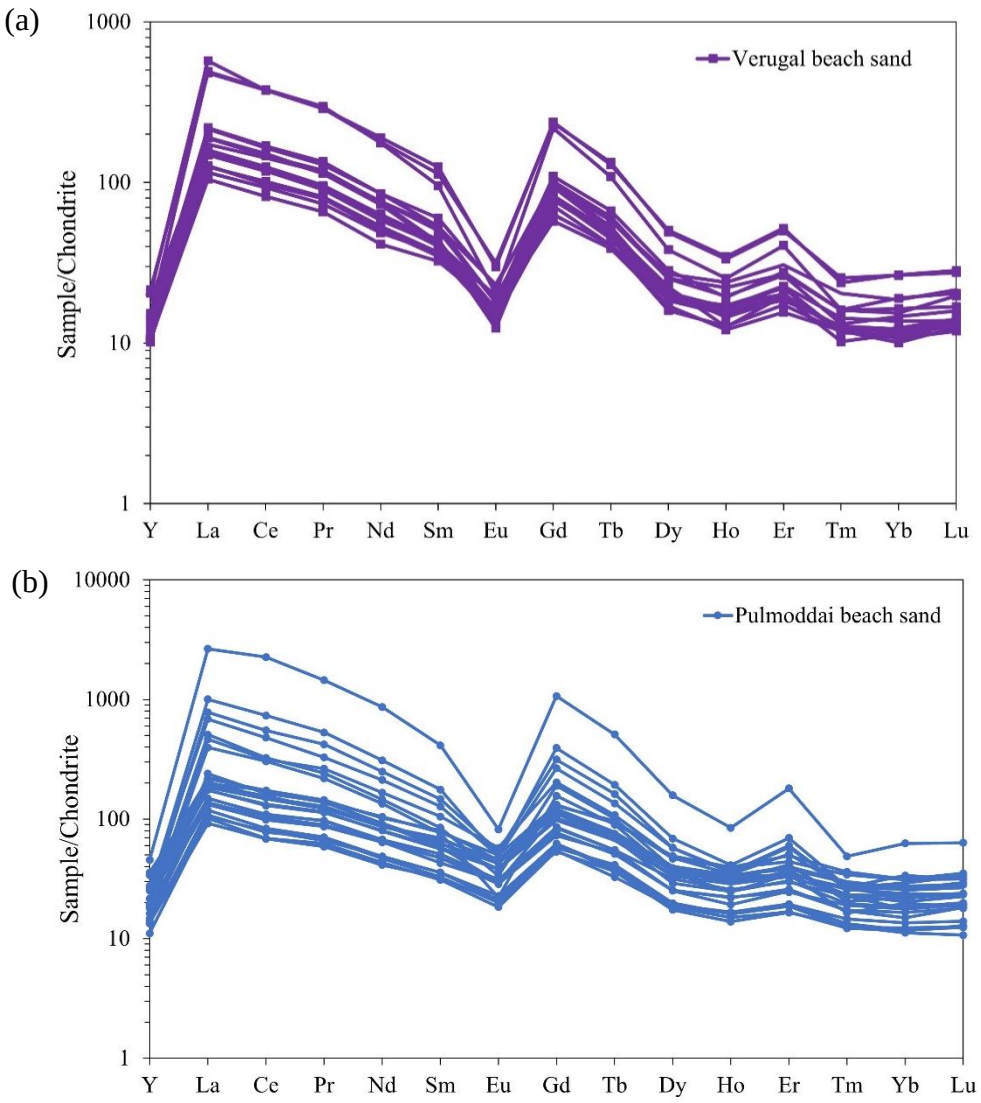

Figure 4.3: Chondrite-normalized REE distribution patterns of beach placers in the (a) Verugal deposit (18 samples) and (b) Pulmoddai deposit (26 samples).

4.1.4. REE content in beach placers along the southwest coast

REE, Th, and U concentrations of beach placers along the southwest coast are shown in Table 4.4. According to Table 4.4, TREE, LREE, and HREE concentrations of beach placers along the southwest coast ranged from 27.94 – 1359 mg/kg, 18.54 – 1209 mg/kg, and 6.09 – 150 mg/kg, respectively. The trend of individual REE concentrations followed a decreasing order of Ce > Nd > La > Y > Gd >Er > Pr > Dy > Sm > Yb > Tb > Ho > Eu > Tm > Lu, where Ce was found as the dominant REE in the southwest coastal line with concentrations ranging from 9.4 –669 mg/kg. The

Table 4.4: REE, Th, and U concentrations (mg/kg) of beach placers along the southwest coast

Element	SW-1	SW-2	SW-3	SW-4	SW-5	SW-6	SW-7	SW-8	SW-9	SW-10	SW-11	SW-12	SW-13	SW-14	SW-15	SW-16	SW-17	SW-18
La	13.35	85.72	39.24	14.66	27.78	25.99	8.19	20.52	13.07	8.32	12.10	3.46	5.68	54.06	13.67	4.72	116.9	247.0
Ce	38.16	225.0	124.2	37.48	87.47	91.76	25.91	54.22	35.77	25.02	31.22	9.36	15.09	157.2	39.08	13.10	352.6	669.1
Pr	3.27	17.07	9.44	3.34	6.60	6.31	2.02	4.26	2.78	1.91	2.56	0.72	1.37	11.41	3.16	1.09	25.56	49.81
Nd	15.46	76.28	41.45	16.58	31.06	33.61	10.16	22.07	14.61	10.66	12.25	4.04	6.92	48.24	15.82	5.95	131.6	211.6
Sm	2.87	11.89	7.18	2.89	4.79	5.41	1.79	3.90	2.51	2.14	1.94	0.77	1.37	7.62	2.82	0.97	18.21	29.96
Eu	0.74	0.93	0.87	0.69	0.59	1.20	0.51	1.28	0.66	0.50	0.35	0.19	0.28	0.62	0.63	0.15	1.24	2.02
Gd	4.23	21.22	11.53	3.98	7.06	6.76	2.21	4.43	2.92	1.68	2.40	0.69	1.19	9.46	2.65	0.89	17.52	33.82
Tb	1.90	8.06	4.43	1.76	2.73	3.12	1.02	2.18	1.29	0.91	0.98	0.33	0.52	3.33	1.37	0.41	7.15	14.02
Dy	3.22	7.43	5.22	2.58	3.71	5.70	1.98	4.93	3.00	3.27	2.09	1.13	1.49	5.97	3.82	0.93	10.15	19.00
Ho	0.92	2.17	1.66	0.69	1.12	1.52	0.61	1.51	1.02	1.15	0.58	0.33	0.42	1.54	1.19	0.28	2.90	5.38
Er	3.84	14.14	9.06	3.98	6.02	7.98	2.41	6.01	3.65	4.09	2.71	1.42	1.86	8.73	4.35	1.24	17.00	35.31
Tm	0.38	0.62	0.52	0.31	0.38	0.61	0.29	0.58	0.37	0.50	0.24	0.07	0.17	0.55	0.43	0.10	0.89	1.59
Yb	2.92	8.96	5.48	2.39	3.67	5.04	1.74	3.70	2.73	2.39	1.65	0.76	0.94	4.69	2.72	0.64	7.18	15.19
Lu	0.33	0.78	0.59	0.25	0.42	0.61	0.21	0.48	0.33	0.36	0.16	0.08	0.13	0.52	0.40	0.09	0.87	1.75
Y	8.89	12.12	9.15	4.78	6.59	12.16	5.58	22.13	12.85	7.63	7.92	4.59	6.07	10.82	9.94	1.52	10.98	23.55
Th	10.00	158.0	45.22	9.54	34.41	31.36	3.34	5.53	9.24	8.77	16.07	8.75	2.88	177.6	9.47	3.03	171.1	429.5
U	1.58	8.39	4.61	1.54	2.50	5.86	1.40	4.62	3.75	2.90	2.91	1.87	2.83	9.24	3.10	0.80	9.56	19.98
LREE	73.84	416.9	222.3	75.64	158.3	164.3	48.57	106.2	69.39	48.55	60.41	18.54	30.71	279.2	75.18	25.97	646.0	1209.5
HREE	26.62	75.50	47.63	20.72	31.68	43.49	16.04	45.94	28.15	21.99	18.72	9.41	12.79	45.61	26.86	6.09	74.63	149.6
TREE	100.5	492.4	270.0	96.36	190.0	207.8	64.61	152.2	97.54	70.54	79.13	27.94	43.50	324.8	102.0	32.06	720.7	1359.1
LREE/HREE	2.77	5.52	4.67	3.65	5.00	3.78	3.03	2.31	2.47	2.21	3.23	1.97	2.40	6.12	2.80	4.26	8.66	8.08
Eu/Eu*	0.36	0.10	0.17	0.35	0.17	0.34	0.44	0.53	0.42	0.45	0.28	0.45	0.37	0.13	0.40	0.27	0.12	0.11
Ce/Ce*	0.79	0.80	0.88	0.73	0.88	0.98	0.87	0.79	0.81	0.86	0.77	0.81	0.74	0.86	0.81	0.79	0.88	0.82

LREE/HREE ratios of beach placers along the southwest coast ranged between 1.9 and 8.6, respectively (Table 4.4). Furthermore, relatively high Th and U concentrations were evident in the southwest beach placers that ranged from 2.88 – 429 mg/kg and 0.8 – 19.98 mg/kg, respectively. However, Th was significantly enriched in the beach placers along the southwest coast compared to U concentrations.

The chondrite normalized REE distribution patterns of beach placers in each location along the southwest coast are illustrated in Figure 4.4. All the REE distribution patterns followed the same trend with strong negative Eu anomalies and positive Tb and Er anomalies. However, locations SW-8 (Benthota) and SW-10 (Ahungalla) had slightly different distribution patterns with no Eu anomalies. Eu/Eu* of the southwest beach placers ranged between 0.1–0.3, whereas Ce/Ce* were in the ranges of 0.7–0.8 (Table 4.4). Therefore, beach placers along the southwest coast can be characterized by prominent negative Eu anomalies and weak negative Ce anomalies.

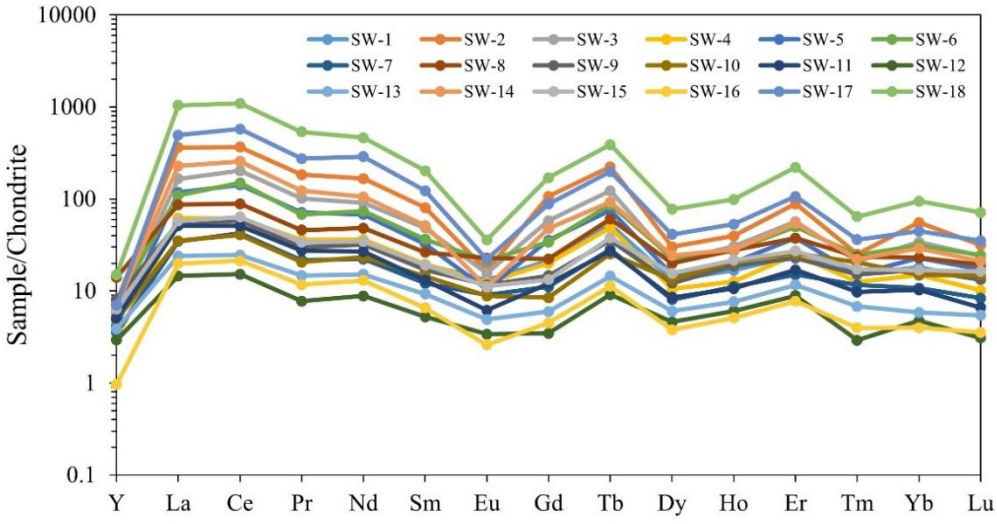

Figure 4.4: Chondrite-normalized REE distribution patterns of beach placers along the southwest coast (18 samples).

4.1.5. REE content in the Walave river basin

REE, Th, and U concentrations in stream sediments of Belihul Oya, Walave river, and Kiriketi Oya are presented in Table 4.5. Accordingly, TREE contents in the

Table 4.5: REE, Th, and U concentrations (mg/kg) of alluvial placers in the Walave river basin

Element	Belihul Oya									Walave River							Kiriketi Oya			
	B-1	B-2	B-3	B-4	B-5	B-6	B-7	B-8	B-9	W-1	W-2	W-3	W-4	W-5	W-6	W-7	K-1	K-2	K-3	K-4
La	95.40	46.83	55.99	48.19	51.57	70.30	55.91	64.86	68.56	71.59	45.97	28.34	48.90	73.96	84.14	29.72	56.55	44.00	51.38	59.21
Ce	142.8	41.65	84.03	47.47	47.76	104.7	49.40	92.55	59.83	67.02	42.47	49.92	71.59	103.9	111.9	42.64	58.68	40.61	75.47	110.6
Pr	37.44	12.53	23.75	13.30	12.92	27.80	13.33	26.70	16.37	19.08	11.40	7.98	21.59	29.78	34.69	7.63	14.94	12.09	13.70	27.35
Nd	86.13	28.30	58.65	34.16	28.50	62.07	32.39	64.62	38.01	45.38	28.53	21.20	51.54	73.22	78.09	19.62	38.95	32.98	33.99	61.43
Sm	12.04	5.30	8.38	5.78	5.33	9.38	5.10	9.60	5.91	8.42	4.45	3.68	8.07	10.85	14.64	3.72	7.39	7.05	6.55	11.41
Eu	1.43	1.18	1.35	1.55	1.31	1.26	1.02	1.45	0.94	2.06	0.85	1.18	1.32	1.55	2.58	1.04	2.90	2.88	2.88	3.36
Gd	15.77	5.70	10.99	6.81	6.05	11.94	6.30	12.13	7.19	9.11	5.28	3.88	9.65	13.43	16.67	4.04	7.90	7.63	7.90	13.10
Tb	2.97	1.30	2.22	1.48	1.29	2.23	1.31	2.42	1.45	2.01	1.07	0.90	2.12	2.71	3.82	1.04	2.11	2.32	1.99	3.05
Dy	4.89	3.63	5.05	4.23	3.87	4.09	2.86	4.82	2.79	5.28	2.52	2.60	4.84	5.77	10.91	3.59	7.36	10.10	8.03	9.25
Ho	0.97	0.77	1.04	0.82	0.77	0.77	0.58	0.98	0.59	1.14	0.52	0.51	1.05	1.18	2.41	0.79	1.65	2.22	1.64	2.02
Er	4.71	2.75	4.13	3.05	2.79	3.78	2.35	4.18	2.56	4.22	2.00	2.07	4.03	4.84	8.79	2.52	5.33	6.89	5.56	6.92
Tm	0.33	0.29	0.41	0.33	0.31	0.28	0.22	0.37	0.21	0.49	0.18	0.24	0.42	0.43	1.05	0.36	0.69	1.03	0.76	0.89
Yb	2.91	2.21	3.04	2.25	2.21	2.41	1.65	2.70	1.77	3.30	1.48	1.50	3.00	3.30	7.38	2.33	4.95	7.11	5.03	6.12
Lu	0.38	0.33	0.43	0.32	0.34	0.33	0.22	0.38	0.25	0.49	0.22	0.24	0.47	0.49	1.06	0.38	0.77	1.07	0.80	0.93
Y	15.06	14.01	19.00	13.75	14.18	12.91	10.15	17.54	10.08	18.96	9.01	9.64	18.46	20.08	23.44	14.14	27.90	47.16	29.17	35.22
Th	110.1	22.51	80.26	44.96	46.41	98.61	44.20	89.35	54.89	57.55	39.22	17.80	78.69	95.33	112.6	42.50	45.53	554.7	45.36	58.45
U	13.53	2.98	5.29	3.67	2.57	10.38	3.32	7.07	3.80	7.67	2.58	1.71	8.84	11.15	9.54	5.72	4.47	28.46	4.32	7.67
LREE	375.2	135.8	232.1	150.4	147.4	275.5	157.2	259.8	189.6	213.6	133.7	112.3	203.0	293.3	326.0	104.4	179.4	139.6	184.0	273.4
HREE	47.97	30.98	46.33	33.05	31.80	38.74	25.65	45.51	26.89	44.99	22.26	21.59	44.04	52.23	75.53	29.17	58.65	85.51	60.88	77.49
TREE	423.2	166.8	278.5	183.5	179.2	314.2	182.8	305.3	216.5	258.6	155.9	133.9	247.0	345.5	401.5	133.5	238.1	225.1	244.8	350.9
LREE/HREE	7.82	4.38	5.01	4.55	4.64	7.11	6.13	5.71	7.05	4.75	6.00	5.20	4.61	5.61	4.32	3.58	3.06	1.63	3.02	3.53
Eu/Eu*	0.18	0.37	0.24	0.42	0.40	0.21	0.31	0.23	0.25	0.41	0.30	0.54	0.26	0.22	0.28	0.46	0.65	0.67	0.69	0.47
Ce/Ce*	0.33	0.23	0.31	0.26	0.25	0.32	0.25	0.30	0.24	0.25	0.25	0.45	0.30	0.30	0.28	0.39	0.28	0.24	0.39	0.38

stream sediments of Belihul Oya, Walave river, and Kiriketi Oya ranged between 167–423 mg/kg (avg. = 250 mg/kg), 134–402 mg/kg (avg. = 239 mg/kg), and 225–351 mg/kg (avg. = 265 mg/kg), respectively. Moreover, LREE concentrations in sediments of the Walave river basin were in the range of 104 – 375 mg/kg, whereas relatively low HREE contents were observed ranging from 21.59 – 47.97 mg/kg. Furthermore, individual REE concentrations in the Walave basin river sediments followed a decreasing order of Ce > La > Nd > Pr > Y > Gd > Sm > Dy > Er > Yb > Tb > Eu > Ho > Lu > Tm, where Ce was the dominant REE with a content ranging from 40.61 – 143 mg/kg. In addition, a LREE/HREE ratio of 1.6 to 7.8 was observed in the sediments of the Walave river basin. According to Table 4.5, considerable levels of Th and U concentrations were observed in the river sediments of the Walave river basin. While Th content ranged between 17.8 – 555 mg/kg, U content was in the range of 1.71 – 28.46 mg/kg.

According to Figure 4.5, chondrite normalized REE distribution patterns of stream sediments in Belihul Oya, Walave river, and Kiriketi Oya generally followed the same trend with some slight differences. Strong negative Ce anomalies were evident in the sediments of the Walave river basin while prominent negative Eu anomalies were only observed in the sediments of Belihul Oya and Walave river,

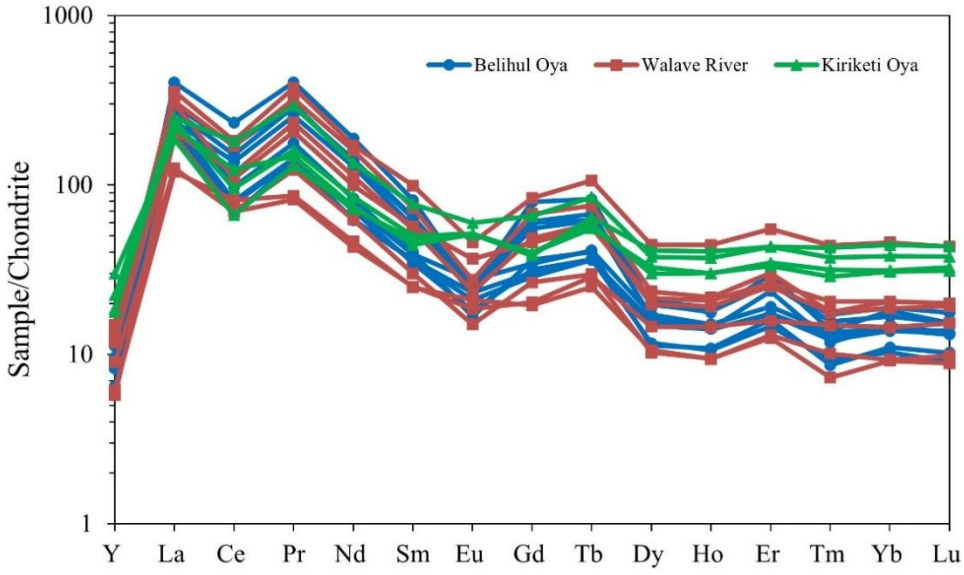

Figure 4.5: Chondrite-normalized REE distribution patterns of alluvial placers in the Walave river basin (20 samples).

where Kiriketi Oya sediments showed weak negative to positive Eu anomalies. This was further proved by the Eu/Eu* and Ce/Ce* values in the sediments of Belihul Oya (Eu/Eu* = 0.18 – 0.25, Ce/Ce* = 0.23 – 0.33), Walave river (Eu/Eu* = 0.22 – 0.54, Ce/Ce* = 0.25 – 0.45), and Kiriketi Oya (Eu/Eu* = 0.47 – 0.69, Ce/Ce* = 0.24 – 0.39) (Table 4.5).

4.1.6. REE content in Thonigala granite

In Thonigala granite, TREE content was in the range of 142 – 615 mg/kg (avg. = 329 mg/kg) with LREE and HREE contents ranging from 125 – 536 mg/kg (avg. = 286 mg/kg) and 17.59 – 79.13 mg/kg (avg. = 43.07 mg/kg), respectively (Table 4.6). The trend of individual REE contents in Thonigala was in decreasing order of Ce > Nd > La > Gd > Pr > Sm > Dy > Er > Tb > Eu > Yb > Ho > Tm > Lu, where Ce had the highest concentration (avg. = 116 mg/kg) and Lu, was the least abundant REE (avg. = 0.18 mg/kg). The LREE/HREE ratio of Thonigala granite ranged between 6.02 – 7.97.

According to Figure 4.6, the chondrite normalized REE plots of rock samples of the Thonigala granite generally showed similar REE patterns with prominent downward slopes and strong negative Eu anomalies. Moreover, weak negative Ce anomalies were evident in the REE distribution patterns of the Thonigala granite. In addition, Gd displayed prominent positive anomalies in the Thonigala granite. Table 4.6 presents Eu/Eu* and Ce/Ce* values ranging from 0.06 – 0.34 and 0.31 – 0.53, respectively, by which Thonigala granite can be characterized with strong negative Eu anomalies and weak negative Ce anomalies.

Table 4.6: REE concentrations (mg/kg) in rock samples of Thonigala granite

Element	**TG1**	**TG2**	**TG3**	**TG4**	**TG5**	**TG6**	**TG7**	**TG8**	**TG9**	**TG10**	**TG11**	**TG12**	**TG13**	**TG14**	**TG15**	**TG16**	**TG17**
La	52.58	51.74	65.39	98.35	51.54	73.25	104.3	76.75	71.09	33.08	49.31	60.87	48.82	40.90	100.5	67.60	61.86
Ce	144.2	104.6	117.7	209.5	68.04	76.92	195.1	90.62	88.96	58.23	108.2	133.9	105.3	65.16	226.7	109.0	63.72
Pr	25.84	20.92	28.19	37.17	11.39	14.48	42.20	16.10	17.39	6.78	22.23	25.33	23.13	8.77	45.06	26.17	12.56
Nd	78.69	60.53	81.27	112.1	35.57	45.69	134.5	48.82	49.37	21.29	68.24	74.31	71.43	27.21	139.0	75.99	38.89
Sm	15.62	11.59	14.12	20.40	8.28	8.27	23.73	10.91	9.04	4.71	12.49	14.20	14.02	7.48	23.19	13.24	8.15
Eu	1.14	0.85	0.92	1.68	1.44	0.97	1.34	1.47	0.84	0.58	0.78	0.94	1.24	2.04	1.23	0.91	0.90
Gd	34.32	25.04	31.99	52.93	17.19	18.89	53.69	25.02	21.67	12.58	27.01	33.56	29.16	14.69	58.45	30.45	17.43
Tb	2.58	2.00	2.40	3.77	1.37	1.48	4.32	1.87	1.59	0.78	2.18	2.52	2.35	1.14	3.97	2.51	1.51
Dy	6.49	4.38	5.69	9.17	4.11	3.58	10.99	5.13	3.91	2.07	5.48	6.46	6.37	2.68	8.50	5.93	4.57
Ho	0.75	0.48	0.57	1.10	0.58	0.41	1.33	0.70	0.44	0.30	0.61	0.81	0.77	0.50	0.80	0.71	0.67
Er	3.93	2.85	3.67	5.59	2.27	2.24	6.63	2.92	2.31	1.19	3.15	4.06	3.61	1.62	5.68	3.80	2.68
Tm	0.15	0.09	0.10	0.22	0.16	0.11	0.28	0.17	0.09	0.08	0.12	0.17	0.17	0.26	0.18	0.16	0.19
Yb	1.15	0.78	0.85	1.76	0.94	0.75	2.09	1.19	0.71	0.50	1.11	1.33	1.27	0.67	1.32	1.24	1.32
Lu	0.18	0.11	0.12	0.26	0.14	0.11	0.31	0.18	0.10	0.08	0.16	0.20	0.19	0.23	0.23	0.18	0.21
LREE	318.1	250.2	307.6	479.2	176.3	219.6	501.2	244.7	236.7	124.7	261.2	309.6	263.9	151.6	535.6	292.9	186.1
HREE	49.52	35.73	45.40	74.79	26.75	27.55	79.62	37.18	30.80	17.59	39.81	49.11	43.87	21.79	79.13	44.98	28.58
TREE	367.6	286.0	353.0	554.0	203.0	247.1	580.8	281.8	267.5	142.3	301.0	358.7	307.8	173.3	614.7	337.9	214.7
LREE/HREE	6.42	7.00	6.77	6.41	6.59	7.97	6.30	6.58	7.68	7.09	6.56	6.30	6.02	6.96	6.77	6.51	6.51
Eu/Eu*	0.08	0.09	0.07	0.09	0.21	0.13	0.06	0.15	0.10	0.13	0.07	0.07	0.11	0.34	0.06	0.08	0.13
Ce/Ce*	0.53	0.43	0.37	0.47	0.38	0.32	0.40	0.35	0.35	0.53	0.45	0.47	0.43	0.47	0.46	0.35	0.31

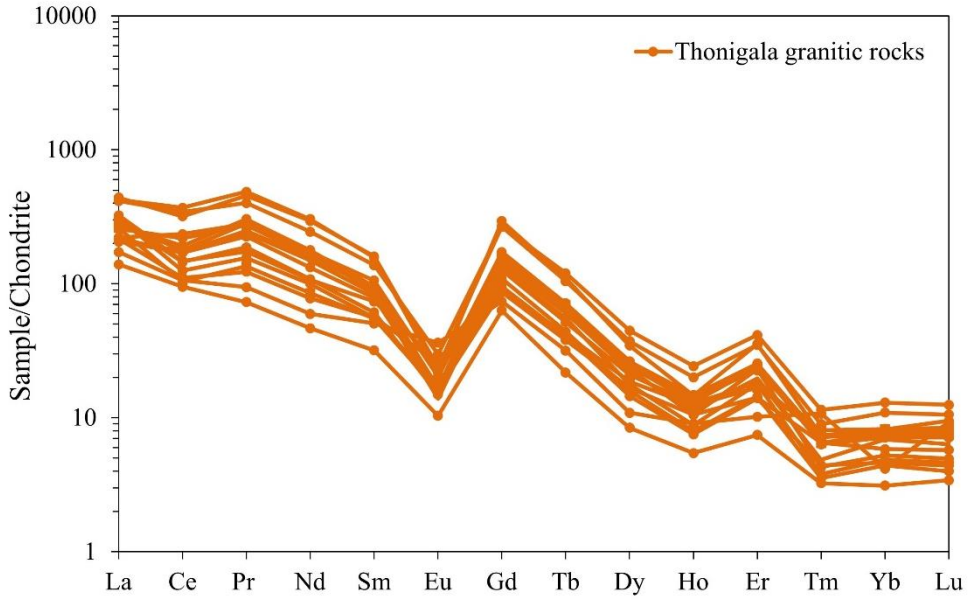

Figure 4.6: Chondrite-normalized REE distribution patterns of the Thonigala granite (17 samples).

4.1.7. REE content in Arangala granite

Arangala granite showed a TREE content ranging between 555 – 1358 mg/kg (avg. = 932 mg/kg) (Table 4.7). Moreover, the LREE and HREE contents were in the range of 395 – 987 mg/kg (avg. = 672 mg/kg) and 160 – 381 mg/kg (avg. = 260 mg/kg), respectively. The individual REE content trend of Arangala granite displayed a decreasing order of Ce > Nd > Gd > La > Y > Pr > Dy > Sm > Er > Tb > Yb > Ho > Eu > Lu > Tm with Ce being the most abundant REE (avg. = 303 mg/kg) while Tm showed the lowest content (avg. = 0.61 mg/kg). The LREE/HREE of Arangala granite ranged between 2.46 – 2.66 with an average of 2.58. All the collected granitic rock samples from Arangala followed similar chondrite normalized REE distribution patterns with highly prominent negative Eu anomalies (Figure 4.7). According to Table 4.7, the average Eu/Eu* and Ce/Ce* values of the Arangala granite were 0.02 and 0.61, respectively. This indicated that the Arangala granite can be characterized by strong negative Eu anomalies and weak negative Ce anomalies.

Table 4.7: REE concentrations (mg/kg) in rock samples of Arangala granite

Element	AR-1	AR-2	AR-3	AR-4	AR-5	AR-6
La	65.02	165.8	120.5	89.11	103.0	173.5
Ce	176.6	437.5	291.0	205.4	264.2	445.4
Pr	23.78	56.49	37.46	25.19	33.46	57.42
Nd	112.7	269.2	175.5	120.4	157.6	271.9
Sm	15.78	35.17	22.59	16.22	20.05	37.67
Eu	0.46	0.93	0.73	0.59	0.55	1.24
Gd	91.27	221.2	150.4	103.1	135.4	225.1
Tb	4.01	9.22	5.96	4.03	5.27	8.95
Dy	19.15	44.74	30.18	19.97	25.68	43.77
Ho	1.64	3.64	2.50	1.58	2.04	3.37
Er	7.35	16.66	11.12	7.05	9.37	15.59
Tm	0.38	0.92	0.67	0.39	0.49	0.84
Yb	3.44	6.91	4.74	2.81	4.07	6.25
Lu	0.52	1.10	0.73	0.44	0.61	1.00
Y	32.83	76.56	46.78	33.20	39.63	66.06
LREE	394.3	965.1	647.8	457.0	578.9	987.2
HREE	160.6	380.9	253.1	172.5	222.5	370.9
TREE	554.9	1346.0	900.9	629.5	801.4	1358.1
LREE/HREE	2.46	2.53	2.56	2.65	2.60	2.66
Eu/Eu*	0.02	0.02	0.02	0.02	0.02	0.02
Ce/Ce*	0.61	0.62	0.59	0.59	0.61	0.61

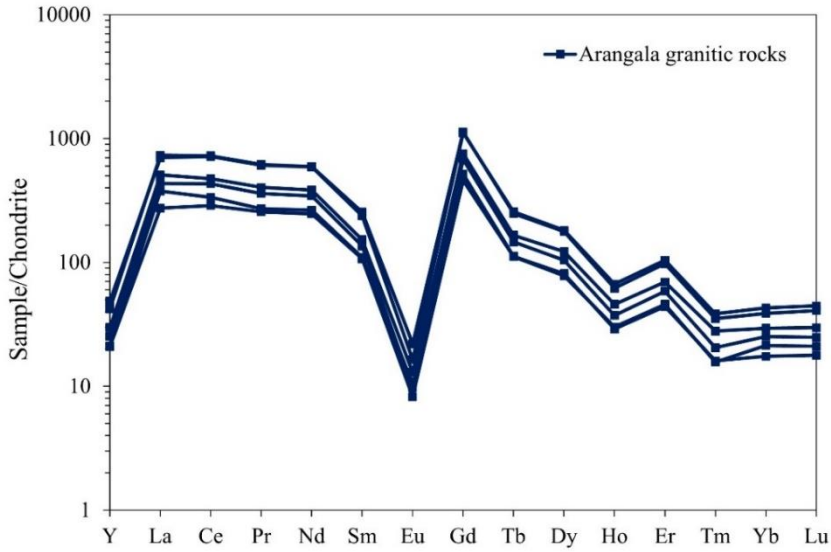

Figure 4.7: Chondrite-normalized REE distribution patterns of the Arangala granite (6 samples).

4.1.8. REE content in Massenna granite

TREE content of Massenna granite ranged between 65.29 – 2153 mg/kg (avg. = 937 mg/kg), whereas LREE and HREE contents were in the ranges of 60.21 – 1918 mg/kg (avg. = 846 mg/kg) and 5.08 – 235 mg/kg (avg. = 90.98 mg/kg), respectively (Table 4.8). The individual REE contents of Massenna granite decreased in the order of Ce > Nd > La > Pr > Gd > Sm > Y > Er > Dy > Tb > Eu > Yb > Ho > Lu > Tm with Ce being the most concentrated REE (avg. = 364 mg/kg) while the lowest content was reported for Tm (avg. = 0.30 mg/kg). Massenna granite showed a LREE/HREE ratio ranging from 8.16 – 11.84 with an average of 9.91.

Table 4.8: REE concentrations (mg/kg) in rock samples of Massenna granite

Element	**MG1**	**MG2**	**MG3**	**MG4**	**MG5**	**MG6**	**MG7**	**MG8**	**MG9**	**MG10**
La	439.8	288.3	199.5	97.31	105.3	12.96	109.9	222.6	350.8	84.51
Ce	696.2	425.3	490.6	197.6	140.6	30.46	262.9	471.9	728.2	197.2
Pr	141.5	69.04	56.86	23.33	22.53	2.98	32.42	58.89	98.56	23.26
Nd	561.8	264.2	229.6	88.24	87.40	10.77	122.6	223.1	372.3	95.73
Sm	69.24	30.85	29.76	11.55	9.79	1.53	18.52	31.26	56.55	13.26
Eu	9.91	6.62	4.13	3.90	3.48	1.51	2.75	6.43	8.89	5.68
Gd	111.8	49.53	43.10	17.67	18.04	2.31	25.64	47.63	81.15	19.02
Tb	19.48	8.81	8.74	3.20	3.09	0.41	4.82	8.52	15.07	3.53
Dy	19.46	8.82	8.33	3.13	2.70	0.46	4.96	8.90	15.33	3.83
Ho	3.12	1.44	1.55	0.52	0.48	0.08	0.85	1.56	2.78	0.64
Er	30.02	14.31	12.67	5.00	4.88	0.60	8.19	14.14	23.31	5.51
Tm	0.63	0.35	0.31	0.16	0.17	0.05	0.18	0.38	0.61	0.20
Yb	8.27	4.12	4.59	1.62	1.30	0.22	2.49	4.61	7.54	1.94
Lu	0.79	0.36	0.39	0.15	0.13	0.02	0.22	0.42	0.74	0.15
Y	41.42	18.30	19.38	7.06	5.75	0.94	10.42	21.71	34.50	8.13
LREE	1918.5	1084.3	1010.4	421.9	369.2	60.2	549.0	1014.2	1615.3	419.7
HREE	235.0	106.0	99.1	38.5	36.5	5.1	57.8	107.9	181.0	42.9
TREE	2153.4	1190.4	1109.5	460.4	405.7	65.3	606.8	1122.1	1796.4	462.6
LREE/HREE	8.16	10.23	10.20	10.96	10.11	11.84	9.50	9.40	8.92	9.77
Eu/Eu*	0.19	0.29	0.20	0.47	0.45	1.38	0.22	0.29	0.23	0.62
Ce/Ce*	0.38	0.41	0.63	0.57	0.39	0.67	0.60	0.56	0.53	0.61

Most samples from Massenna granite had similar downward-sloping REE patterns with small negative Eu and Ce anomalies (Figure 4.8). Eu/Eu* (0.19 – 1.38)

and Ce/Ce* (0.38 – 0.67) values presented in Table 4.8 further prove the above characteristics of the Massenna granite.

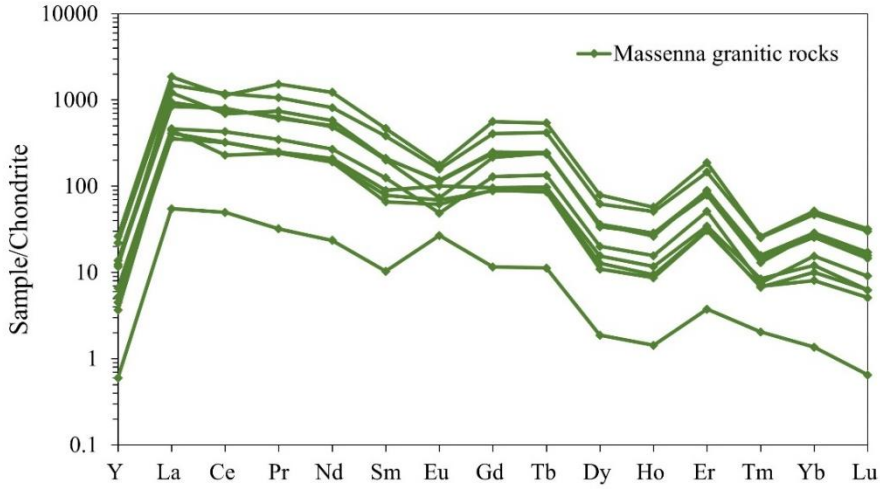

Figure 4.8: Chondrite-normalized REE distribution patterns of the Massenna granite (10 samples).

4.1.9. REE content in Ambagaspitiya granite

In the Ambagaspitiya granite, TREE content ranged between 98.54 – 1192 mg/kg (avg. = 317 mg/kg), whereas LREE and HREE contents were in the ranges of 68.82 – 811 mg/kg (avg. = 216 mg/kg) and 29.72 – 381 mg/kg (avg. = 100 mg/kg), respectively (Table 4.9). The individual REE contents of Ambagaspitiya granite decreased in the order of Ce > Nd > Gd > Y > La > Pr > Dy > Sm > Er > Tb > Yb > Ho > Eu > Lu > Tm with Ce being the most concentrated REE (avg. = 107 mg/kg) while the lowest content was reported for Tm (avg. = 0.29 mg/kg). Ambagaspitiya granite showed a LREE/HREE ratio ranging from 1.78 – 2.81 with an average of 2.22.

Although almost all the samples collected from Ambagaspitiya granite had similar REE distribution patterns with strong negative Eu anomalies and weak negative Ce anomalies, a few deviations were observed in some samples (Figure 4.9). This was further proved by the average Eu/Eu* (0.14) and Ce/Ce* (0.87) values of the Ambagaspitiya granite (Table 4.9).

Table 4.9: REE concentrations (mg/kg) in rock samples of Ambagaspitiya granite

Element	AMB-1	AMB-2	AMB-3	AMB-4	AMB-5	AMB-6
La	12.54	12.00	12.59	22.65	25.95	14.73
Ce	29.27	437.5	30.45	56.95	49.85	41.75
Pr	3.80	56.49	3.99	7.70	5.39	5.80
Nd	19.27	269.2	19.79	36.92	26.37	29.51
Sm	3.32	35.17	4.26	7.82	3.70	6.82
Eu	0.62	0.93	0.95	1.41	0.70	1.23
Gd	15.44	221.2	16.65	29.64	24.94	22.45
Tb	0.75	9.22	0.78	1.64	0.90	1.37
Dy	3.77	44.74	3.92	8.10	4.24	7.24
Ho	0.34	3.64	0.35	0.82	0.37	0.87
Er	1.27	16.66	1.56	3.14	1.46	2.97
Tm	0.11	0.92	0.14	0.24	0.09	0.24
Yb	0.61	6.91	0.53	1.36	0.49	1.44
Lu	0.09	1.10	0.11	0.22	0.09	0.24
Y	7.35	76.56	8.47	18.58	7.17	19.13
LREE	68.82	811.2	72.02	133.4	112.0	99.84
HREE	29.73	380.9	32.52	63.72	39.75	55.95
TREE	98.54	1192.2	104.5	197.2	151.7	155.8
LREE/HREE	2.32	2.13	2.21	2.09	2.82	1.78
Eu/Eu*	0.15	0.02	0.19	0.16	0.12	0.17
Ce/Ce*	0.58	2.29	0.59	0.59	0.58	0.62

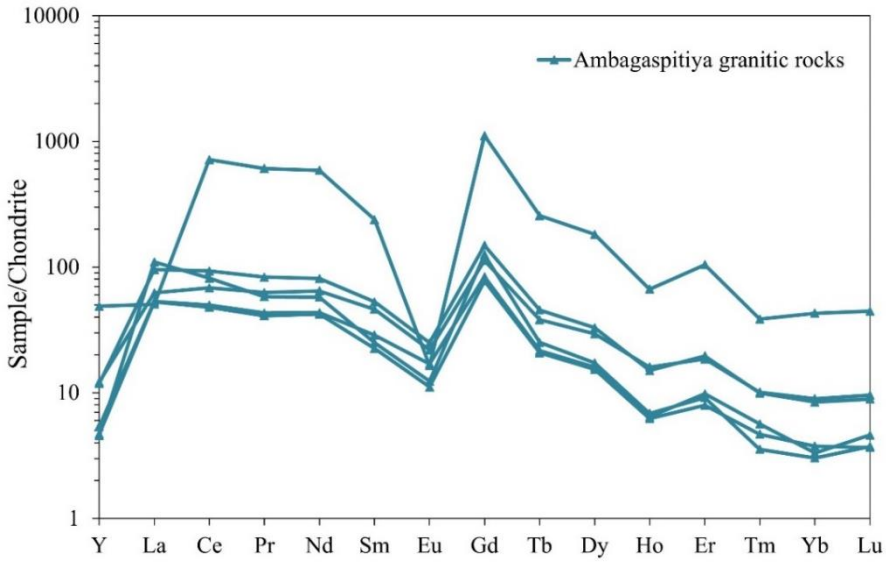

Figure 4.9: Chondrite-normalized REE distribution patterns of the Ambagaspitiya granite (6 samples).

4.1.10. REE content in Ratthota pegmatite, Matale

In Ratthota pegmatite, TREE content ranged between 19.6 – 271 mg/kg (avg. = 80.34 mg/kg), whereas LREE and HREE contents were in the ranges of 3.4 – 105 mg/kg (avg. = 36.38 mg/kg) and 16.3 – 166 mg/kg (avg. = 43.97 mg/kg) (Table 4.10). Moreover, rock samples in the Rattotha pegmatite showed a low LREE/HREE ratio ranging between 0.14 – 4.41 (avg. = 1.46). The individual REE content trend was also not the same as other derived trends and it ranged in the decreasing order of Y > La > Nd > Ce > Dy > Er > Pr > Sm > Gd > Yb > Ho > Tb > Eu > Tm > Lu with Y being the most abundant REE (avg. = 26.68 mg/kg) while the lowest content was reported for Lu (avg. = 0.4 mg/kg).

Table 4.10: REE concentrations (mg/kg) in rock samples of Ratthota pegmatite

Element	**R1**	**R2**	**R3**	**R4**	**R5**	**R6**
La	5.26	33.00	15.97	9.69	1.10	0.89
Ce	9.73	7.75	22.87	6.87	1.19	1.00
Pr	1.47	11.43	4.56	2.04	0.41	0.24
Nd	3.81	37.27	12.11	5.06	1.46	0.69
Sm	0.95	12.52	2.00	1.03	1.23	0.41
Eu	0.26	2.61	1.05	0.11	0.12	0.15
Gd	0.95	11.13	2.11	1.09	1.13	0.46
Tb	0.33	3.90	0.53	0.32	0.53	0.25
Dy	1.66	20.86	1.41	1.15	3.25	1.75
Ho	0.44	5.05	0.30	0.25	0.82	0.45
Er	1.39	14.97	1.13	0.75	2.17	1.30
Tm	0.19	1.99	0.15	0.08	0.33	0.21
Yb	1.14	10.53	0.86	0.57	2.04	1.28
Lu	0.18	1.57	0.13	0.10	0.35	0.21
Y	11.76	96.12	6.67	7.11	28.07	10.35
LREE	21.5	104.6	58.6	24.8	5.5	3.4
HREE	18.0	166.1	13.3	11.4	38.7	16.3
TREE	39.5	270.7	71.9	36.2	44.2	19.6
LREE/HREE	1.19	0.63	4.41	2.17	0.14	0.21
Eu/Eu*	0.48	0.38	0.88	0.18	0.17	0.58
Ce/Ce*	0.48	0.05	0.37	0.21	0.24	0.30

Based on Figure 4.10, almost all the samples of Ratthota pegmatite showed different chondrite-normalized REE patterns with relatively flat slopes. But some distribution patterns had slightly downward slopes. While strong negative Eu anomalies were absent in most of the samples, only a few exhibited significant negative Eu anomalies. In addition, several distribution patterns showed distinct negative Ce anomalies.

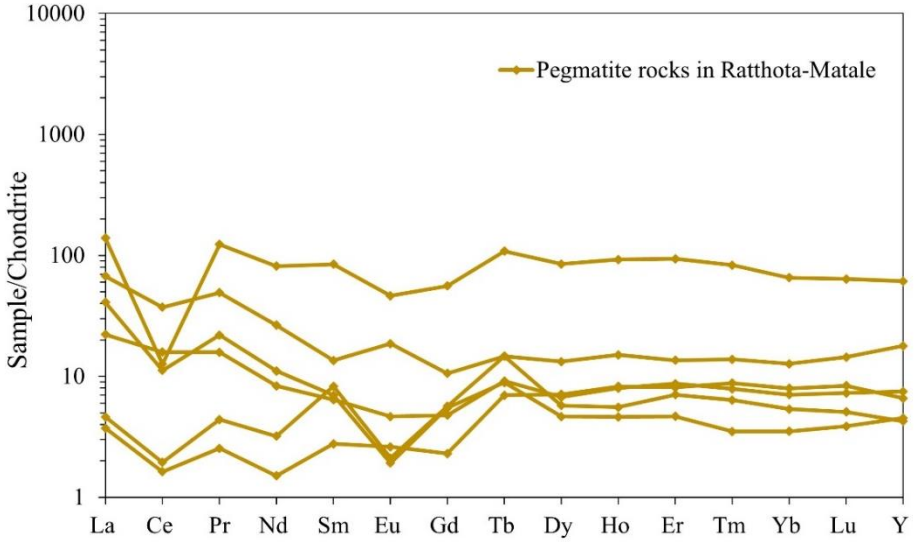

Figure 4.10: Chondrite-normalized REE distribution patterns of the Ratthota pegmatite (6 samples).

4.2. Enrichment of REEs in different geological formations of Sri Lanka

4.2.1. REE enrichment in residual laterites

Out of the two types of residual lateritic formations explored in the present study (carbonatite-associated and serpentinite-associated), the EPD is extremely enriched in REEs (apatite crystals avg. = 4072 mg/kg, secondary phosphate matrix avg. = 4063 mg/kg) than the Ginigalpelessa serpentinite deposit (avg. = 90.50 mg/kg). It is also well-observed in the comparison between average chondrite-normalized REE distribution patterns of the EPD and the Ginigalpelessa serpentinite deposit (Figure 4.11). The enrichment of REEs in weathering profiles is mainly reflected by the degree of REE enrichment in the respective primary host rocks (Jaireth et al., 2014). Accordingly, significantly higher REE enrichment in the secondary weathering

profiles at the EPD than the Ginigalpelessa serpentinite deposit is a result of great REE depletion in the Ginigalpelessa serpentinite rocks (northern carbonatite = 959 mg/kg, southern carbonatite = 742 mg/kg, Ginigalpelessa serpentinite rock = 0.59 – 30.89 mg/kg). Therefore, the presence of REE-enriched host rocks in residual lateritic deposits is important for the formation of secondary weathering profiles with elevated REE contents.

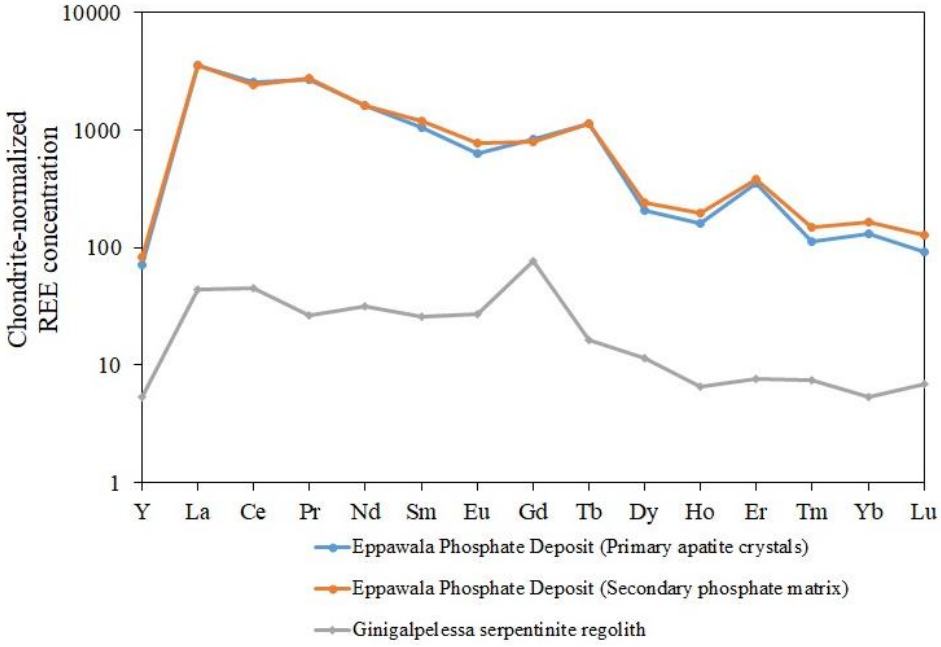

Figure 4.11: Comparison between chondrite-normalized REE distribution patterns of the Eppawala phosphate deposit and the Ginigalpelessa serpentinite deposit.

The EPD has a higher LREE/HREE ratio than the Ginigalpelessa serpentinite deposit inferring that the EPD is significantly enriched of LREE, whereas the latter may have a potential for HREEs. However, the EPD shows high enrichments of REEs, such as La, Ce, Pr, Nd, Gd, Tb, and Er while the Ginigalpelessa serpentinite deposit is enriched in only La, Ce, and Gd.

4.2.2. REE enrichment in beach placers

Figure 4.12 shows the relative enrichment of individual REEs in the studied beach placer deposits, namely the Pulmoddai deposit, Verugal deposit, and southwest coast beach placers. Based on it, the Pulmoddai deposit has the highest enrichment of REEs in terms of beach placers in Sri Lanka. However, in the Verugal deposit and

southwest coast beach placers, certain fluctuations are observed for several REEs. For example, while enrichments of some REEs, such as La, Pr, Sm, Gd, and Y are higher in the Verugal deposit, several HREEs like Tb, Ho, Er, Tm, and Yb showed greater enrichments in the southwest coast beach placers. The degree of REE enrichment in beach placers is governed by the geochemical characteristics of the source rock (provenance), whereas the type of REE-bearing minerals present, in particular, monazite, xenotime, and zircon may control the relative proportions of individual REEs (Papadopoulos et al., 2019; Paulick and Machacek, 2017).

Pronounced negative Eu anomalies evident in the chondrite-normalized REE distribution patterns in these beach placers (Figure 4.12) indicate that they may have been derived from granites and granitic pegmatites in the local inland terrains (Veerasamy et al., 2021). It has been reported that one of the major sources of beach placers in the northeast coast is sediments transported through the Mahaweli River, the

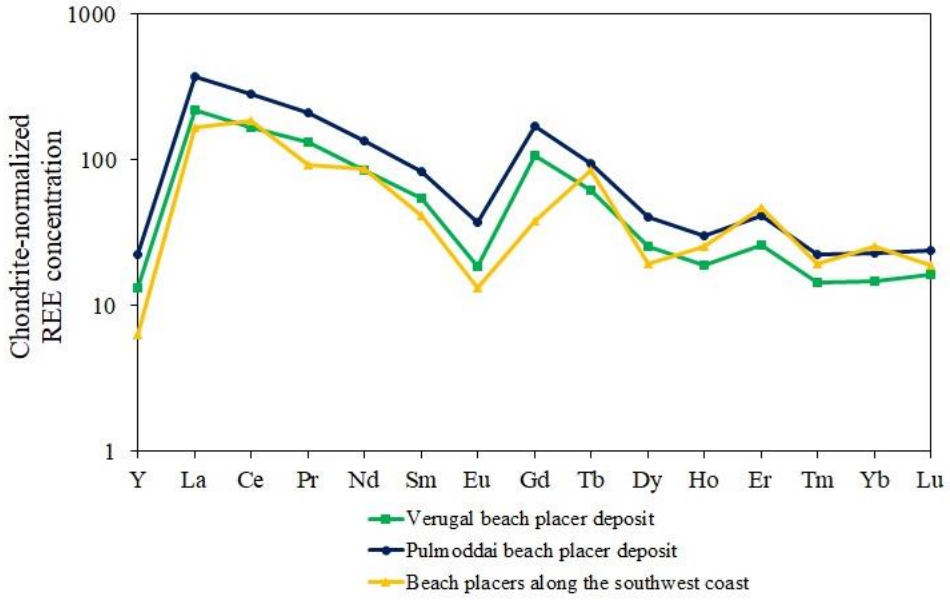

Figure 4.12: Comparison of chondrite-normalized REE distribution patterns of Pulmoddai, Verugal, and southwest coast beach placers.

largest terrestrial sediment-loaded river. The catchment of the Mahaweli river mainly consists of high-grade metamorphic rocks covering approximately one-sixth of Sri Lanka. Furthermore, there may be a minor contribution from eastern Indian clastic sediments to the northeast beach placers (Amalan et al., 2018). In contrast, eroded

sediments of granites, charnockites, khondalites, and granitoid rocks present in the inland drainage basins could be the possible sources of beach placers along the southwest coast (Amalan et al., 2018; Batapola et al., 2021).

Since beach placers are dynamic resources, temporal variation of REE enrichment can be observed with seasonal changes. Usually, northeast coast beach placers are replenished with heavy minerals during the northeastern monsoon while heavy mineral volumes on the southwest coast are higher during the southwestern monsoon (Amalan et al., 2018). Therefore, it is important to consider the heavy mineral percentages present at the time of sampling as it affects the REE content of the beach placers. In the present study, average heavy mineral percentages in Pulmoddai, Verugal, and southwest coast beach placers were obtained as 50-65%, 25-30%, and 7-12% respectively. However, in Amalan et al. (2018), they were reported as 70-85%, 45-50%, and 10%, respectively.

4.2.3. REE enrichment in alluvial placers

Figure 4.13 shows the relative enrichment of REEs in the Walave river sediments compared to the respective chondrite values. River sediments in Belihul Oya, Walave River, and Kiriketi Oya showed similar but medium enrichments of

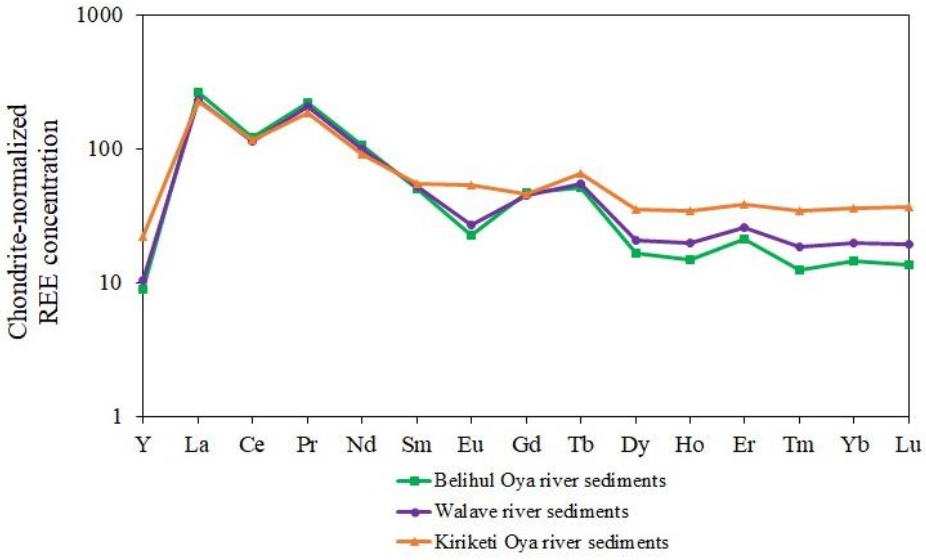

Figure 4.13: Comparison of chondrite-normalized REE distribution patterns of Belihul Oya, Walave river, and Kiriketi Oya sediments.

REEs (avg. TREE, Belihul Oya sediments = 250 mg/kg, Walave river sediments = 239 mg/kg, and Kiriketi Oya sediments = 265 mg/kg) particularly in LREEs. However, HREE enrichment in the sediments of the Walave river basin varies among rivers with the highest enrichment observed in Kiriketi Oya followed by Walave river and Belihul Oya. REE enrichment in river sediments are closely related to sediment provenance and chemical weathering (Li et al., 2013). Therefore, similar enrichment levels in these sediments suggest that they have been derived from the same source rocks in the catchment of the Walave river basin that constitutes granitic pegmatite occurrences.

However, the types of heavy minerals present in river sediments can largely influence the fractionation of LREEs and HREEs (Yang et al., 2002). Therefore, the high enrichment of HREEs in Kiriketi Oya sediments could be due to the presence of HREE-bearing heavy minerals, such as xenotime and allanite. Especially, it is indicated by the relative Y enrichment in Kiriketi Oya sediments since xenotime and allanite are Y-bearing phosphates and silicate minerals. Thus, mineralogical studies must be carried out to reveal REE-bearing minerals in these river sediments. In addition, REEs, such as La, Pr, Nd, and Tb show higher enrichments in sediments of the Walave river basin.

4.2.4. REE enrichment in magmatic deposits

The enrichment of REEs in the studied granitic rocks increases in the order of Ambagaspitiya (317 mg/kg), Thonigala (329 mg/kg), Arangala (932 mg/kg), and Massenna (937 mg/kg). This order of enrichment is also observed in the comparison of chondrite-normalized REE distribution patterns of the above granites (Figure 4.14a). Moreover, the average LREE/HREE ratios of Massenna (9.91) and Thonigala (6.73) granites are high meaning that they are significantly LREE-enriched. However, Arangala and Ambagaspitiya granites contain relatively low LREE/HREE ratios (~3.0), which indicate their potential for HREEs.

The magmatic differentiation (changing towards a more felsic composition during the crystallization of magma) through fractionation (As minerals crystallize, ions of those are depleted in the melt) causes the REE enrichment in the granites since

REEs tend to concentrate in the melt as incompatible elements. However, the level of enrichment and whether they are LREE- or HREE-enriched depend on the degree of fractionation and highly-fractionated granites favor the HREE enrichment (Sanematsu et al., 2009). Therefore, the fractionation of the granitic rocks may also increase in the following order: Ambagaspitiya, Thonigala, Arangala, and Massenna. All these granites, however, are not highly fractionated resulting in the absence of significant HREE enrichments in them. However, these granites contain increased enrichments of critical REEs, such as Nd, Pr, Gd, and Er.

The results of the present study show that REE enrichment in pegmatite at Ratthota, Matale is lower compared to the studied granites. The low REE contents and

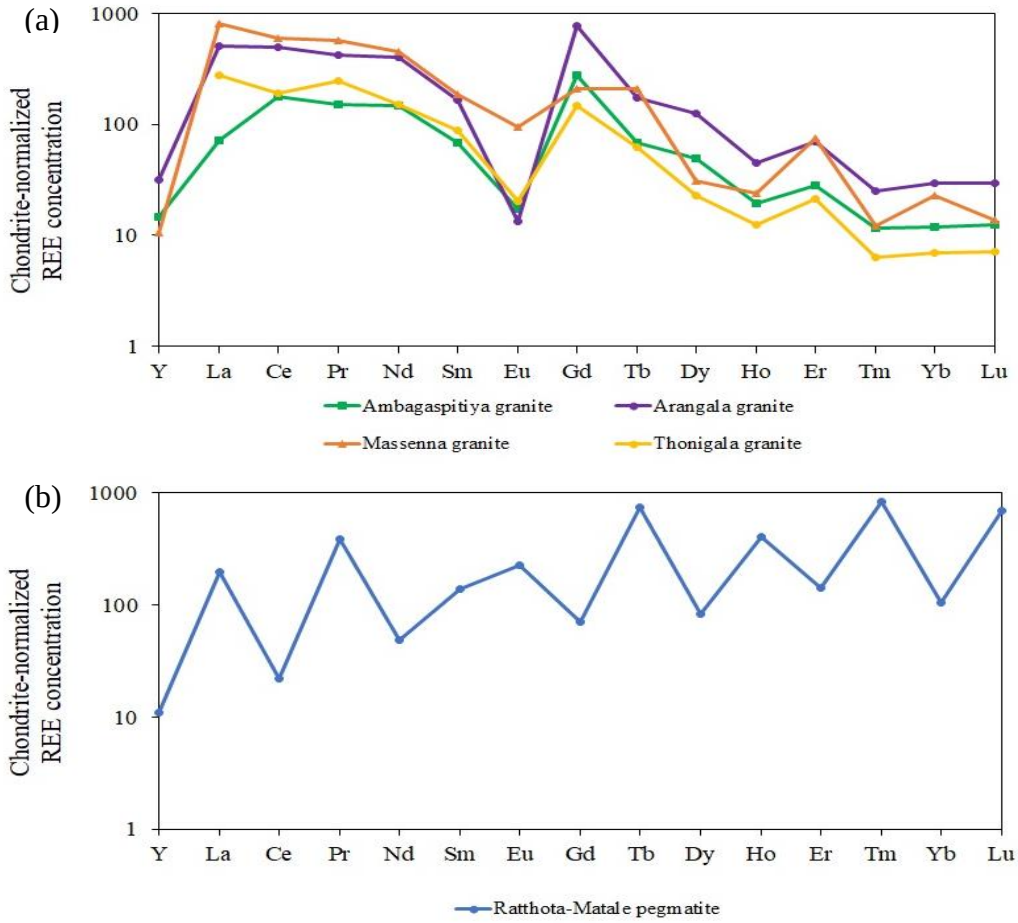

Figure 4.14: Comparison of chondrite-normalized REE distribution patterns of (a) Ambagaspitiya, Thonigala, Arangala, and Massena granites; (b) Ratthota-Matale pegmatite.

the relatively flattened REE distribution patterns of this pegmatite indicate a crystallization from fluids that originated from extremely late stages of the solidification of a parental granitic melt (Schilling et al., 2014). The different chondrite-normalized REE patterns (Figure 4.10) are probably because of the vast mineralogical and compositional variation within the Ratthota pegmatite, which is also in accordance with the literature (Dharmapriya et al., 2021; Möller, 1989). Therefore, the mineralogy in this pegmatite must be explored in detail to understand its potential as a source of REEs. As far as the average chondrite-normalized REE distribution pattern of the Ratthota pegmatite is concerned, its upward slope and low LREE/HREE ratio (1.46) suggest the potential for HREE enrichment (Figure 4.14b). In particular, it shows relatively high enrichments of several critical HREEs, such as Dy, Er, and Y along with Nd and Ce enrichments. However, more detailed sampling and geochemical analyses are needed for this prospect owing to its complex mineralogy and the potentiality of rarer and rather expensive HREEs.

4.3. Potential REE prospects in Sri Lanka

Typically, the potential of many metal deposits, such as gold, iron, or copper mainly depends on the grade and tonnage in the deposits. However, the case of REEs is distinct because the potential of a REE deposit can vary based on multiple factors, such as grade, tonnage, RE mineralogy, characteristics of LREE/HREE ratios, and the enrichment of critical REEs (Paulick and Machacek, 2017). In this section, we investigate the potential REE prospects in Sri Lanka concerning the above-mentioned factors. Accordingly, Table 4.11 summarizes the TREE contents, TREO grades, LREE/HREE ratio, and enriched REEs in the studied geological resources. However, tonnage and REE-bearing minerals were not considered here due to the lack of published data. In addition, these resources are compared against similar global occurrences to assess their potential in the global context.

In terms of TREE content and TREO grade, the EPD, Massenna granite, Arangala granite, and Pulmoddai deposit have higher potential relative to other studied resources (Table 4.11). However, the potential of a REE deposit cannot be assessed by only considering their grade. Generally, most REE deposits have a higher abundance

Table 4.11: A comparison of TREE concentrations and REO grades of the studied prospects in Sri Lanka against the global occurrences

Deposit type		**Deposit name**	T**REE content (mg/kg)**	**Average TREO grade (wt%)**	**LREE/HREE Ratio**	**Enriched REEs**	**Global examples (TREO wt%, TREE mg/kg)**
Residual lateritic regolith	Carbonatite-associated	Eppawala phosphate deposit (EPD)	Apatite crystals: 2676 – 6486 (avg. = 4072) Secondary phosphate matrix: 3253 – 5120 (avg. = 4063)	0.31 – 0.76	High, strongly enriched in LREEs relative to HREEs	La, Ce, Pr, Nd, Gd, Tb, Er	Kola, Russia (0.8-1 wt%); Khibiny, Russia (0.35-4 wt%); Zhijin, China (0.05-0.13 wt%); Kiirunavaara, Sweden (0.07-0.83 wt%); Gloserheia, Norway (0.06-0.36 wt%) (Source: Åmli, 1975; Harlov et al., 2002; Nie et al., 2013; Zaitsev et al., 2015; Zielinski et al., 1993)
	Serpentinite-associated	Ginigalpelessa serpentinite deposit	19.29 – 143 (avg. = 90.5)	0.01 – 0.02	Low, slightly enriched in LREEs relative to HREEs	La, Ce, Gd	-
Placers	Beach placers	Verugal deposit	144 – 612 (avg. = 274)	0.02 – 0.07	Low,slightly enriched in LREEs relative to HREEs	La, Ce, Pr, Nd, Gd, Tb, Er	Chatrapur, India (2402 mg/kg); Andra Pradesh, India (52 – 4597 mg/kg);

		Pulmoddai deposit	137 – 2996 (avg. = 454)	0.02 – 0.35	Low, slightly enriched in LREEs relative to HREEs	La, Ce, Pr, Nd, Gd, Tb, Er	Kavala-Nea Permos, Greece (58 – 10,879 mg/kg); Sithonia, Greece (14 – 6474 mg/kg) (Source: Batapola et al., 2021; Singh, 2020)
		Southwest coast	27.94 - 1359	0.01 – 0.16	Medium, moderately enriched in LREEs relative to HREEs	La, Ce, Pr, Nd, Tb, Er, Yb	
	Alluvial placers	Belihul Oya	167 – 423 (avg. = 250)	0.02 – 0.05	Medium, moderately enriched in LREEs relative to HREEs	La, Pr, Nd, Tb	Taiwanese rivers, Taiwan (122 – 323 mg/kg); Changjiang, China (162 – 211 mg/kg); Huanghe (106 – 249 mg/kg); Zhujiang, China (162 – 362 mg/kg) (Source: Li et al., 2013)
		Walave River	134 – 402 (avg. = 239)	0.02 – 0.05			
		Kiriketi Oya	225 – 351 (avg. = 265)	0.03 – 0.04			
Magmatic deposits	Granites	Thonigala	142 – 615 (avg. = 329)	0.02 – 0.07	High, strongly enriched in LREEs relative to HREEs	La, Pr, Nd, Gd, Er	Bokan, USA (0.61 wt%); Toongi, Australia (0.89 wt%); Brockman, Australia (0.21 wt%) (Source: Dostal, 2017)
		Arangala	555 – 1358 (avg. = 932)	0.06 – 0.16	Low, slightly enriched in LREEs relative to HREEs	La, Ce, Gd	

		Massenna	65.29 – 2153 (avg. = 937)	0.01 – 0.25	High, strongly enriched in LREEs relative to HREEs	Ce, Nd, La, Pr, Gd	
		Ambagaspitiya	98.54 – 1192 (avg. = 317)	0.01 – 0.14	Low, slightly enriched in LREEs relative to HREEs	Ce, Nd, Gd, Y, La	
	Pegmatites	Ratthota	19.6 – 217 (avg. = 80.34)	0.002 – 0.032	Low, slightly enriched in LREEs relative to HREEs	Y, Nd, Ce, Dy, Er	Strange Lake, Canada (0.87 wt%) (Source: Orris and Grauch, 2002)

of LREEs than HREEs. As a result, while LREE production volumes for LREEs, such as La, Ce, and Nd are in the order of tens of thousand tonnes, production volumes for most HREEs are typically less than 1000 tonnes. Therefore, the 'balance problem' (i.e., overproduction of LREEs over HREEs) in the REE market has caused the deterioration of LREE prices in recent years while demand and prices for HREEs have increased substantially due to their rarity and importance in modern high-tech products and renewable technologies. Therefore, when prospecting for potential REE deposits, it is important to take into consideration the relative enrichment of HREEs over LREEs (Paulick and Machacek, 2017).

In this context, the EPD and Massenna granite are highly enriched in LREEs, whereas the Pulmoddai deposit and Arangala granite have a lesser LREE enrichment than others, thus not causing the 'balance problem'. However, in terms of granitic occurrences with REE potential, technological challenges arise when they are converted to exploitable mineral reserves. Since granites mostly contain non-traditional REE-bearing silicate minerals, immense R&D is required for viable processing methods to commercially extract REEs from such sources (Paulick and Machacek, 2017; Sanematsu et al., 2009). However, granites have a higher potential for HREEs than other resources, thus they could be prospective in the future if extraction techniques are developed for silicate minerals. In contrast, the EPD and Pulmoddai deposit have processable REE-bearing minerals. The EPD mainly contains apatite-group minerals, whereas the Pulmoddai deposit consists of monazite. Monazite is currently commercially processed to produce REEs and different novel extraction methodologies have been developed for apatite. Therefore, the EPD and Pulmoddai deposit could be considered as the potential REE prospects in Sri Lanka out of the explored geological resources in this study.

In comparison to similar occurrences of REE deposits in the world, the studied prospects in Sri Lanka are relatively low-grade, even in the case of the EPD and Pulmoddai deposit (Table 4.11). However, with the exponential consumption of REEs and the development of novel extraction techniques for low-grade REE resources, such as bio-leaching and Phyto-extraction (Rötzer and Schmidt, 2018), these low-grade REE resources in Sri Lanka could also be economically viable in the future.

Furthermore, the economic viability of REE extraction from a geological source is not entirely dependent on its REE content or grade, but also on REE mineralogy. REE-bearing minerals present within these units play a key role in concentrating REEs as well as in the economic viability of REE extraction (potentially acid-leachable minerals) (Jowitt et al., 2017). Therefore, the REE mineralization of these sources must be fully characterized to understand their potential as future REE prospects.

As future potential REE prospects in Sri Lanka, the EPD is more favored over the Pulmoddai deposit in the present study, considering the environmental and radioactive challenges associated with the latter deposit. Furthermore, the EPD is currently mined for the production of phosphate rock, which is applied in raw form as fertilizers for perennial crops. Thus, a significant amount of REEs is wasted by this usage of phosphate rock in raw form. In this regard, recovering REEs as a by-product after developing the existing phosphate fertilizer production flow at the EPD while producing a more soluble form of phosphate fertilizers creates a sub-economic potential for the EPD.

4.4. Eppawala phosphate deposit as a future prospect for REEs

Figure 4.15 illustrates a comparison of REE abundance in the EPD with the median abundances of REEs of the phosphate rocks in the world. Most of the REEs in the EPD (La, Ce, Pr, Nd, Sm, Eu, Gd, Tb, Er, and Yb) had higher abundances compared to their median values in phosphate rocks, while the rest (Dy, Ho, Tm, Lu, and Y) fell within the same or lower range as of their medians. Among the highly enriched REEs in the EPD, LREEs shared a great percentage, while only HREEs, such as Tb and Er showed significant enrichments.

In the sense of economic and scarcity potential (ESP), most LREEs like La and Ce are less in demand due to their insignificance in clean energy (Pell et al., 2019). However, despite being LREEs, the demand for Nd and Pr is increasing due to their importance in the production of permanent magnets used in many high-tech applications. It has been forecasted that the demand for Nd will increase by 700% within the next two decades, leading to rapid growth in the price of neodymium oxide

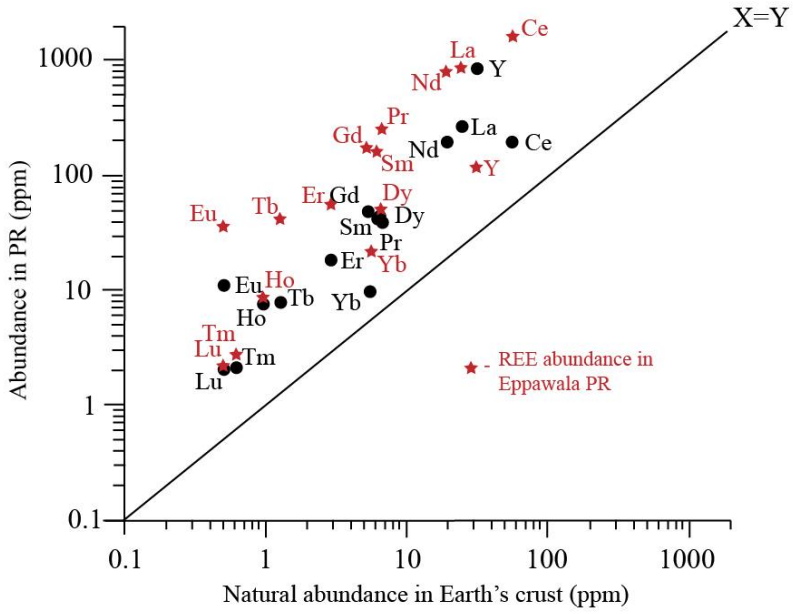

Figure 4.15: A comparison of the REE abundances in the Eppawala Phosphate Deposit with the median abundances of phosphate rocks in the world,
Source: adapted from Chen and Graedel (2015)

in the market. Based on the role in renewable energy as well as supply risk, the US Department of Energy has identified five REEs as critical rare earth elements (CREEs)for both short and long terms, namely Nd, Eu, Tb, Dy, and Y. In addition, Pr is also considered critical since it acts as a substitution for Nd in permanent magnets used in renewable energy components (e.g., electric vehicles and direct drive wind turbines). Therefore, these elements will experience high demand growth in the future with strong price performance due to inadequate supply caused by various environmental and geopolitical concerns (U.S. Department of Energy, 2011). The prices of Nd, Eu, Tb, Dy, Y, and Pr per tonne in 2020 were U.S. $49,144, U.S. $30,000, U.S. $671,000, U.S. $260,000, U.S. $2,940, and U.S. $45,763, respectively (Statista, 2020). It indicates that Tb and Dy share the highest market prices among the CREEs, while Nd, Pr, and Eu also have significantly high prices. Moreover, Pell et al. (2019) forecasted that the price of neodymium oxide will increase to the U.S. $77,500 by 2025. Therefore, the discovery of new and alternative supply chains for these CREEs (particularly Tb, Dy, Nd, Pr, and Eu) is a timely requirement.

In this context, higher abundances of Tb, Nd, Pr, and Eu in the EPD compared to median abundances in phosphate rocks highlight the economic importance of the EPD as a source for these CREEs. Considering the average grades of these elements and the reserve capacity of 60 million tonnes, Tb, Nd, Pr, and Eu contents could be roughly estimated as 2,897 tonnes, 54,468 tonnes, 17,994 tonnes, and 2,508 tonnes, respectively. Therefore, the EPD could be considered as a possible source for these CREEs, especially Nd and Pr. However, detailed exploration works along with economic viability studies must be carried out to assess the actual potential of these CREEs.

Based on the present work, the average TREO grades in the apatite crystals and secondary phosphate matrix of the EPD were obtained as 0.49 wt% TREO and 0.48 wt% TREO, respectively. Moreover, the average light rare earth oxide (LREO) and heavy rare earth oxide (HREO) grades of the apatite crystals and secondary phosphate matrix were 0.43 wt% LREO, 0.06 wt% HREO, and 0.42 wt% LREO, 0.06 wt% HREO, respectively. Therefore, the EPD might be significant as a diverse source for REEs in Sri Lanka, especially for HREEs that are rarer and less concentrated but highly demanded and priced due to their importance in permanent magnets and renewable energies. Moreover, considering an average TREO grade of 0.48%, the average REE reserve at the EPD is estimated at approximately 0.29 million tonnes of TREO. Furthermore, average LREE and HREE reserves at the EPD are about 0.26 million tonnes of LREO (using an average grade of 0.43% LREO) and 0.03 million tonnes of HREO (using an average grade of 0.06% HREO), respectively.

The outstripping REE demand over supply and the global attempt to diversify the world's REE production will promote even low-grade REE sources to become economically viable in the future. In this regard, the EPD could be a strategic target for future REE supply considering its ability to recover REEs as a by-product from the currently available phosphate production flow. Therefore, the EPD could be identified as the most potential REE prospect out of the studied geological formations in Sri Lanka. However, more detailed sampling, geochemical evaluations, mineralogical analyses, and volume calculations are required before the true potential of these prospects can be determined.

CHAPTER 5: CONCLUSIONS

Although several geological and geochemical research have reported high concentrations of REEs in different geological formations in Sri Lanka, they have never been explored in detail to find out their true potential as future REE prospects. In this context, the present study has revealed a few potential REE prospects in Sri Lanka that are associated with residual lateritic formations, beach placers, and magmatic occurrences.

In the studied residual lateritic regolith in Sri Lanka, the EPD showed the highest potential with extreme REE enrichment compared to the Ginigalpelessa serpentinite deposit. The possible cause for this higher REE enrichment in the weathered profile of the EPD is related to the degree of REE enrichment in the parent carbonatite rock at the EPD. Pulmoddai is the highest REE-enriched beach placer deposit in Sri Lanka, whereas Verugal and southwest coast beach placers have similar, but medium enrichments of REEs. The provenance of beach placers on the northeast coast may be associated with high-grade metamorphic rocks in the catchment of the Mahaweli river and eastern Indian clastic sediments to a lesser extent. However, the possible sources of beach placers along the southwest coast could be related to granites, charnockites, khondalites, and granitoid rocks present in the inland drainage basins. The studied alluvial placers in the Walave river basin do not exhibit significant REE enrichment levels, but Kiriketi Oya sediments showed relatively high enrichments for HREEs. In terms of magmatic deposits, REE enrichments in the studied granites increased in the order of Ambagaspitiya < Thonigala < Arangala < Massenna. The observed difference in REE enrichment in the granites is possibly due to the degree of fractionation and highly fractionated granites favor the HREE enrichment. However, all these granites are not highly fractionated resulting in the absence of significant HREE enrichments in them. Pegmatite in Ratthota-Matale showed the lowest potential of REEs in magmatic deposits, but it has a higher enrichment of HREEs.

Out of the studied geological resources in the present study, the EPD, Massenna granite, Arangala granite, and Pulmoddai deposit were identified as the

prospective source/s in Sri Lanka. Although granitic rocks in Sri Lanka indicate high REE potential, they are difficult to consider as exploitable mineral reserves due to the lack of commercial REE processing technologies for REE-bearing silicate minerals. However, the EPD and Pulmoddai deposit contain currently processable apatite and monazite as RE minerals, thus they are more exploitable than other studied prospects. Even though the Pulmoddai deposit is a prospective source for REEs in Sri Lanka, environmental and radioactive issues associated with the processing of monazite pose significant challenges in converting such deposits into exploitable reserves. Therefore, in the present study, the EPD was identified as the most prospective REE source in Sri Lanka, considering its sub-economic potential to extract REEs as a by-product from the phosphate production flow.

In this regard, the EPD could be considered a potential source of REEs, especially for LREEs. However, LREEs, such as La and Ce are less in demand due to their insignificance in clean energy, while the demand for Nd and Pr is high. Therefore, the EPD could become a potential diverse source for Nd and Pr, considering their susceptibility to high supply risk in the future. Moreover, the EPD could be an unconventional source for Tb as well, which is a critical HREE due to its importance in renewable energy and possible supply risk. The EPD has a TREO grade of 0.48% with an estimated reserve of 0.29 million tonnes of REOs. In comparison to most other phosphate deposits in the world, TREO grade in the EPD is lower, however, the EPD could become a potential secondary REE source, considering the rapid outstripping demand over limited REE supply. Therefore, REE extraction technologies must be developed to recover REEs as a by-product of the EPD, which could ultimately contribute to the local and global REE supply chains as a sustainable, diverse REE source.

CHAPTER 6: RECOMMENDATIONS

The present study reveals that the EPD has a sub-economic potential for REEs to be recovered as a by-product of phosphate fertilizer production. However, more detailed geological, mineralogical, and geochemical explorations are required in the EPD to delineate its actual potential for REEs. Furthermore, economic feasibility studies must be carried out in the EPD, and if viable suitable extraction techniques must be developed to extract REEs as a by-product. Moreover, two intrusive prospects with high REE potential, namely Massenna and Arangala granites must be fully characterized for their mineralogy and geology since the potentiality of REEs in a deposit also depends on factors, such as ore minerals, textures, and grain size.

Pulmoddai mineral sand deposit was also identified as one of the most potential REE prospects in this study and it is well-known for monazite enrichment. According to the present study, the average REE content of this deposit is relatively low. However, the sampling was carried out during the inter-monsoon period after the mining of beach sand started. Therefore, further sampling is recommended in the Pulmoddai deposit during the northeastern monsoon when these beaches are replenished with heavy minerals. In addition, we proposed to assess the potential of REEs in the monazite concentrates separated in the processing plant at the Pulmoddai deposit since only a few preliminary works have been carried out in this regard. Moreover, suitable extraction techniques must be developed to recover REEs from monazite at the Pulmoddai deposit. However, the environmental concerns and radioactive issues must be carefully addressed if the Pulmoddai deposit is considered to be a prospect for REEs in Sri Lanka.

In addition, the literature shows that IOCG deposits are a prospective source of REEs, and thus it is also important to investigate the REE potential in iron ore deposits of Sri Lanka. Although Samarakoon et al. (2021) have explored the REE potential in three iron ore deposits in Sri Lanka, namely Panirendawa, Dela, and Buttala, their results were not significant. However, since Seruwila Cu-Magnetite deposit has not yet been explored for REEs, which is also an iron ore deposit in Sri Lanka, we further recommend investigating the REE potential in this prospect as well.

REFERENCES

Aide, M., Smith-Aide, C., 2003. Assessing soil genesis by rare-earth elemental analysis. Soil Sci. Soc. Am. J. 67, 1470–1476.

Alonso, E., Sherman, A.M., Wallington, T.J., Everson, M.P., Field, F.R., Roth, R., Kirchain, R.E., 2012. Evaluating rare earth element availability: A case with revolutionary demand from clean technologies. Environ. Sci. Technol. 46, 3406–3414.

Altschuler, Z.S., Berman, S., Cuttitta, F., 1967. Rare earths in phosphorites—geochemistry and potential recovery 125–135.

Amalan, K., Ratnayake, A.S., Ratnayake, N.P., Weththasinghe, S.M., Dushyantha, N., Lakmali, N., Premasiri, R., 2018. Influence of nearshore sediment dynamics on the distribution of heavy mineral placer deposits in Sri Lanka. Environ. earth Sci. 77, 737.

Athurupane, B.M.B., 2014. Rare earth mineral resources in sri lanka.

Balaram, V., 2019. Rare earth elements: A review of applications, occurrence, exploration, analysis, recycling, and environmental impact. Geosci. Front. 10, 1285–1303.

Bao, Z., Zhao, Z., 2008. Geochemistry of mineralization with exchangeable REY in the weathering crusts of granitic rocks in South China. Ore Geol. Rev. 33, 519–535.

Barakos, G., Mischo, H., Gutzmer, J., 2016. An outlook on the rare earth elements mining industry. AusIMM Bull. 62–66.

Barnes, R., Jaireth, S., Miezitis, Y., Suppel, D., 1999. Regional mineral potential assessments for land use planning; GIS-based examples from eastern Australia: publication series, in: Australas. Inst. Min. Metall. pp. 4–99.

Batapola, N., Dushyantha, N., Ratnayake, N., Premasiri, R., Abeysinghe, B., Dissanayake, O., Rohitha, S., Ilankoon, S., Dharmaratne, P., 2021. Rare earth element potential in the beach placers along the southwest coast of Sri Lanka, in:

2021 Moratuwa Engineering Research Conference (MERCon). IEEE, pp. 415–420.

Batapola, N.M., Dushyantha, N.P., Premasiri, H.M.R., Abeysinghe, A., Rohitha, L.P.S., Ratnayake, N.P., Dissanayake, D., Ilankoon, I., Dharmaratne, P.G.R., 2020. A comparison of global rare earth element (REE) resources and their mineralogy with REE prospects in Sri Lanka. J. Asian Earth Sci. 200, 104475.

Berger, A., Janots, E., Gnos, E., Frei, R., Bernier, F., 2014. Rare earth element mineralogy and geochemistry in a laterite profile from Madagascar. Appl. geochemistry 41, 218–228.

Binnemans, K., Jones, P.T., Blanpain, B., Van Gerven, T., Yang, Y., Walton, A., Buchert, M., 2013. Recycling of rare earths: a critical review. J. Clean. Prod. 51, 1–22.

Cassidy, K.F., Towner, R.R., Ewers, G.R., 1997. Rare earth elements in Australia. AGSO Confid. Rep.

center for Strategic International Studies, 2022. Does China Pose a Threat to Global Rare Earth Supply Chains? [WWW Document].

Černý, P., Ercit, T.S., 2005. The classification of granitic pegmatites revisited. Can. Mineral. 43.

Černý, P., London, D., Novák, M., 2012. Granitic pegmatites as reflections of their sources. Elements 8, 289–294.

Chakhmouradian, A.R., Zaitsev, A.N., 2012. Rare earth mineralization in igneous rocks: sources and processes. Elements 8, 347–353.

Chandrajith, R., Dissanayake, C.B., Tobschalll, H.J., 2000. The Stream Sediment Geochemistry of the Walawe Ganga Basin of Sri Lanka - Implications for Gondwana Mineralization 189–204.

Chandrakumara, G.T.D., Balasooriya, N.W.B., Mantilaka, M., Lottermorser, B.G., Pitawala, H., 2021. Geochemical and mineralogical characterization of phosphatic crusts developed on the basement carbonatites of Sri Lanka: towards

a better understanding of the weathering process. Ceylon J. Sci. 50.

Chen, W.T., Zhou, M.-F., 2015. Mineralogical and geochemical constraints on mobilization and mineralization of rare Earth elements in the Lala Fe-Cu-(Mo, Ree) deposit, SW China. Am. J. Sci. 315, 671–711.

Cocker, M.D., 2014. Lateritic, supergene rare earth element (REE) deposits.

Coomáraswámy, A.K., 1904. VII.—Contributions to the Geology of Ceylon: III. The Balangoda Group. Geol. Mag. 1, 418–422.

Cooray, P.G., 1994. The precambrian of Sri Lanka: a historical review. Precambrian Res. 66, 3–18.

Cooray, Percival Gerald, 1984. An introduction to the geology of Sri Lanka (Ceylon). National museums of Sri Lanka publication.

Cooray, P. G., 1984. An Introduction to The Geology of Sri Lanka, 2nd Revise. ed. National Museums of Sri Lanka Publication, Colombo.

Cox, C., Kynicky, J., 2018. The rapid evolution of speculative investment in the REE market before, during, and after the rare earth crisis of 2010–2012. Extr. Ind. Soc. 5, 8–17.

Dahanayake, K., Subasinghe, S.M.N.D., 1991. Mineralogical, chemical and solubility variations in the Eppawala phosphate deposit of Sri Lanka - a case for selective mining for fertilizers. Fertil. Res. 28, 233–238. https://doi.org/10.1007/BF01049756

Dharmapriya, P.L., Disanayaka, D.W.M., Martin, R.F., Pitawala, H., Malaviarachchi, S.P.K., 2021. Granitic pegmatites in Sri Lanka: A concise review leading to insights and predictions. Ore Energy Resour. Geol. 6, 100011.

Dinalankara, D., 1995. Eppawala phosphate deposit of Sri Lanka-present status. Direct Appl. phosphate rock Appropr. Technol. Fertil. Asia–what hinders Accept. growth. Inst. Fundam. Stud. Sri Lanka 153–163.

Dissanayaka, C.B., 1982. The geology and geochemistry of the Uda Walawe

serpentinite. Sri Lanka. J Natn Sci Coun Sri Lanka 10, 13–34.

Dostal, J., 2017. Rare earth element deposits of alkaline igneous rocks. Resources 6, 34.

Dostal, J., 2016. Rare metal deposits associated with alkaline/peralkaline igneous rocks.

Dushyantha, N., Batapola, N., Ilankoon, I., Rohitha, S., Premasiri, R., Abeysinghe, B., Ratnayake, N., Dissanayake, K., 2020. The story of rare earth elements (REEs): Occurrences, global distribution, genesis, geology, mineralogy and global production. Ore Geol. Rev. 122, 103521.

Dushyantha, N., Weerawarnakula, S., Premasiri, R., Abeysinghe, B., Ratnayake, N., Batapola, N., Ranasinghe, M., 2021. Potential ecological risk assessment of heavy metals (Cr, Ni, and Co) in serpentine soil at Ginigalpelessa in Sri Lanka. Arab. J. Geosci. 14, 1–12.

Dushyantha, N.P., Hemalal, P.V.A., Jayawardena, C.L., Ratnayake, A.S., Ratnayake, N.P., 2019. Application of geochemical techniques for prospecting unconventional phosphate sources: A case study of the lake sediments in Eppawala area Sri Lanka. J. Geochemical Explor. 201, 113–124.

Fernando, G., Pitawala, A., Amaraweera, T., 2011. Emplacement and evolution history of pegmatites and hydrothermal deposits, Matale district, Sri Lanka.

Fernando, L.J.D., 1986. Mineral Resources of Sri Lanka.

Fernando, L.J.D., 1954. Progress of the Geological Survey of Ceylon. Bull. Ceylon geogr. Soc 8, 1–10.

Filippelli, G.M., 2011. Phosphate rock formation and marine phosphorus geochemistry: the deep time perspective. Chemosphere 84, 759–766.

Filippelli, G.M., 2008. The global phosphorus cycle: past, present, and future. Elements 4, 89–95.

Folger, T., 2011. The secret ingredients of everything. Natl. Geogr. Mag. 6.

Garnett, R.H.T., Bassett, N.C., 2005. Placer deposits.

Goodenough, K.M., Schilling, J., Jonsson, E., Kalvig, P., Charles, N., Tuduri, J., Deady, E.A., Sadeghi, M., Schiellerup, H., Müller, A., 2016. Europe's rare earth element resource potential: An overview of REE metallogenetic provinces and their geodynamic setting. Ore Geol. Rev. 72, 838–856.

Goodenough, K.M., Wall, F., Merriman, D., 2018. The rare earth elements: demand, global resources, and challenges for resourcing future generations. Nat. Resour. Res. 27, 201–216.

Groves, D.I., Bierlein, F.P., Meinert, L.D., Hitzman, M.W., 2010. Iron oxide copper-gold (IOCG) deposits through Earth history: Implications for origin, lithospheric setting, and distinction from other epigenetic iron oxide deposits. Econ. Geol. 105, 641–654.

GSMB, 2001. Sri Lanka 1:100 000 Geology (Provincial Map Series) Sheet 7 and 8 [WWW Document]. Geol. Surv. mines Bur. (GSMB), Sr Lanka.

Gupta, C.K., Krishnamurthy, N., 2005. Extractive metallurgy of rare earths CRC press. Boca Raton, Florida 65, 70–75.

Hampel, C.A., Kolodney, M., 1961. Rare metals handbook. J. Electrochem. Soc. 108, 248C.

Haxel, G.B., Hedrick, J.B., Orris, G.J., Stauffer, P.H., Hendley II, J.W., 2002. Rare earth elements: critical resources for high technology.

Hein, J.R., Conrad, T., Koshinsky, A., 2011. Comparison of land-based REE ore deposits with REE-rich marine Fe-Mn crusts and nodules. Miner. Mag 75, 1000.

HERATH, J.W., 1980. Mineral Resources of Sri Lanka. Geological Survey Econ. Bull 1–72.

Hewawasam, T., 2013. Tropical weathering of apatite-bearing rocks of Sri Lanka: Major element behaviour and mineralogical changes. J. Geol. Soc. Sri Lanka 15, 31–46.

Hewawasam, T., Fernando, G., Priyashantha, D., 2014. Geo-vegetation mapping and soil geochemical characteristics of the Indikolapelessa serpentinite outcrop, southern Sri Lanka. J. Earth Sci. 25, 152–168.

Hoatson, D.M., Jaireth, S., Miezitis, Y., 2011. The major rare-earth-element deposits of Australia: geological setting, exploration, and resources. Geoscience Australia.

Hoshino, M., Sanematsu, K., Watanabe, Y., 2016. REE mineralogy and resources. Handb. Phys. Chem. Rare Earths 49, 129–291.

Ilankoon, I., Dushyantha, N.P., Mancheri, N., Edirisinghe, P.M., Neethling, S.J., Ratnayake, N.P., Rohitha, L.P.S., Dissanayake, D., Premasiri, H.M.R., Abeysinghe, A., 2022. Constraints to rare earth elements supply diversification: Evidence from an industry survey. J. Clean. Prod. 331, 129932.

Ilankoon, I.M.S.K., Tang, Y., Ghorbani, Y., Northey, S., Yellishetty, M., Deng, X., Mcbride, D., 2018. The current state and future directions of percolation leaching in the Chinese mining industry : Challenges and opportunities. Miner. Eng. 125, 206–222.

IPO Future Earth Coasts, 2009. R&S 32. LOICZ Global Change Assessment and Synthesis of River Catchment -Coastal Sea Interaction and Human Dimensions. https://doi.org/10.13140/RG.2.1.2300.0804

Jackson, W.D., Christiansen, G., 1984. International Strategic Minerals Inventory Summary Report--rare-earth Oxides. US Government Printing Office.

Jaireth, S., Hoatson, D.M., Miezitis, Y., 2014. Geological setting and resources of the major rare-earth-element deposits in Australia. Ore Geol. Rev. 62, 72–128.

Jaques, A.L., Jaireth, S., Walshe, J.L., 2002. Mineral systems of Australia: an overview of resources, settings and processes. Aust. J. Earth Sci. 49, 623–660.

Jayawardena, D., 2011. Assessment of rare earth elements in SL For use in hi-tech products and strategic defence systems. Isl. Editor. Anal. Comment. 8.

Jayawardena, D.E. de S., 1978. The Eppawala carbonatite complex in north-west Sri Lanka (Ceylon). Geological Survey Department.

Jayawardena, D.E. de S., Carswell, D.A., 1976. The geochemistry of'charnockites' and their constituent ferromagnesian minerals from the Precambrian of south-east Sri Lanka (Ceylon). Mineral. Mag. 40, 541–554.

Jordens, A., Cheng, Y.P., Waters, K.E., 2013. A review of the beneficiation of rare earth element bearing minerals. Miner. Eng. 41, 97–114.

Jowitt, S.M., Medlin, C.C., Cas, R.A.F., 2017. The rare earth element (REE) mineralisation potential of highly fractionated rhyolites: A potential low-grade, bulk tonnage source of critical metals. Ore Geol. Rev. 86, 548–562.

Kanazawa, Y., Kamitani, M., 2006. Rare earth minerals and resources in the world. J. Alloys Compd. 412, 1339–1343.

Kato, Y., Fujinaga, K., Nakamura, K., Takaya, Y., Kitamura, K., Ohta, J., Toda, R., Nakashima, T., Iwamori, H., 2011. Deep-sea mud in the Pacific Ocean as a potential resource for rare-earth elements. Nat. Geosci. 4, 535.

King, H.M., 2015. Pegmatite [WWW Document]. Geology.com. URL https://geology.com/rocks/pegmatite.shtml (accessed 12.10.21).

Kingsnorth, D.J., 2010. Rare earths: facing new challenges in the new decade, in: Presented by Clinton Cox, SME Annual Meeting.

Kreuzer, O.P., Markwitz, V., Porwal, A.K., McCuaig, T.C., 2010. A continent-wide study of Australia's uranium potential: Part I: GIS-assisted manual prospectivity analysis. Ore Geol. Rev. 38, 334–366.

Kroner, A., 1991. Lithotectonic subdivision of the Precambrian basement in Sri Lanka. In The Crystalline Crust of Sri Lanka, Part I. Summary and Research of the German-Sri Lanka Consortium. Geol. Surv. Dep. Sri Lanka, Prof. Pap. 5, 5–21.

Kröner, A., Cooray, P.G., Vitanage, P.W., 1991. Lithotectonic subdivision of the Precambrian basement in Sri Lanka., In: ed, The crystalline crust of Sri Lanka, Part 1, Summary of Research of the German-Sri Lankan Consortium. Geol. Surv. Dept. Prof. Paper 5., Sri Lanka.

Lanka Mineral Sands Ltd, 2022. Products & Annual Production [WWW Document].

URL https://lankamineralsands.com/products/ (accessed 9.17.22).

Li, M.Y.H., Zhou, M.-F., 2020. The role of clay minerals in formation of the regolith-hosted heavy rare earth element deposits. Am. Mineral. J. Earth Planet. Mater. 105, 92–108.

Li, M.Y.H., Zhou, M.-F., Williams-Jones, A.E., 2019. The genesis of regolith-hosted heavy rare earth element deposits: Insights from the world-class Zudong deposit in Jiangxi Province, South China. Econ. Geol. 114, 541–568.

Li, X.-C., Zhou, M.-F., 2018. The nature and origin of hydrothermal REE mineralization in the Sin Quyen deposit, northwestern Vietnam. Econ. Geol. 113, 645–673.

Li, X., Li, H., Yang, G., 2017. Electric fields within clay materials: How to affect the adsorption of metal ions. J. Colloid Interface Sci. 501, 54–59.

Long, K.R., Gosen, B.S. Van, Foley, N.K., Cordier, D., 2012. The principal rare earth elements deposits of the United States: a summary of domestic deposits and a global perspective, in: Non-Renewable Resource Issues. Springer, pp. 131–155.

Lottermoser, B.G., 1990. Rare-earth element mineralisation within the Mt. Weld carbonatite laterite, Western Australia. Lithos 24, 151–167.

Mahmoud, S.A.E.A., 2019. Geology, mineralogy and mineral chemistry of the NYF-type pegmatites at the Gabal El Faliq area, South Eastern Desert, Egypt. J. Earth Syst. Sci. 128, 1–24.

Mancheri, N.A., Sprecher, B., Bailey, G., Ge, J., Tukker, A., 2019. Effect of Chinese policies on rare earth supply chain resilience. Resour. Conserv. Recycl. 142, 101–112.

Manthilake, M., Sawada, Y., Sakai, S., 2008. Genesis and evolution of Eppawala carbonatites, Sri Lanka. J. Asian earth Sci. 32, 66–75.

Marks, M.A.W., Hettmann, K., Schilling, J., Frost, B.R., Markl, G., 2011. The mineralogical diversity of alkaline igneous rocks: critical factors for the transition from miaskitic to agpaitic phase assemblages. J. Petrol. 52, 439–455.

Mazdab, F.K., Johnson, D.A., Barton, M.D., 2008. Trace element characteristics of hydrothermal titanite from iron-oxide-Cu-Au (IOCG) mineralization. Geochim. Cosmochim. Acta 72, A609.

McDonough, W.F., Sun, S.-S., 1995. The composition of the Earth. Chem. Geol. 120, 223–253.

McLemore, V.T., 2015. Rare earth elements (REE) deposits in New Mexico: Update. New Mex. Geol. 37, 59–69.

Mertzman, S., 2019. What are rare earths, crucial elements in modern technology? 4 questions answered [WWW Document]. Conversat. URL https://theconversation.com/what-are-rare-earths-crucial-elements-in-modern-technology-4-questions-answered-101364 (accessed 10.21.19).

Migdisov, A.A., Williams-Jones, A.E., 2014. Hydrothermal transport and deposition of the rare earth elements by fluorine-bearing aqueous liquids. Miner. Depos. 49, 987–997.

Moldoveanu, G.A., Papangelakis, V.G., 2016. An overview of rare-earth recovery by ion-exchange leaching from ion-adsorption clays of various origins. Mineral. Mag. 80, 63–76.

Nawaratne, S.W., 2009. Feldspar and vein quartz mineralization in Sri Lanka: a possible post metamorphic mid-Paleozoic pegmatiticpneumatolitic activity. J Geol Soc Sri Lanka 13, 83–96.

Nawaratne, S.W., Wijeratne, G.N., 1995. The source of placer gold in the Walawe Ganga basin, Sri Lanka.

Novák, M., Škoda, R., Gadas, P., Krmíček, L., Černý, P., 2012. Contrasting origins of the mixed (NYF+ LCT) signature in granitic pegmatites, with examples from the Moldanubian Zone, Czech Republic. Can. Mineral. 50, 1077–1094.

Oreskes, N., Einaudi, M.T., 1990. Origin of rare earth element-enriched hematite breccias at the Olympic Dam Cu-U-Au-Ag deposit, Roxby Downs, South Australia. Econ. Geol. 85, 1–28.

Orris, G., Grauch, R., 2002. Rare earth element mines, deposits, and occurrences.

Pell, R.S., Wall, F., Yan, X., Bailey, G., 2019. Applying and advancing the economic resource scarcity potential (ESP) method for rare earth elements. Resour. Policy 62, 472–481.

Pitawala, A., Lottermoser, B.G., 2012. Petrogenesis of the Eppawala carbonatites, Sri Lanka: A cathodoluminescence and electron microprobe study. Mineral. Petrol. 105, 57–70.

Pitawala, A., Schidlowski, M., Dahanayake, K., Hofmeister, W., 2003. Geochemical and petrological characteristics of Eppawala phosphate deposits, Sri Lanka. Miner. Depos. 38, 505–515.

Pohl, J.G., Emmermann, R., 1991. Chemical composition of the Sri Lanka Precambrian basement, In: Kröner. ed, The Crystalline Crust of Sri Lanka, Part I. Summary of Research of the German–Sri Lankan Consortium. Geol. Surv. Dept., Sri Lanka.

Rajakaruna, N., Bohm, B.A., 2002. Serpentine and its vegetation: a preliminary study from Sri Lanka. J. Appl. Bot. 76, 20–28.

Ratnayake, A.S., Dushyantha, N., De Silva, N., Somasiri, H.P., Jayasekara, N.N., Weththasinghe, S.M., Samaradivakara, G.V.I., Vijitha, A.V.P., Ratnayake, N.P., 2017. Sediment and physicochemical characteristics in Madu-ganga Estuary, southwest Sri Lanka. J. Geol. Soc. Sri Lanka 18, 43–52.

Sameera, K.A.G., Wickramasinghe, W., Harankahawa, S.B., Welikanna, C.R., De Silva, K., 2020. Radiometric surveying for Th and U mineralization in southwestern, Sri Lanka: radiological, mineralogical and geochemical characteristics of the radioactive anomalies. J. Geol. Soc. Sri Lanka 21.

Sanematsu, K., Watanabe, Y., 2016. Characteristics and genesis of ion adsorption-type rare earth element deposits.

Schmid, M., 2019. Mitigating supply risks through involvement in rare earth projects: Japan's strategies and what the US can learn. Resour. Policy 63, 101457.

Schüler, D., Buchert, M., Liu, R., Dittrich, S., Merz, C., 2011. Study on rare earths and their recycling. Öko-Institut eV Darmstadt 49, 30–40.

Senaratne, A., RUPASINGHE, M.S., DISSANGAYAKE, C.B., 1987. Rare earth elements in some residual, alluvial and inter-tidal sediments of Sri Lanka. Chemie der Erde 47, 31–40.

Sengupta, D., Van Gosen, B.S., 2016. Placer-type rare earth element deposits: Chapter 4.

Siegel, K., Vasyukova, O. V, Williams-Jones, A.E., 2018. Magmatic evolution and controls on rare metal-enrichment of the Strange Lake A-type peralkaline granitic pluton, Québec-Labrador. Lithos 308, 34–52.

Simandl, G.J., 2014. Geology and market-dependent significance of rare earth element resources. Miner. Depos. 49, 889–904.

Simandl, G.J., Paradis, S., 2018. Carbonatites: related ore deposits, resources, footprint, and exploration methods. Appl. Earth Sci. 127, 123–152.

Sinclair, W.D., Jambor, J.L., Birkett, T.C., 1992. Rare earths and the potential for rare-earth deposits in Canada. Explor. Min. Geol. 1, 265–281.

Singh, Y., 2020. Rare earth element resources: Indian context. Springer.

Skirrow, R.G., Bastrakov, E.N., Barovich, K., Fraser, G.L., Creaser, R.A., Fanning, C.M., Raymond, O.L., Davidson, G.J., 2007. Timing of iron oxide Cu-Au-(U) hydrothermal activity and Nd isotope constraints on metal sources in the Gawler craton, South Australia. Econ. Geol. 102, 1441–1470.

Skirrow, R.G., Jaireth, S., Huston, D.L., Bastrakov, E.N., Schofield, A., Van der Wielen, S.E., Barnicoat, A.C., 2009. Uranium mineral systems: processes, exploration criteria and a new deposit framework. Geosci. Aust. Rec. 20, 44.

Smith, M.P., Moore, K., Kavecsánszki, D., Finch, A.A., Kynicky, J., Wall, F., 2016. From mantle to critical zone: A review of large and giant sized deposits of the rare earth elements. Geosci. Front. 7, 315–334.

Spandler, C., Morris, C., 2016. Geology and genesis of the Toongi rare metal (Zr, Hf, Nb, Ta, Y and REE) deposit, NSW, Australia, and implications for rare metal mineralization in peralkaline igneous rocks. Contrib. to Mineral. Petrol. 171, 1–24.

Statista, 2020. Rare earth oxide demand worldwide from 2017 to 2025 [WWW Document].

Taylor, S.R., McLennan, S.M., 1985. The continental crust: its composition and evolution.

Thilakanayaka, T., 2015. Quantification of Radioactive and Heavy Minerals in Uswetakeiyawa area (Sri Lanka) 5.

Timofeev, A., Williams-Jones, A.E., 2015. The origin of niobium and tantalum mineralization in the Nechalacho REE Deposit, NWT, Canada. Econ. Geol. 110, 1719–1735.

Udarika, R.M.L., Udayakumara, E.P.N., Amalan, K., Ratnayake, N.P., Premasiri, H.M.R., 2016. Comparison of heavy mineral composition along Mahaweli River with placer deposits at North East Coast of Sri Lanka, in: International Symposium on Agriculture and Environment.

Ugbe, F.C., 2011. Basic engineering geological properties of lateritic soils from Western Niger Delta. Res. J. Environ. Earth Sci. 3, 571–577.

United States Geological Survey (USGS), 2022. Mineral Commodity Summaries 2022.

United States Geological Survey (USGS), 2021. Mineral Commodity Summaries.

United States Geological Survey (USGS), 2011. Mineral Commodity Summaries 2011.

Van Gosen, B.S., Verplanck, P.L., Long, K.R., Gambogi, J., Seal II, R.R., 2014. The rare-earth elements: vital to modern technologies and lifestyles. US Geological Survey.

Vithanage, M., Rajapaksha, A.U., Oze, C., Rajakaruna, N., Dissanayake, C.B., 2014. Metal release from serpentine soils in Sri Lanka. Environ. Monit. Assess. 186, 3415–3429.

Wadia, D.N., Fernando, L.J.D., 1945. Gems and semi-precious stones of Ceylon. Ceylon Dep. Mineral. Prof. Pap. 2, 13–44.

Wall, F., Mariano, A.N., 1995. Rare earth minerals in carbonatites: a discussion centred on the Kangankunde Carbonatite, Malawi. Mineral. Soc. Ser. 7, 193–226.

Walters, A., Lusty, P., 2010. Rare earth elements. British Geological Survey.

Wang, L., Liang, T., 2016. Anomalous abundance and redistribution patterns of rare earth elements in soils of a mining area in Inner Mongolia, China. Environ. Sci. Pollut. Res. 23, 11330–11338.

Wang, X., Yao, M., Li, J., Zhang, K., Zhu, H., Zheng, M., 2017. China's rare earths production forecasting and sustainable development policy implications. Sustainability 9, 1003.

Weng, Z., Jowitt, S.M., Mudd, G.M., Haque, N., 2015. A detailed assessment of global rare earth element resources: opportunities and challenges. Econ. Geol. 110, 1925–1952.

Wickremeratne, W.S., 1986. Preliminary studies on the offshore occurrences of monazite-bearing heavy-mineral placers, southwestern Sri Lanka. Mar. Geol. 72, 1–9.

Williams-Jones, A.E., Migdisov, A.A., Samson, I.M., 2012. Hydrothermal mobilisation of the rare earth elements–a tale of "ceria" and "yttria." Elements 8, 355–360.

Williams, P.J., Barton, M.D., Johnson, D.A., Fontboté, L., De Haller, A., Mark, G., Oliver, N.H.S., Marschik, R., 2005. Iron oxide copper-gold deposits: Geology, space-time distribution, and possible modes of origin.

Winter, J.D., 2013. Principles of igneous and metamorphic petrology. Pearson education.

Woolley, A.R., Kjarsgaard, B., 2004. Carbonatites of the world: map and database.

Zepf, V., 2013. Rare earth elements: a new approach to the nexus of supply, demand and use: exemplified along the use of neodymium in permanent magnets. Springer Science & Business Media.

Zhou, B., 2017. Global Potential of Rare Earth Resources and Rare Earth Demand from Clean Technologies. Minerals 7, 203–217. https://doi.org/10.3390/min7110203